REPORT DOCUMENTATION PAGE

Form Approved
OMB No. 0704-0188

PLEASE DO NOT RETURN YOUR FORM TO THE ABOVE ADDRESS.

1. REPORT DATE *(DD-MM-YYYY)*	2. REPORT TYPE	3. DATES COVERED *(From - To)*
25/Jun/2001	THESIS	

4. TITLE AND SUBTITLE
SIMULTANEOUS ATTITUDE CONTROL AND ENERGY STORAGE USING VSCMGS: THEORY AND SIMULATION

5a. CONTRACT NUMBER

5b. GRANT NUMBER

5c. PROGRAM ELEMENT NUMBER

6. AUTHOR(S)
CAPT RICHIE DAVID J

5d. PROJECT NUMBER

5e. TASK NUMBER

5f. WORK UNIT NUMBER

7. PERFORMING ORGANIZATION NAME(S) AND ADDRESS(ES)
GEORGIA INSTITUTE OF TECHNOLOGY

8. PERFORMING ORGANIZATION REPORT NUMBER
CI01-125

9. SPONSORING/MONITORING AGENCY NAME(S) AND ADDRESS(ES)
THE DEPARTMENT OF THE AIR FORCE
AFIT/CIA, BLDG 125
2950 P STREET
WPAFB OH 45433

10. SPONSOR/MONITOR'S ACRONYM(S)

11. SPONSOR/MONITOR'S REPORT NUMBER(S)

12. DISTRIBUTION/AVAILABILITY STATEMENT
Unlimited distribution
In Accordance With AFI 35-205/AFIT Sup 1

13. SUPPLEMENTARY NOTES

14. ABSTRACT

15. SUBJECT TERMS

16. SECURITY CLASSIFICATION OF:			17. LIMITATION OF ABSTRACT	18. NUMBER OF PAGES	19a. NAME OF RESPONSIBLE PERSON
a. REPORT	b. ABSTRACT	c. THIS PAGE		142	19b. TELEPHONE NUMBER *(Include area code)*

Simultaneous Attitude Control and Energy Storage using VSCMGs: Theory and Simulation

A Thesis
Presented to
The Academic Faculty

by

David James Richie

In Partial Fulfillment
of the Requirements for the Degree of
Master of Science in Aerospace Engineering

Georgia Institute of Technology
April 2001

Simultaneous Attitude Control and Energy Storage using VSCMGs: Theory and Simulation

Approved:

Panagiotis Tsiotras, Chairman

Dewey Hodges

Amy Pritchett

Date Approved by Chairman 4/17/01

Date Approved _____

GOVERNMENT DISCLAIMER

The views expressed in this thesis are those of the author and do not necessarily reflect the official policy or position of the Department of Defense or the United States Government.

DEDICATION

For Melissa, the shining light in a often dark world

Contents

List of Tables

List of Figures

ACKNOWLEDGEMENTS

I would like to thank the following individuals that made this research effort possible: First and foremost is my research and thesis advisor, Dr. Panagiotis Tsiotras. Over the course of the last year and a half, he pushed me to new academic heights I never dreamed I could reach. At times I struggled but he never gave up on me and always knew I could do better. His love for research is unparalleled and I am truly grateful for all he has done.

Second, is my thesis committee, Dr. Dewey Hodges and Dr. Amy Pritchett. Dr. Hodges was instrumental in helping me come to Georgia Tech in the first place. He served as an excellent role model for me to follow when I become an educator. I appreciate his expertise and experience and am thankful for his service on my committee.

Dr. Pritchett opened the door to the fascinating world of simulation for me. She has shown me how to model many physical machines, vehicles, and processes (i.e anything that can be described by a differential equation). This has greatly added to my personal "skills toolbox." Furthermore, she always took it upon herself to ensure that my education was of the highest quality even though I was not her advisee. Dr. Pritchett was clearly an excellent choice for my committee.

Third, there is my mentor and customer, Dr. Jerry Fausz. He taught me many of the ins and outs of graduate school and life as a professional controls engineer. Because of his efforts, I was able to spend an eventful summer semester at the Air Force Research Laboratory in Albuquerque, New Mexico. That experience proved to be the cornerstone for this research effort.

In relation to my work with Dr. Fausz, I also would like to thank Dr. Marc Jacobs of AFOSR for funding this research. One should note that part of this work was carried out during my visit to the AFRL/VS Directorate (mentioned above) through the Educational Partnership Agreement between AFRL and the Georgia Institute of Technology (Contract no: 2000-AFRL/VS-EPA-15).

Fifth, my trusted colleague and mentor – Haijun Shen. From my first campus visit to Georgia Tech, Haijun helped me understand what it takes to be an Aerospace Engineering graduate student. He gave me tremendous technical support and tips on my research topic as I followed a research effort parallel to his. Haijun's help is greatly appreciated!

Sixth, my friend and fellow advisee, Brian Wilson. His ability to translate theoretical issues to real problems and vice versa is remarkable. He has a good knack for re-explaining the more difficult control concepts in simple terms. Based on his general love and zest for controls work, I know his limits are unbounded!

Seventh, my trusted fellow advisee – Hyungjoo Yoon. I am greatly indebted to Yoon for his help in validating the simulation software and providing a benchmark

for comparison purposes. This helped ensure the resulting software is as accurate as possible given the complex nature of the supporting equations.

Eighth, my lab mates – Byungmoon Kim and Stathis Valenis. I cannot count the number of times these individuals explained to me the finer points of the various computer tools I learned while at Georgia Tech as well as helped me understand controls concepts so that I could apply these concepts to real systems.

Ninth, I would like to thank many of the administrative personnel at Georgia Tech that have made this a wonderful experience. Namely Vivian and Loretta in the School of Aerospace Engineering. Both these individuals were always there for help and were valuable assets during times of need in the strenuous graduate school environment.

More importantly, I would not have been able to complete this research effort without the relentless support, continuous sacrifice (for long hours everyday), and unconditional love of my tremendously wonderful wife Melissa. She even helped me handle last minute draft thesis printing problems, no small task. She is truly my better half!

Finally, I would like to thank the Lord our God for giving me the opportunity to further investigate the physical world of aircraft and satellites as well as complete my Master's of Science Degree at the internationally esteemed Georgia Institute of Technology.

SUMMARY

This work examines the simultaneous use of single-gimbal Variable Speed Control Moment Gyroscopes (VSCMGs) as spacecraft attitude control actuators and energy storage devices. The resulting theory is then used as the foundation for designing the VSCMG Workbench, a simulation tool designed to meet the Air Force Research Laboratory's need for a realistic/flexible computer simulation for conceptual analysis and hardware-in-the-loop testing. This tool allows both Georgia Tech and AFRL's Space Vehicles Directorate a low-cost alternative for analyzing the feasibility of employing a combined attitude control/energy storage system as well as the technical details to create such a system for different types of spacecraft. Its modularity permits adding more model fidelity in the future with little user training required.

ACRONYMS LIST

Symbol	Definition
AFRL	Air Force Research Laboratory
ADCS	Attitude Dynamics and Control System
PMAD	Power Management and Distribution System
IPACS	Integrated Power and Attitude Control System
FACETS	Flywheel Attitude Control, Energy Transmission and Storage System
NASA	National Aeronautics and Space Administration
ASTREX	Advanced Space Structures Technology Research Experiments
RWA/RWAs	Reaction Wheel Assembly/Assemblies
RW	Reaction Wheel
CMG/CMGs	Control Moment Gyroscope/Gyroscopes
VSCMG/VSCMGs	Variable Speed Control Moment Gyroscope/Gyroscopes
ACES	Attitude Control and Energy Storage
FESS	Flywheel Energy Storage System

DEFINITIONS AND NOMENCLATURE LIST

Bodies :

P $\triangleq$ spacecraft platform without VSCMGs

G $\triangleq$ gimbal structure

W $\triangleq$ wheel

Mass Center points :

P* $\triangleq$ center of spacecraft body without VSCMGs

G* $\triangleq$ center of VSCMG gimbal structure

W* $\triangleq$ center of VSCMG wheel (coincides with G* by assumption)

O $\triangleq$ combined system center of mass (assumed constant in frame $\mathcal{N}$ described below)

Coordinate Reference Frames :

$\mathcal{B} \triangleq$ ref frame that rotates with the spacecraft body and is centered at P*

$\mathcal{G} \triangleq$ ref frame that rotates with VSCMG about gimbal axis

$\mathcal{N} \triangleq$ inertial reference frame

$\mathcal{G}_0 \triangleq$ body fixed, VSCMG installation ref frame (note that $\mathcal{G}$ coincides with $\mathcal{G}_0$ at the initial time)

$\hat{g}_s, \hat{g}_t, \hat{g}_g$ = Unit vectors for VSCMG spin, transverse, and gimbal axes

g_s, g_t, g_g = VSCMG unit vecs expressed as components in $\mathcal{B}$

τ_r = torque required for stable regulation or tracking

$\boldsymbol{L}_{BN}$ = Transformation from $\mathcal{N}$ to $\mathcal{B} = \boldsymbol{L}_{NB}^T$

$\boldsymbol{L}_{RN}$ = Transformation from $\mathcal{N}$ to $\mathcal{R} = \boldsymbol{L}_{NR}^T$

$\boldsymbol{L}_{BR}$ = Transformation from $\mathcal{R}$ to $\mathcal{B} = \boldsymbol{L}_{RB}^T = \boldsymbol{L}_{BN}\boldsymbol{L}_{RN}^T$

β = column matrix of euler parameters representing rotation from $\mathcal{N}$ to $\mathcal{B}$

β_r = column matrix of euler parameters euler parameter representing rotation $\mathcal{N}$ to $\mathcal{R}$ where $\mathcal{R}$ is fixed to $\mathcal{N}$ in the regulation problem

ω = body angular velocity with respect to $\mathcal{N}$ written in $\mathcal{B}$ (in expanded notation this is written as $(\omega_{B/N})_B$)

ω_r = reference body angular velocity with respect to $\mathcal{N}$ written in $\mathcal{B}$ for regulation and $\mathcal{R}$ for tracking

$\dot{\omega} = \frac{d}{dt}\omega$

$\dot{\omega}_r = \frac{d}{dt}\omega_r$ (zero for the regulation case)

$\dot{\boldsymbol{L}}_{BN}$ = Inertial derivative of $\boldsymbol{L}_{BN} = \frac{d}{dt}\boldsymbol{L}_{BN}$

$\dot{\boldsymbol{L}}_{RN}$ = Inertial derivative of $\boldsymbol{L}_{RN} = \frac{d}{dt}\boldsymbol{L}_{RN}$

$\dot{\mathbf{R}}_{BR}$ = Inertial derivative of $\boldsymbol{L}_{BR} = \frac{d}{dt}\boldsymbol{L}_{BR}$

$\delta\beta$ = error euler paramter column matrix representing a transform from $\mathcal{B}$ to $\mathcal{R}$

$\delta\omega$ = angular velocity error

$\delta\omega = \omega - \boldsymbol{L}_{BR}\omega_r$

$\delta\dot{\omega}$ = inertial derivative of angular velocity error

$\delta\dot{\omega} = \dot{\omega} - \boldsymbol{L}_{BR}\dot{\omega}_r - \dot{\boldsymbol{L}}_{BR}\omega_r$

CHAPTER 1

INTRODUCTION

1.1 Overview

1.1.1 Problem Background

Space vehicle programs consistently seek to reduce satellite bus mass to increase payload capacity and/or reduce launch and fabrication costs. In addition, satellite system performance demands continually challenge space vehicle designers. Specifically, larger space structures require finer, more accurate three-axis attitude control methods. One of the most popular methods for this type of control is by employing gas jet thrusters to provide the necessary vehicle control torque. Unfortunately, as mentioned in reference [1], the plumes of such thrusters often impinge on critical vehicle components such as communications equipment, sensors, and subsystem actuators.

For this reason, internal vehicle three-axis control methods with lower mass are needed. Flywheel-based systems providing both energy storage and attitude control

address the need for combined energy storage and attitude control. In particular, the Air Force Research Laboratory (AFRL)'s Flywheel Attitude Control, Energy Transmission and Storage (FACETS) program will combine all or part of the energy storage, attitude control, and power management and distribution (PMAD) subsystems into a single system, significantly decreasing bus mass (and volume) by eliminating the need for conventional chemical batteries [2].

1.1.2 IPACS

An Integrated Power and Attitude Control System (IPACS) such as FACETS employs flywheels as "mechanical batteries" to perform the attitude control and energy storage functions. The IPACS concept eliminates vehicle mass while improving system performance and lifetime. The results of a recent Air Force trade study are reflected in figure 1.1. This figure shows the 45-50 percent cost savings such a system attains as it removes the typical satellite's most expensive subsystem, the batteries. Up until now, the well-documented IPACS concept was never implemented due to high flywheel spin rates (on the order of 40K to 80K RPM versus less than 5K RPM for conventional Control Moment Gyroscopes (CMGs) or momentum wheel actuators). At such high speeds, the actuators quickly wear out mechanical bearings. Additional challenges include flywheel material mass/durability and stiffness inadequacies. Recently, the advent of composite materials and magnetic bearing technology has enabled realistic IPACS development [2, 3].

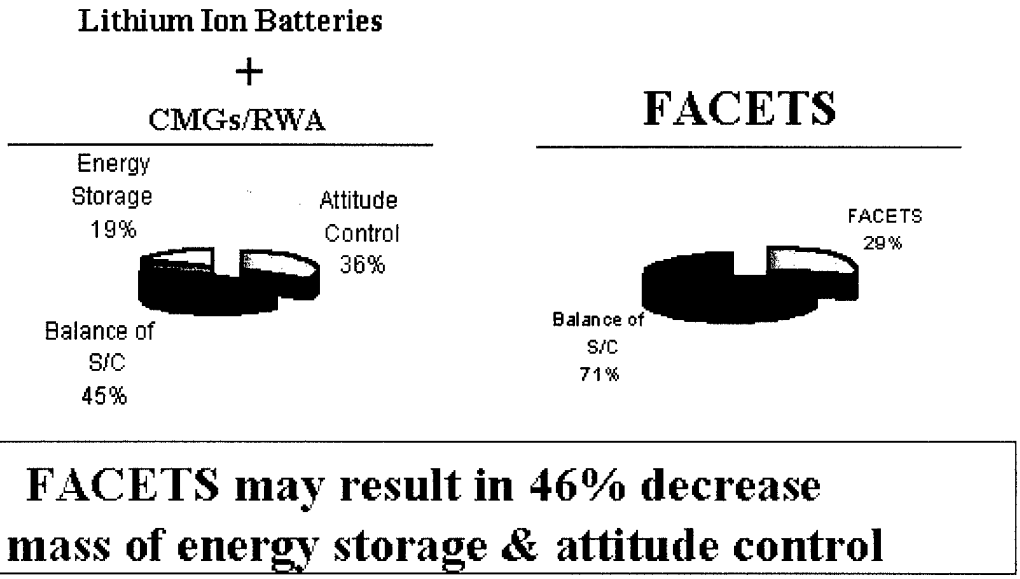

Figure 1.1: USAF Trade Study Results

1.1.3 Simultaneous Control Difficulty

The control problem of simultaneous energy storage and attitude control is far from trivial, even in its simplest conceivable form. While decoupling the attitude control and energy storage functions may be a workable solution, research in related areas suggests it may not be the best approach [2].

1.1.4 Momentum Wheel Concept

It has been shown in [4, 5] that simultaneous momentum management and power tracking can be accomplished with four or more wheels in reaction wheel (RW) mode. This is done by adjusting the wheel acceleration in the null subspace of the required attitude control torque dynamics matrix in such a way as to generate the required

vehicle power while not imparting adverse external torque on the spacecraft. Furthermore, this method was shown to be practical for tracking the required time history profiles for several types of satellites [3, 4].

1.1.5 AFRL's FACETS

AFRL's FACETS program intends to employ VSCMGs on the Advanced Space Structures Technology Research Experiments (ASTREX) test article (depicted in figure 1.2) using a concept similar to that for momentum wheels described in section 1.1.4. This test article rests on an air bearing and provides one of the best ground-based test environments for simulating on-orbit satellite motion. Tests using this structure produce results that are very close to that experienced by the real space vehicle. The ASTREX platform helps reduce satellite program costs since problems can be eliminated long before payloads are launched into orbit.

Figure 1.3 shows a CMG actuator configuration previously used on the ASTREX structure in the early 1990s. A similar configuration is planned for the new FACETS flywheel actuator installation. There are different kinds of actuators that could be used for an on-orbit IPACS. Figure D.2 shows a few of these along with each alternative's associated specifications.

1.2 Problem Statement

Simultaneous attitude and power tracking for a rigid spacecraft using Variable Speed Control Moment Gyroscopes (VSCMGs) is possible. This work examines the theoretical background governing the use of VSCMG actuators, presents a simulation software tool designed to investigate systems using these actuators, and analyzes the results of several simulation runs using this software tool for a simultaneous attitude control and energy storage system.

In this work, the exact nonlinear equations, never apparently derived in the literature, governing such an attitude control/energy storage system are derived and examined. The derivation is based on n VSCMGs, n being an arbitrary number. The resulting equations are independent of any particular actuator configuration. The explicit derivation enables direct application of the theory to an actual satellite system. The generality of the theory permits application to a wide variety of spacecraft missions. This creates flexibility for future space systems contemplating an IPACS using VSCMGs for attitude control and energy storage. In addition, the design of a SIMULINK-based software simulation tool for analyzing these types of spacecraft actuators, called the VSCMG Workbench, is presented. This software will be used by AFRL to analyze the application of simultaneous attitude control/energy storage to different satellite programs. Finally, results from several simulation runs using two different designed control algorithms for two different control cases – attitude regulation and attitude tracking – are presented. From these controller scenario tests as

well as overall system performance tests, the effects that several parameters have on the system are analyzed.

1.3 Research Outline

The structure of this document supports the goals just presented in section 1.2. In order to achieve these goals, one must investigate several aspects of the problem. These aspects are decomposed into 7 chapters with further supporting details contained in the Appendices.

Chapter 2 provides a review of the countless documents related to this topic. Much of this research directly builds on the work of others in further developing the theory, proposing a simulation analysis tool, and testing the results. Therefore, it is very important that one is able to put the past work into historical perspective. Chapter 2 aims to do just that.

Chapter 3 investigates the intricate details of the theory. This chapter is the backbone upon which the analytical results are based. It shows the nuts and bolts of the integration of previous results related to spacecraft attitude control and energy storage using VSCMGs.

Chapter 4 presents the VSCMG Workbench, a software simulation tool to analyze the application of simultaneous energy storage and attitude control for satellites. The generality and modularity of this tool renders it a robust computer platform that can be modified for countless satellite programs contemplating using the simultaneous

spacecraft energy storage and attitude control methodology presented.

Chapter 5 outlines the large battery of VSCMG Workbench simulation tests performed to gain system insight. This chapter centers only on the testing structure and not on the test result analysis.

Chapter 6 presents the results of running the battery of tests presented in chapter 5. These results illustrate several lessons learned about the example system and reflect the different parameter effects on the spacecraft system overall as well as in terms of its subsystems. This type of analysis allows users to see what they can learn by running the VSCMG Workbench and applying the concepts to a particular satellite and/or satellite mission.

Chapter 7 summarizes the different conclusions one can draw from this research. Thus, this chapter highlights the most important lessons learned during the research effort.

Finally, chapter 8 describes potential areas for further study. This research raises exciting questions about spacecraft systems employing simultaneous 3-axis attitude control and energy storage methods. Such further study will help researchers learn more about this interesting concept.

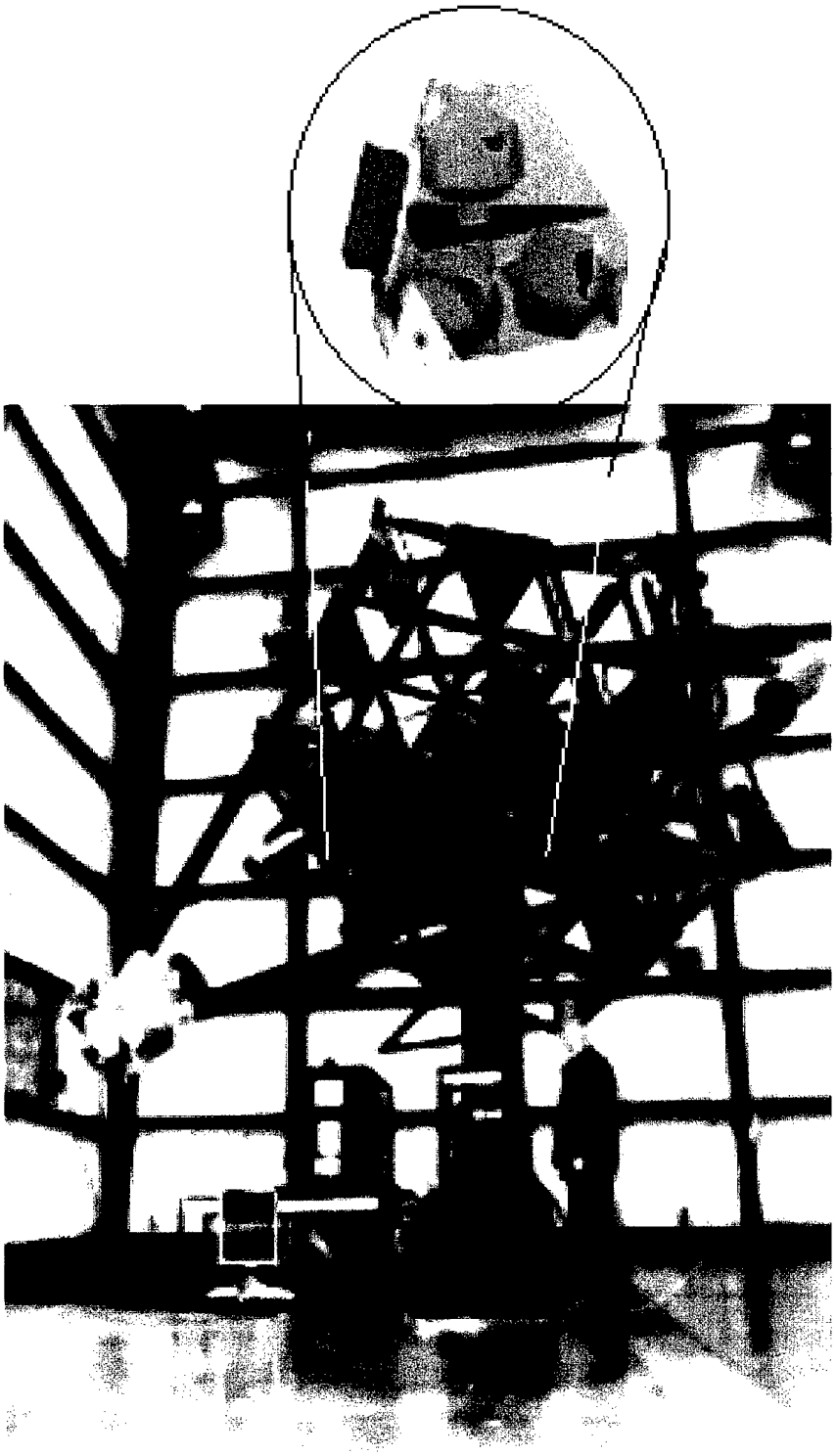

Figure 1.2: ASTREX Test Article

Figure 1.3: CMG Actuators

Attitude Control

CMGs for 2 transverse axes
RWA for polar axis

Honeywell M325S CMG
Nominal Torque: 440 N-m
Momentum: 440 N-m-s
Mass: 65.3 kg

Honeywell HR150 RWA
Nominal Torque: 1.62 N-m
Momentum: 203 N-m-s
Mass: 27.7 kg

Energy Storage

Nickel-Hydrogen or Lithium
Ion Battery

Lithium Ion Battery
Specific Energy: 110 W-h/kg
Depth of Discharge: 46%

Nickel-Hydrogen Battery
Specific Energy: 50 W-h/kg
Depth of Discharge: 56%

Combined Attitude Control & Energy Storage

FACETS
Nominal Torque: 580 N-m
Momentum: 5858 N-m-s
Specific Energy: 50 W-h/kg
Depth of Discharge: 82%

Figure 1.4: Actuator Alternatives

CHAPTER 2

LITERATURE REVIEW

Combined spacecraft attitude control and energy storage is a well-studied problem. In fact, the concept of using flywheel based actuators for energy storage and attitude control has been around since the 1960s [3]. This chapter will review the significant literature related to the problem of simultaneous attitude control/energy storage using VSCMGs. The relevant literature can be broken down into two parts: i) flywheels used for energy storage (terrestrially and in space) and ii) control moment gyroscopes for attitude control. Reference [3] gives an excellent overview of the pertinent literature on the former part and [6] remarkably summarizes the latter.

2.1 Flywheel Energy Storage

The roots of the concept of using flywheels to store energy came to light in the 1960s during investigation of high performance kinetic energy storage systems [3]. As Hall mentions in [3],"the use of flywheels instead of batteries to store energy on spacecraft was suggested as early as 1961 (by Roes), when a 17 W hr/kg composite

flywheel spinning at 10 to 20 thousand RPM on magnetic bearings was proposed. The configuration included two counter-rotating flywheels, and the author did not mention the possibility of using the momentum for attitude control." Meanwhile, the use of reaction wheels for large spacecraft precision pointing and attitude control has been around for well over 30 years [7, 8]. As Hall states, once the concept of using flywheels for energy storage arose, it only made sense that such flywheels could be combined as momentum wheels for attitude control and energy storage [3].

Energy storage flywheels rapidly increased in popularity during the late 1970s and early 1980s as a result of the "energy crisis" [9]. Several industries are now employing the use of such flywheels in some fashion (such as for industrial plants, energy efficient automobiles, and for use in uninterruptible Power Supplies (UPS)) [3]. A great conceptual review of flywheel energy storage as it applies to these different industries is given in references [10] and [11].

Research related to flywheel energy storage and its space applications contained in the literature can be further subdivided into three eras: 1970-1980, 1980-1990, and 1990-present. The ensuing sections will recount these eras.

2.1.1 Flywheel Energy Storage in the 1970s

As mentioned, the concept of attitude control and energy storage has been around for a while. Soon after the energy storage idea initially appeared in reference [12], the combined concept arose. There were three primary periods during which the

combined concept was intensively addressed. References [13, 14, 15, 16, 17] cover the first period of investigation (from 1970-1980), during which time Anderson and Keckler coined the term IPACS (Integrated Power and Attitude Control System) to describe such a system. At that time, NASA did some extensive concept feasibility studies and even held a few working groups on the topic in order to investigate potential uses for shuttle-age programs.

2.1.2 Flywheel Energy Storage in the 1980s

References [18, 19, 20, 21, 22, 23, 24, 25, 26, 27] encompass the second period of extensive combined attitude control and energy storage concept exploration in which a Combined Attitude Control and Energy Storage (CARES) system was investigated by the Charles Stark Draper Laboratory as well as investigation into an IPACS for the Space Station was continued by NASA.

The CARES system explored the technological issues related to mounting momentum exchange devices on magnetic bearings. Downer, Eisenhaure, *et al.* published several papers in the mid 1980s that presented the Draper Laboratory's flywheel energy storage and spacecraft attitude control system concept, magnetic suspension design, component specifications, and hardware issues [19, 20, 22]. This system applied magnetic bearing technology developed for the Department of Energy to a spacecraft attitude control problem [20]. As stated in [20], the resulting system provided "attitude control about the roll, pitch, and yaw axes." Reference [20] stated that

two axes were "controlled by utilizing the wheels as control moment gyros, while the third axis (was) controlled by utilizing the wheels as reaction wheels." Interestingly, the magnetic bearing of that system was "used as a 'gimbal' for a control moment gyro" [20].

Excellent summaries of the mid-1980s technological issues facing IPACS implementation were given by Simon and Van Tassel in [26] and by Oglevie and Eisenhaure in [23]. These sources describe the material, durability, and stiffness issues mentioned in chapter 1 along with flywheel magnetic suspension hurdles to implementation and the problem of motor, generator, and electronic technologies in the area of energy conversion. The latter of these references pointed out that "the energy transfer required (for rapidly slewing large satellites) is so large that it imposes very large peak torquing power requirements (many horsepower). The IPACS capability to store and deliver high peak power, and regeneratively brake the rapid slewing maneuver, is ideally suited to these applications" [23]. Olmstead looked at applying flywheel energy storage technology for attitude control using a counter-rotating flywheel concept [24]. Flatley examined the use of four flywheels as reaction wheels in a tetrahedron configuration and the associated voltage regulation problem presented when such a system is used for combined attitude control and energy storage [21]. Studer and Rodriguez provided some of the overarching design issues in implementing an Attitude Control and Energy Storage (ACES) system [27].

As is evident, many technological combined attitude control and energy stor-

age design issues arose and were investigated in the 1980s. Building on concepts introduced in the early 1970s, the research uncovered some of the important design barriers to IPACS implementation. This paved the way for re-examination of the problem in the 1990s.

2.1.3 Flywheel Energy Storage in the 1990s and beyond

The third period of study, addressed by references ([28, 3, 4]), comprises recent investigation due to the advance of enabling technologies mentioned in Chapter 1 such as flywheel durability and magnetic bearing technology. The investigation found in [4] includes a more detailed analysis of the exact, nonlinear equations of motion for flywheels used as momentum wheels. Also, reference [29] is a good source for the Air Force Research Laboratory's current application of flywheel energy storage.

Most of the present spacecraft energy storage research has been sponsored by two government sources, NASA (for future implementation on the International Space Station) and AFRL in its perpetual effort to make next generation spacecraft cheaper and lighter.

2.2 Control Moment Gyroscopes

Similar to flywheel energy storage, control moment gyroscopes have been well-studied over the last 30 years. This research can be broken into three areas: early concepts, on-orbit applications, and theoretical analysis. Each of these areas will be addressed.

In this research, we primarily concentrate on the use of the Single Gimbal CMG (SGCMG) as this device is much simpler than its counterpart, the Double Gimbal CMG (DGCMG).

2.2.1 Early Control Moment Gyroscope Concepts

The concept of using control moment gyroscopes for attitude control arose in the mid-1960s during the modern era of space exploration. One of the first sources that details the concepts, benefits, and potential configurations of CMGs for attitude control is given by Jacot and Liska in [30]. That document reflects a commonality found in several works in the CMG literature – the use of linearized equations of motion. This work shows that the beginning of the use of CMGs started through laboratory investigation of the system and stemmed from the fact that early spacecraft gyroscopic sensors imparted slight torques on a spacecraft during its operation [30]. Application of these devices on spacecraft has mainly been for large angle, three-axis satellite maneuvers due to the CMG's mass and power requirements.

2.2.2 On-Orbit Uses

There have been several large space vehicles that have employed CMG actuators since the 1960s. One spacecraft that used three orthogonally mounted DGCMGs was NASA's Skylab space station [8]. Also, the Russian Space Station MIR has employed six parallel mounted SGCMGs successfully. Third, the International Space Station

uses four parallel mounted DGCMGs, two of which are mounted anti-parallel to the other two. But as Wie states in [8], "control moment gyros have never been used in commercial satellites", perhaps due to the complex nature of these systems and the large satellites they prove cost effective for.

2.2.3 CMG Equations of Motion Analysis

Although the use of CMGs for attitude control concept was born in the 1960s, it was not until the work by Marguilies and Aubrun in 1979 [31] that the first real mathematical development of CMG theory arose. This work centered on the related geometry of using CMGs and introduced some of the properties of CMG singularities.

Oh and Vadali [32] seemed to be the first to seriously investigate the nonlinear CMG equations of motion. References [33, 34, 35, 36] further present the singularity problems that arise from the use of Control Moment Gyroscopes in many applications.

2.2.4 Variable Speed Control Moment Gyroscopes

The first realistic study of combining the two functions of reaction wheel/momentum wheels and control moment gyroscopes was presented by Ford and Hall in [6, 37]. However, as Schaub points out in [38], Ford and Hall stop short of investigating the simultaneous use of reaction wheels and control moment gyroscopes. For this reason, Schaub, Junkins, and Vadali proposed the use of Variable Speed Control Moment Gyroscopes in [38, 39, 40] to help avoid unfavorable classical CMG singularites as

well as develop the governing nonlinear equations of motion associated with this type of system. The research by Schaub et. al. even goes to the point of analyzing the use of null motion by VSCMGs in order to reorient a spacecraft to take advantage of more robust preferred gimbal angle configurations.

2.2.5 The Present Research: VSCMGs for Energy Storage and Attitude Control

The only apparent suggestion of using Variable Speed Control Moment Gyroscopes for combined attitude control and energy storage was made in 1985 by O'Dea et. al. in [22] The authors in that reference mentioned gimballing the motor and used the term "variable-speed" CMGs while proposing that this concept was "promising" but stopped short of developing the governing the nonlinear equations of motion. This left the door open for research into combined attitude control and energy storage using Variable-Speed Control Moment Gyroscopes.

In summary, the present research combines the previous results of other investigations and applies it via simulation to a realistic satellite system. Some of the initial theoretical results of this research are published in [2] as well as in an upcoming American Control Conference paper by Richie, Tsiotras, and Fausz [41]. Although documentation in the literature is very abundant for each of these topics separately (flywheel energy storage, control moment gyroscopes, and variable-speed control moment gyroscopes), the present research combines them into a more general result.

The theoretical results of this study are further presented in the next chapter.

CHAPTER 3

THEORETICAL BACKGROUND

Next, the theory behind a VSCMG-actuated spacecraft attitude control/energy storage system will be discussed.

3.1 Preliminaries

It is necessary to present some key definitions and mathematical relations that will be useful in the subsequent sections so that one can best understand the theory.

3.1.1 Notation

Matrices are presented in bold as in $\boldsymbol{A}$, vectors are presented with an arrow as in $\vec{x}$, and vector components with respect to a particular basis (essentially used as $n \times 1$ column matrices) are denoted in italics as in x. The derivative of a vector $\vec{x}$ with respect to the inertial reference frame is denoted by

$$\frac{^N d}{dt}(\vec{x}) \equiv \dot{\vec{x}} \tag{3.1}$$

For convenience, in representing vector cross products, define the skew symmetric matrix $\tilde{\boldsymbol{x}} \in \mathbb{R}^{3\times 3}$, for $x \in \mathbb{R}^3$, which allows one represent $\vec{x} \times \vec{y} = \tilde{\boldsymbol{x}} y$ in terms of a column matrix of its components in the same basis as that in which the components of are represented in x and y. Thus the components of $\vec{x} \times \vec{y}$ are written as $\tilde{bx}$ where

$$\tilde{\boldsymbol{x}} = \begin{bmatrix} 0 & -x_3 & x_2 \\ x_3 & 0 & -x_1 \\ -x_2 & x_1 & 0 \end{bmatrix} \tag{3.2}$$

The $\otimes$ operator represents the Kronecker product of two matrices. For any two matrices $A \in \mathbb{R}^{n\times m}$ and $B \in \mathbb{R}^{p\times q}$ the matrix $A \otimes B$ is the $\mathbb{R}^{mp\times nq}$ matrix given by

$$A \otimes B = \begin{bmatrix} a_{11}B & a_{12}B & \cdots & a_{1n}B \\ a_{21}B & a_{22}B & \cdots & a_{2n}B \\ \vdots & \vdots & & \vdots \\ a_{m1}B & a_{m2}B & \cdots & a_{mn}B \end{bmatrix}$$

3.1.2 Assumptions and Definitions

Now, one can make several key assumptions throughout the derivation of the system model. These assumptions will be identified individually in the text as they become appropriate. For the development of the equations of motion, one should consider a system consisting of a rigid spacecraft with body-fixed reference frame, $\mathcal{B}$, which includes an array of n rigid VSCMGs with reference frames fixed to each of the VSCMG gimbals, $\mathcal{G}_1, \mathcal{G}_2, \ldots, \mathcal{G}_n$. Figure 3.1 (taken from [40]) illustrates the $\mathcal{G}$ frame for one VSCMG. As shown in Fig. 3.1, the frames attached to the n VSCMGs, $\mathcal{G}_j$,

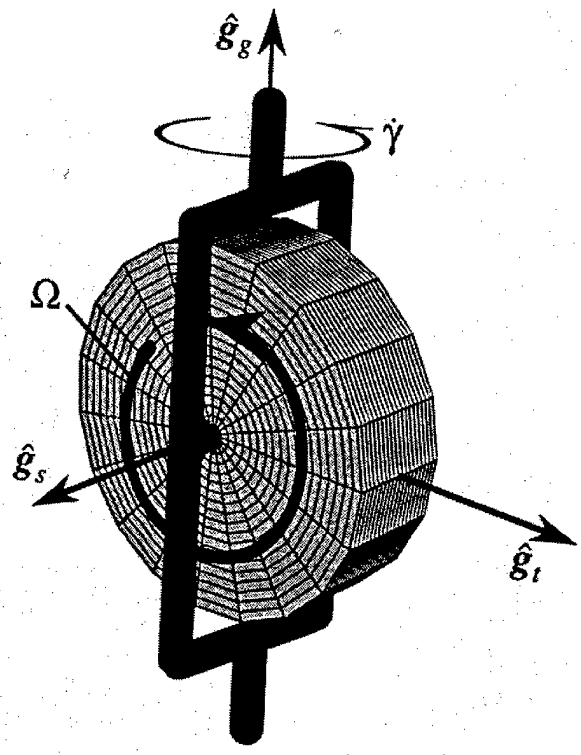

Figure 3.1: Variable Speed Control Moment Gyro

$j = 1, ..., n$, are characterized by an orthogonal set of unit vectors, $\hat{g}_{sj}$, $\hat{g}_{tj}$, and $\hat{g}_{gj}$, $j = 1, ..., n$, where the subscripts s, t, and g denote the spin, transverse and gimbal axes, respectively, satisfying the relation

$$\hat{g}_{gj} \times \hat{g}_{sj} = \hat{g}_{tj} \tag{3.3}$$

The matrix $\boldsymbol{L}_{BGj} \in \mathbb{R}^{3\times3}$ is the rotation matrix transforming vectors expressed as components in reference frame $\mathcal{G}_j$ to frame $\mathcal{B}$ and conversely, $\boldsymbol{L}_{GjB} = \boldsymbol{L}_{BGj}^T$ is the rotation matrix from $\mathcal{B}$ to $\mathcal{G}_j$. Conveniently, the matrix $\boldsymbol{L}_{BGj} \in \mathbb{R}^{3\times3}$ can be defined

as

$$\boldsymbol{L}_{BGj} = [g_{sj}\ g_{tj}\ g_{gj}] \tag{3.4}$$

where the column matrices g_{sj}, g_{tj}, and g_{gj} contain the components of the unit vectors $\hat{g}_{sj}$, $\hat{g}_{tj}$, and $\hat{g}_{gj}$ expressed in $\mathcal{B}$.

Next, let $\Omega \in \mathbb{R}^n$ be the column matrix that contains the wheel rotational speeds of the n VSCMGs, Ω_j, $j = 1, \ldots, n$, and let $\gamma \in \mathbb{R}^n$ be the column matrix that contains the gimbal angles of the n VSCMGs, γ_j, $j = 1, \ldots, n$. Then, $\dot{\Omega} \in \mathbb{R}^n$, $\dot{\gamma} \in \mathbb{R}^n$, and $\ddot{\gamma} \in \mathbb{R}^n$ are defined similarly.

To simplify the presentation of the results, one first defines $\boldsymbol{G}_s \in \mathbb{R}^{3\times n}$ as a matrix whose columns are measure numbers of $\hat{g}_{sj}$ in the $\mathcal{B}$ basis, so that

$$\boldsymbol{G}_s = [g_{s1} \cdots g_{sn}] \tag{3.5}$$

and then defines $\boldsymbol{G}_t$ and $\boldsymbol{G}_g$ similarly for the transverse and gimbal axis unit vectors, respectively. One must also define the matrix $\boldsymbol{G}_{sd} \in \mathbb{R}^{3n\times n}$ such that

$$\boldsymbol{G}_{sd} = \text{diag}\ [g_{s1}, g_{s2}, \ldots, g_{sn}] \tag{3.6}$$

and similarly for $\boldsymbol{G}_{td}$ and $\boldsymbol{G}_{gd}$.

Next, it will be convenient that one define several matrices involving the inertia properties of the VSCMGs. The inertia values of each VSCMG is decomposed into the contributions of the wheel and the gimbal structure using the scalar variables $I_{W_{sj}}$, $I_{W_{tj}}$, $I_{W_{gj}}$, $I_{G_{sj}}$, $I_{G_{tj}}$, and $I_{G_{gj}}$, $j = 1, \ldots, n$, where the subscripts W and G denote the wheel and gimbal structure contributions along the s, t, and g axes, respectively. It

should be noted that the assumption is made (as is done in [39]) that all VSCMGs are perfectly balanced and aligned so that the unit vectors $\hat{g}_{sj}$, $\hat{g}_{tj}$, and $\hat{g}_{gj}$, $j = 1, \ldots, n$, represent principal directions for the VSCMG reference frames.

Now, the reader can define the following inertia matrices:

$$\begin{aligned} \boldsymbol{I}_{G_j} &= \text{diag}\left[I_{G_{sj}}, I_{G_{tj}}, I_{G_{gj}}\right] \\ \boldsymbol{I}_{G_s} &= \left[I_{G_{s1}} I_{G_{s2}} \cdots I_{G_{sn}}\right] \\ \boldsymbol{I}_{G_{sd}} &= \text{diag}\left[\boldsymbol{I}_{G_s}\right] \\ \boldsymbol{I}_{G_{sm}} &= \boldsymbol{I}_{G_{sd}} \otimes \boldsymbol{I}_3 \end{aligned} \tag{3.7}$$

where $\boldsymbol{I}_{G_j} \in \mathbb{R}^3$, $\boldsymbol{I}_{G_s} \in \mathbb{R}^{1\times n}$, $\boldsymbol{I}_{G_{sd}} \in \mathbb{R}^{n\times n}$, and $\boldsymbol{I}_{G_{sm}} \in \mathbb{R}^{3n\times 3n}$. Similarly, one can define matrices for the other gimbal structure inertias: $\boldsymbol{I}_{G_t} \in \mathbb{R}^{1\times n}$, $\boldsymbol{I}_{G_g} \in \mathbb{R}^{1\times n}$, $\boldsymbol{I}_{G_{td}} \in \mathbb{R}^{n\times n}$, $\boldsymbol{I}_{G_{gd}} \in \mathbb{R}^{n\times n}$, $\boldsymbol{I}_{G_{tm}} \in \mathbb{R}^{n\times n}$, and $\boldsymbol{I}_{G_{gm}} \in \mathbb{R}^{n\times n}$; as well as for the wheel inertias: $\boldsymbol{I}_{W_j} \in \mathbb{R}^3$, $\boldsymbol{I}_{W_s} \in \mathbb{R}^{1\times n}$, $\boldsymbol{I}_{W_t} \in \mathbb{R}^{1\times n}$, $\boldsymbol{I}_{W_g} \in \mathbb{R}^{1\times n}$, $\boldsymbol{I}_{W_{sd}} \in \mathbb{R}^{n\times n}$, $\boldsymbol{I}_{W_{td}} \in \mathbb{R}^{n\times n}$, $\boldsymbol{I}_{W_{gd}} \in \mathbb{R}^{n\times n}$, $\boldsymbol{I}_{W_{sm}} \in \mathbb{R}^{3n\times 3n}$, $\boldsymbol{I}_{W_{tm}} \in \mathbb{R}^{3n\times 3n}$, and $\boldsymbol{I}_{W_{gm}} \in \mathbb{R}^{3n\times 3n}$; and that $\boldsymbol{I}_3$ is the 3×3 identity matrix.

At times it is convenient to combine the inertia contributions of the wheel and gimbal structure, so define $\boldsymbol{J}_j \in \mathbb{R}^{3\times 3}$, $\boldsymbol{J}_s \in \mathbb{R}^{1\times n}$, $\boldsymbol{J}_{sm} \in \mathbb{R}^{3n\times 3n}$, and $\boldsymbol{J}_{sb} \in \mathbb{R}^{3\times 3n}$

such that

$$\begin{aligned} \boldsymbol{J}_j &= \boldsymbol{I}_{G_j} + \boldsymbol{I}_{W_j} \\ \boldsymbol{J}_s &= \boldsymbol{I}_{G_s} + \boldsymbol{I}_{W_s} \\ \boldsymbol{J}_{sm} &= \boldsymbol{I}_{G_{sm}} + \boldsymbol{I}_{W_{sm}} \\ \boldsymbol{J}_{sb} &= \boldsymbol{J}_s \otimes \boldsymbol{I}_3 \end{aligned}$$

and similarly for $\boldsymbol{J}_t \in \mathbb{R}^{1\times n}$, $\boldsymbol{J}_g \in \mathbb{R}^{1\times n}$, $\boldsymbol{J}_{tm} \in \mathbb{R}^{3n\times 3n}$, $\boldsymbol{J}_{gm} \in \mathbb{R}^{3n\times 3n}$, $\boldsymbol{J}_{tb} \in \mathbb{R}^{3\times 3n}$, and $\boldsymbol{J}_{gb} \in \mathbb{R}^{3\times 3n}$. Finally, one defines matrices $\boldsymbol{\Omega}_d \in \mathbb{R}^{n\times n}$ and $\boldsymbol{\omega}_d \in \mathbb{R}^{3n\times n}$ such that

$$\boldsymbol{\omega}_d = \text{diag } [\omega, \omega, \ldots, \omega] = \boldsymbol{I}_n \otimes \omega \tag{3.8}$$

$$\boldsymbol{\Omega}_d = \text{diag } [\Omega_1, \Omega_2, \ldots, \Omega_n] \tag{3.9}$$

where the spacecraft body angular velocity vector $\omega \in \mathbb{R}^3$ is repeated n times in the definition of $\boldsymbol{\omega}_d$.

3.2 Dynamics

In this section the spacecraft dynamic system model extending the results of Oh and Vadali [32] to the case of VSCMGs is presented. More details of this derivation can be found in Appendix A. The equations of motion are derived using Euler's equation [42]

$$\vec{\tau}^{\text{sys}/O} = \frac{^N d}{dt}\left(\vec{h}^{\text{sys}/O}\right) \tag{3.10}$$

where $\vec{h}^{sys/O}$ is the total angular momentum of the spacecraft and the VSCMG cluster about the combined system center of mass (point O), given by

$$\vec{h}^{sys/O} = \vec{h}^{P/P^*} + \vec{h}^{P^*/O} + \vec{h}^{W/W^*}$$
$$+\vec{h}^{W^*/O} + \vec{h}^{G/G^*} + \vec{h}^{G^*/O} \tag{3.11}$$

and $\vec{\tau}^{sys/O}$ is the sum of the moments of all external forces about point O and of all external torques on the spacecraft. $\vec{h}^{P/P^*}$ is the angular momentum of the spacecraft platform (without the VSCMGs installed) about its own center of mass P^*. Similarly, $\vec{h}^{G/G^*}$ is the sum of the n-VSCMG gimbal structure angular momenta about each gimbal structure's center of mass, G_j^*, and $\vec{h}^{W/W^*}$ is the sum of n-VSCMG wheel angular momenta about each wheel's center of mass, W_j^*, respectively. For the remainder of this thesis, it is assumed that the points G_j^* and W_j^* coincide for each VSCMG. Additionally, $\vec{h}^{P^*/O}$ is the angular momentum of the center of mass of the platform (located at P^*) with respect to point O, $\vec{h}^{W^*/O}$ is the sum total of each wheel's center of mass angular momentum (located at point G_j^*) with respect to point O , and $\vec{h}^{G^*/O}$ is the sum total of each gimbal structure's center of mass angular momentum (located at point G_j^*) with respect to point O.

Let τ be $\vec{\tau}^{sys/O}$ expressed in $\mathcal{B}$. Then, the system dynamic equations of motion, derived in Appendix A and simplified in Appendix B, may be expressed as [32]

$$\tau = \boldsymbol{I}_T\dot{\omega} + \tilde{\boldsymbol{\omega}}\boldsymbol{I}_T\omega + \boldsymbol{B}\ddot{\gamma} + \boldsymbol{D}_s\dot{\gamma} + \boldsymbol{E}\dot{\Omega} + \boldsymbol{F}\Omega \tag{3.12}$$

where ω is the angular velocity vector of the spacecraft body with respect to frame $\mathcal{N}$

expressed in frame $\mathcal{B}$, τ is as defined above, and $\boldsymbol{I}_T$ is the *total* inertia matrix given by

$$\boldsymbol{I}_T = \boldsymbol{I}_{sc} + \sum_{j=1}^{N} \boldsymbol{L}_{BGj} \boldsymbol{J}_j \boldsymbol{L}_{BGj}^T \tag{3.13}$$

$\boldsymbol{I}_{sc}$ is the spacecraft platform inertia about point O matrix plus the total point mass inertia matrix of the $n-$ VSCMGs. The total VSCMG point mass inertia matrix can be further subdivided into the total wheel point mass inertia matrix and the total gimbal structure point mass inertia matrix. The total wheel point mass inertia matrix is the matrix obtained by summing the individual wheel point mass inertia matrices. Each wheel point mass inertia matrix represents the inertia about point O of a particle located at W_j^* that contains the entire mass of that wheel. The gimbal structure point mass inertia matrix is defined identically to that of its wheel counterpart. This is expressed mathematically as:

$$\boldsymbol{I}_{sc} = \boldsymbol{I}^{\mathrm{P/O}} + \boldsymbol{I}^{\mathrm{G^*/O}} + \boldsymbol{I}^{\mathrm{W^*/O}} \tag{3.14}$$

Note that the summation term in (3.13) is the time varying portion of the total inertia that changes as the VSCMGs move on the spacecraft. In addition, the coefficient matrices in (3.12) are given by

$$\boldsymbol{B} = \boldsymbol{G}_g \left(\boldsymbol{I}_{Ggd} + \boldsymbol{I}_{Wgd} \right) \tag{3.15}$$

$$\boldsymbol{D}_s(\omega, \Omega, \gamma) = \boldsymbol{D}_1 + \boldsymbol{D}_2 + \boldsymbol{D}_3 \tag{3.16}$$

$$\boldsymbol{E}(\gamma) = \boldsymbol{G}_s \boldsymbol{I}_{Wsd} \tag{3.17}$$

$$\boldsymbol{F}(\omega, \gamma) = \tilde{\boldsymbol{\omega}} \boldsymbol{G}_s \boldsymbol{I}_{Wsd} \tag{3.18}$$

where

$$\begin{aligned} \boldsymbol{D}_1(\omega,\Omega,\gamma) &= \left(\boldsymbol{G}_t\,\boldsymbol{G}_{sd}^T\,\boldsymbol{I}_{W_{sm}} - \boldsymbol{G}_s\,\boldsymbol{G}_{td}^T\,\boldsymbol{I}_{W_{tm}}\right)\boldsymbol{\omega}_d \\ &\quad + \boldsymbol{G}_t\,\boldsymbol{I}_{W_{sd}}\,\boldsymbol{\Omega}_d \end{aligned} \tag{3.19}$$

$$\boldsymbol{D}_2(\omega) = \tilde{\boldsymbol{\omega}}\boldsymbol{G}_g\boldsymbol{J}_{gd} \tag{3.20}$$

$$\begin{aligned} \boldsymbol{D}_3(\omega,\gamma) &= [(\boldsymbol{G}_t\boldsymbol{G}_{sd}^T\boldsymbol{I}_{G_{sm}} - \boldsymbol{G}_s\boldsymbol{G}_{td}^T\boldsymbol{I}_{G_{tm}}) \\ &\quad -(\boldsymbol{G}_t\boldsymbol{G}_{sd}^T\boldsymbol{J}_{tm} - \boldsymbol{G}_s\boldsymbol{G}_{td}^T\boldsymbol{J}_{sm})]\boldsymbol{\omega}_d \end{aligned} \tag{3.21}$$

3.3 Kinematics

One can represent the spacecraft orientation using Euler parameters corresponding to the transformation from the inertial reference frame, $\mathcal{N}$, to the vehicle body frame, $\mathcal{B}$, as:

$$\beta \triangleq \begin{bmatrix} \beta_0 \\ \beta_1 \\ \beta_2 \\ \beta_3 \end{bmatrix} \tag{3.22}$$

Defining the operator $\boldsymbol{Q}(\beta)$ as:

$$\boldsymbol{Q}\left(\beta\right) \triangleq \begin{bmatrix} -\beta_1 & -\beta_2 & -\beta_3 \\ \beta_0 & -\beta_3 & \beta_2 \\ \beta_3 & \beta_0 & -\beta_1 \\ -\beta_2 & \beta_1 & \beta_0 \end{bmatrix} \tag{3.23}$$

then the spacecraft's kinematic differential equation is:

$$\dot{\beta} \triangleq \frac{1}{2}\boldsymbol{Q}(\beta)\,\omega \tag{3.24}$$

Equations (3.12) and (3.24) together allow for the simulation of the spacecraft's motion.

3.4 Attitude Stability

In this section a control law for attitude tracking using VSCMGs is developed. Note that supplemental details of this derivation are contained in Appendix **??**. One begins by deriving a Lyapunov based steering control law as developed in [32] and then formulates the power tracking control in a somewhat analogous manner to that done for RWs in [3, 5].

As in [32], a positive definite Lyapunov function is defined in terms of the attitude errors $\beta - \beta_r$ and $\omega - \omega_r$ as follows

$$V = k(\beta - \beta_r)^T(\beta - \beta_r) + \tfrac{1}{2}(\omega - \omega_r)^T \boldsymbol{I}_T(\omega - \omega_r) \tag{3.25}$$

where β_r and ω_r are the desired vehicle reference attitude and reference angular velocity, respectively. The derivative of the Lyapunov function can be expressed as

$$\begin{aligned} \dot{V} &= -(\omega - \omega_r)^T \left[\, k\boldsymbol{Q}^T(\beta)\beta_r - \boldsymbol{I}_T(\dot{\omega} - \dot{\omega}_r) \right. \\ &- \left. \tfrac{1}{2}\dot{\boldsymbol{I}}_T(\omega - \omega_r) \,\right] \end{aligned} \tag{3.26}$$

It is evident that $\dot{V}$ can be made non-positive if one sets

$$\left[k\boldsymbol{Q}^T(\beta)\beta_r - \boldsymbol{I}_T\left(\dot{\omega} - \dot{\omega}_r\right) - \tfrac{1}{2}\dot{\boldsymbol{I}}_T\left(\omega - \omega_r\right) \right] \;=\; \boldsymbol{K}\left(\omega - \omega_r\right) \tag{3.27}$$

where $\boldsymbol{K}$ is a positive definite gain matrix. Since $\dot{V}$ is non-negative definite, the resulting system is Lyapunov stable. It can be shown that $\dot{V}$ is zero if and only if $\omega = \omega_r$ and $\beta = \beta_r$. By LaSalle's theorem, one can show that the system trajectories are stabilized about the desired reference attitude. In addition, due to the radial unboundedness of V, the resulting system is actually globally asymptotically stable.

Next, notice that the term $\frac{1}{2}\dot{\boldsymbol{I}}_T(\omega - \omega_r)$ is a linear function of $\dot{\gamma}$. Hence, one can decompose this term as follows

$$\boldsymbol{R}\dot{\gamma} = \tfrac{1}{2}\dot{\boldsymbol{I}}_T(\omega - \omega_r) \tag{3.28}$$

where the term $\boldsymbol{R}$ is given by

$$\boldsymbol{R} = \tfrac{1}{2}\left(\boldsymbol{J}_{sb} - \boldsymbol{J}_{tb}\right)\left(\boldsymbol{G}_{sd}\boldsymbol{G}_{td}^T + \boldsymbol{G}_{td}\boldsymbol{G}_{sd}^T\right)\left(\boldsymbol{\omega}_{rd} - \boldsymbol{\omega}_d\right) \tag{3.29}$$

If a matrix $\boldsymbol{D}$ is defined such that

$$\boldsymbol{D} = \boldsymbol{D}_s + \boldsymbol{R} \tag{3.30}$$

then one can combine (3.12), (3.26), (3.27), (3.29), and (3.30) to yield the condition

$$\boldsymbol{B}\ddot{\gamma} + \boldsymbol{E}\dot{\Omega} + \boldsymbol{D}\dot{\gamma} + \boldsymbol{F}\Omega =$$

$$\boldsymbol{K}(\omega - \omega_r) - k\boldsymbol{Q}^T(\beta)\beta_r - \boldsymbol{I}_T\dot{\omega}_r - \tilde{\boldsymbol{\omega}}\boldsymbol{I}_T\omega + \tau_d \tag{3.31}$$

where τ_d represents a disturbance torque on the vehicle.

3.4.1 Required Torque for Attitude Tracking

Next, if one defines a column matrix containing the measure numbers of the required torque vector, $\tau_r \in \mathbb{R}^3$ as

$$\tau_r = \boldsymbol{K}(\omega - \omega_r) - k\boldsymbol{Q}^T(\beta)\beta_r - \boldsymbol{I}_T\dot{\omega}_r - \tilde{\boldsymbol{\omega}}\boldsymbol{I}_T\omega \tag{3.32}$$

then (3.31) can be written as

$$\boldsymbol{B}\ddot{\gamma} + \boldsymbol{E}\dot{\Omega} + \boldsymbol{F}\Omega + \boldsymbol{D}\dot{\gamma} = \tau_r + \tau_d \tag{3.33}$$

which expresses the torque required for tracking in terms of the physical parameters (or states) of the system.

As shown in [39] if one assumes that the gimbal accelerations are small, then the required torque equation can be rearranged in terms of gimbal rate and wheel acceleration, which represents the parameters typically controlled by commercial CMGs and RWs, respectively. The resulting steering law (known as the velocity steering law) is thus

$$\boldsymbol{E}\dot{\Omega} + \boldsymbol{D}\dot{\gamma} = \tau_r - \boldsymbol{F}\Omega \tag{3.34}$$

3.4.2 Alternative Control Law

An alternative control law to that given by equations (3.33) and (3.32) is derived in Appendix . This control law is more intuitive in the case of attitude tracking. The resulting control law is by first defining the required torque and then using this

required torque in equation (3.33). The required torque in this case is

$$\tau_R = \boldsymbol{K}\omega - \boldsymbol{K}\boldsymbol{L}_{BR}\omega_r - \tilde{\omega}\boldsymbol{I}_T\omega - \boldsymbol{I}_T\boldsymbol{L}_{BR}\dot{\omega}_r + \boldsymbol{I}_T\tilde{\omega}\boldsymbol{L}_{BR}\omega_r - k\begin{bmatrix}\delta\beta_1\\ \delta\beta_2\\ \delta\beta_3\end{bmatrix} \tag{3.35}$$

where $\delta\beta$ is a column matrix of errors in $\beta_j, j = 0, 1, 2, 3$ and describes a transformation between the vehicle body reference frame, $\mathcal{B}$, and the desired vehicle reference frame $\mathcal{R}$ and ω_r is the angular velocity of the desired vehicle orientation (it can be thought of as a virtual rotating spacecraft body [4]) with respect to inertial space (i.e. frame $\mathcal{N}$).

For the remainder of this report, the control law described in the pair of equations (3.33) and (3.32) will be referred to as controller I; and, likewise, the control law described by equations (3.33) and (3.35) will be termed controller II.

3.4.3 Gimbal Acceleration Control

The main advantage of a single-gimbal CMG is its torque amplification property [30]. In order to take advantage of this property, one needs to provide a velocity command $\dot{\gamma}$ to the CMG (and keep $\ddot{\gamma}$ small). In fact, most standard CMG actuators are controlled via gimbal rate and *not* gimbal acceleration. Solving for $\ddot{\gamma}$ directly from (3.33) will require large gimbal acceleration commands and hence, large gimbal motor torques. Alternatively, the analyst can choose a velocity command $\dot{\gamma}$ from (3.34) and then implement this velocity steering law via an outer control loop that will keep the

actual $\dot{\gamma}$ close to the desired gimbal rates. This yields the following equation for the gimbal acceleration command (assuming the desired gimbal acceleration, $\ddot{\gamma}_d$, is negligible):

$$\ddot{\gamma} = \lambda \left(\dot{\gamma}_d - \dot{\gamma} \right), \quad \lambda > 0 \tag{3.36}$$

3.5 Power Tracking

The kinetic energy T_j of the jth actuator is given by:

$$T_{Wj} = \tfrac{1}{2} \omega_{Wj}^T \boldsymbol{I}_{Wj} \omega_{Wj} \tag{3.37}$$

where ω_{Wj} represents the angular velocity of the wheels with respect to the gimbal structure written in $\mathcal{G}_j$ components. This can be re-written as:

$$\omega_{Wj} = \begin{bmatrix} \Omega_j \\ 0 \\ 0 \end{bmatrix} \tag{3.38}$$

Next, note that for n actuators, the total energy is just the sum of each of the individual actuator energies

$$T_W = \sum_{j=1}^{n} T_{Wj} \tag{3.39}$$

As alluded to earlier, taking the first derivative of the energy yields the power generated by the wheels

$$P_W = \Omega^T \boldsymbol{I}_{W_{sd}} \dot{\Omega} \tag{3.40}$$

3.6 Simultaneous Attitude and Power Tracking

The available control inputs are the rate of change of the wheel speeds and the angular velocity of the gimbals (for the case of gimbal velocity steering law). Hence,

$$\dot{\Omega} = u_{\text{mw}} \tag{3.41}$$

$$\dot{\gamma} = u_{\text{cmg}} \tag{3.42}$$

where $u_{\text{mw}} \in \mathbb{R}^n$ and $u_{\text{cmg}} \in \mathbb{R}^n$ are the control inputs in the "momentum wheel" and "CMG" modes, respectively. Let the combined control input $u = [u_{\text{mw}}^T \; u_{\text{cmg}}^T]^T$. Then after some algebraic manipulation one can write

$$\begin{bmatrix} \boldsymbol{C}_{11} & \boldsymbol{C}_{12} \\ \boldsymbol{C}_{21} & \boldsymbol{C}_{22} \end{bmatrix} u = \begin{bmatrix} F_{pv} \\ P_{fv} \end{bmatrix} \tag{3.43}$$

where

$$\boldsymbol{C}_{11} = \boldsymbol{E}, \quad \boldsymbol{C}_{12} = \boldsymbol{D} \tag{3.44}$$

$$\boldsymbol{C}_{21} = \Omega^T \boldsymbol{I}_{W_{sd}}, \quad \boldsymbol{C}_{22} = 0_N \tag{3.45}$$

Furthermore,

$$F_{pv} = \tau_r - \boldsymbol{F}\Omega \qquad \text{and} \qquad P_{fv} = P_W \tag{3.46}$$

where F_{pv} is as defined in (3.34) and P_{fv} is defined in (3.40). This system of equations is similar to the velocity steering laws defined in the literature [32, 40], which involve solving for $\dot{\gamma}$.

Defining $\boldsymbol{C}_1 \equiv [\boldsymbol{C}_{11}\ \boldsymbol{C}_{12}]$ and $\boldsymbol{C}_2 \equiv [\boldsymbol{C}_{21}\ \boldsymbol{C}_{22}]$, the equation for F_{pv} from (3.43) can be written as

$$\boldsymbol{C}_1 u = F_{pv} \tag{3.47}$$

The general solution to (3.47) is given by

$$u = \boldsymbol{C}_1^{\dagger} P_{fv} + u_n \tag{3.48}$$

where the symbol † denotes the suitable generalized inverse, and $\boldsymbol{C}_1 u_n = 0$ (i.e., u_n is in the null space of $\boldsymbol{C}_1$, $\mathcal{N}(\boldsymbol{C}_1)$). Now substitute (3.48) into the equation for P_{fv} from (3.43) so that

$$\boldsymbol{C}_2 u = \boldsymbol{C}_2(\boldsymbol{C}_1^{\dagger} F_{pv} + u_n) = P_{fv} \tag{3.49}$$

and

$$\boldsymbol{C}_2 u_n = P_m \tag{3.50}$$

where $P_m = P_{fv} - \boldsymbol{C}_2 \boldsymbol{C}_1^{\dagger} F_{pv}$. Since $u_n \in \mathcal{N}(\boldsymbol{C}_1)$, one can find a vector ν such that

$$u_n = \boldsymbol{P}_N \nu \tag{3.51}$$

where $\boldsymbol{P}_N = \mathbf{I}_n - \boldsymbol{C}_1^{\dagger} \boldsymbol{C}_1$ is the orthogonal projection onto $\mathcal{N}(\boldsymbol{C}_1)$. Then, from (3.50) and (3.51), and making use of the fact that $\boldsymbol{P}_N$ is a projection matrix, one can see u_n is chosen such that

$$u_n = \boldsymbol{P}_N \boldsymbol{C}_2^{\mathrm{T}} (\boldsymbol{C}_2 \boldsymbol{P}_N \boldsymbol{C}_2^{\mathrm{T}})^{-1} P_m \tag{3.52}$$

This completes the solution for u of (3.48) for combined attitude and power tracking.

In summary, given the reference attitude to track, β_r and ω_r, the required power P_W and the state of the system β, ω, Ω and γ, one calculates the required

attitude tracking torque τ_r from (3.32) and the corresponding control inputs u_{mw} and u_{cgm} from (3.48) and (3.52). If a gimbal acceleration steering law is required (to command the gimbal motors), then equation (3.36) must be used to "back-step" the velocity command $u_{\text{cmg}} = \dot{\gamma}_d$ to an acceleration command. Interestingly, the formulated power equation does not change regardless of these steering laws as $\dot{\gamma}$ and $\ddot{\gamma}$ do not appear in the power equation.

CHAPTER 4

VSCMG WORKBENCH LAYOUT AND DESIGN

The VSCMG workbench is a software program designed for studying the control system design of a spacecraft equipped with VSCMGs for combined attitude control and energy storage. Its modularized structure permits flexibility in implementation.

The several layers of the design are described here as well as basic program operation. Note that a couple more detailed schematics of the system design can be found in Appendix F.

4.1 Main Program Control Module

The first block the user needs is the Main Program Control Module shown in figure 4.1. In this module, the user loads the reference data (which currently involves tailoring a matlab *.m file where the user defines 2 column matrices (one contains the time data, the other contains the parameter time history) for each of the 11 reference

values (these values are the 4-parameter Euler parameter history, 3-parameter vehicle angular velocity (given in the vehicle coordinate reference frame, commonly referred to as p, q, and r), and the 3 angular velocity derivatives (typically referred to as $\dot{p}$, $\dot{q}$, and $\dot{r}$)).

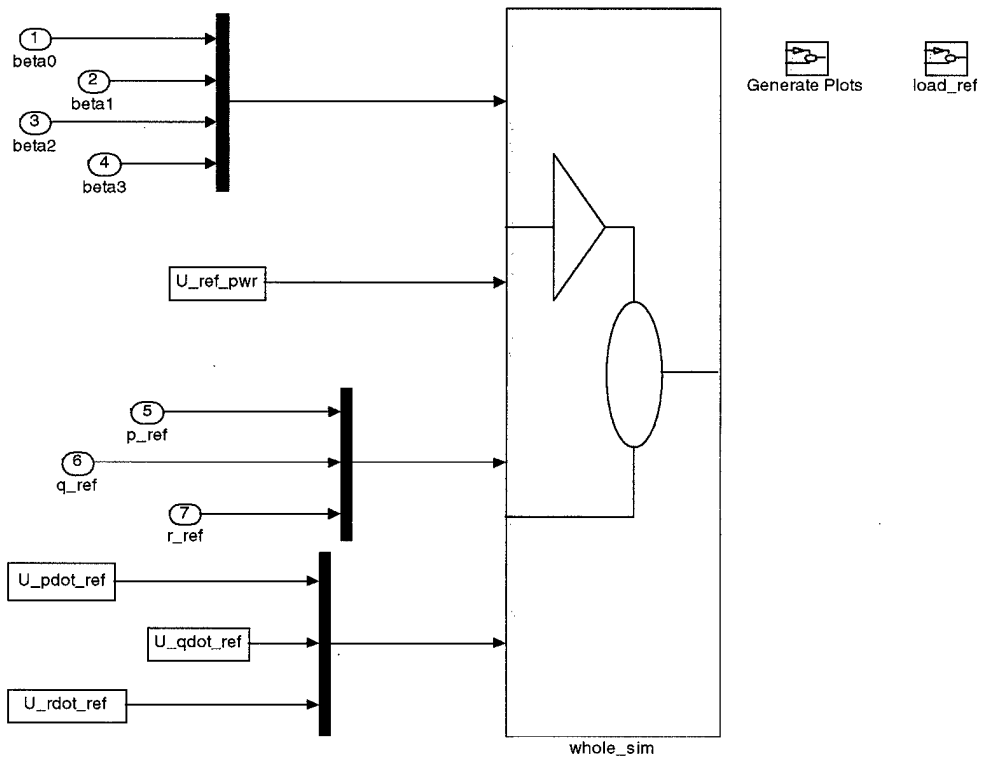

Figure 4.1: Main Program Control Module

4.2 Feedback System Overview

Underneath the Program Control Module mask resides the overall feedback control system. Unless the user intentionally reveals the support code by selecting to look under the SIMULINK mask all underlying subsystems are masked from the user. The underlying system includes modules representing characteristics inherent in a typical control system – the plant module, the plant actuators, the controller, the sensor suite, and the reference values. This is reflected in figure 4.2. Each one of these major subsystems is introduced in this chapter.

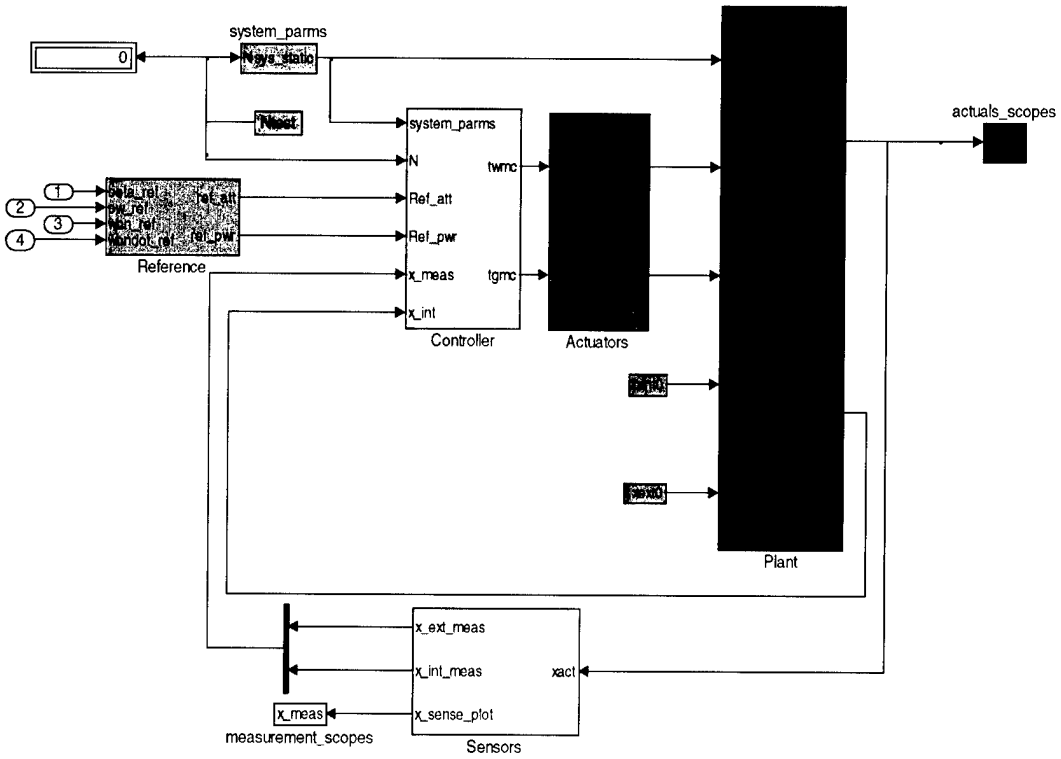

Figure 4.2: System Schematic

4.3 System Parameters Module

The first underlying subsystem is the System Parameters Module reflected in figure 4.3. There are two primary sets of parameters that drive the system configuration. These are set by the user and depend on the number of actuators used. These parameters include the reference VSCMG $\mathcal{G}$ frame installation orientation and the system inertias (as described in section 3.2).

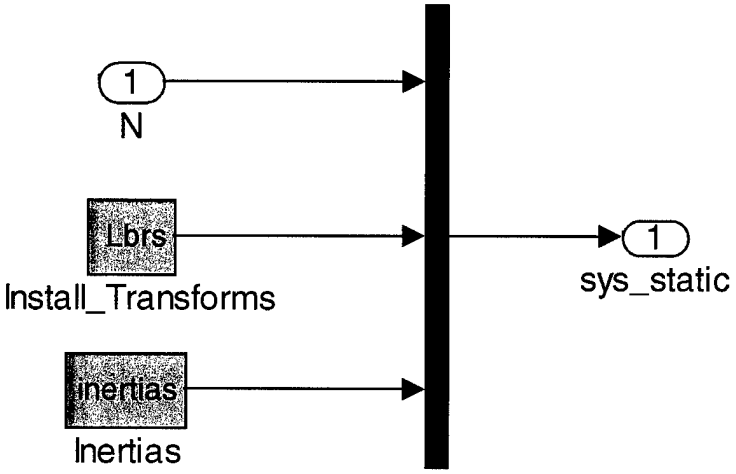

Figure 4.3: System Parameters Overview

4.4 Reference Module

Besides setting the system parameters, another key set of inputs to the control system is the reference attitude and the reference power that the control system is tasked to achieve. The flexibility in the design allows different reference attitude and reference power time histories (in the form of data tables) to be used as input to the system.

These can represent vehicles in different configurations, different vehicles, different actuator systems, and the list goes on.

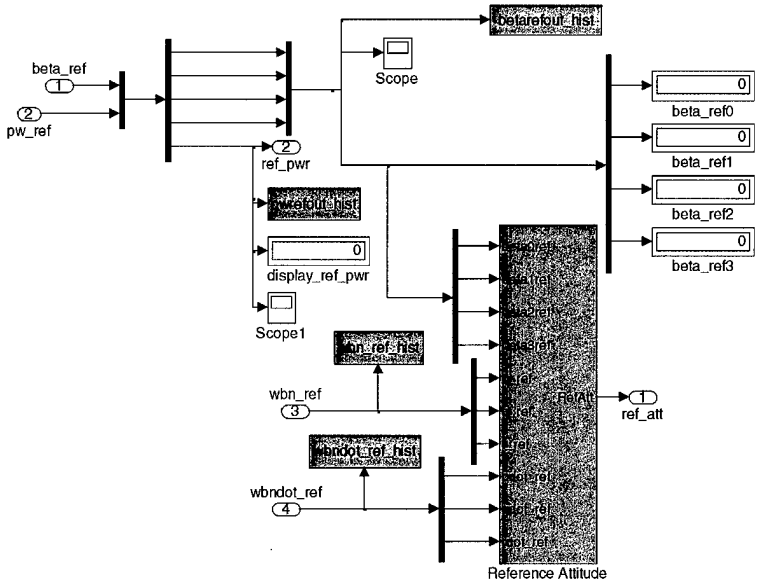

Figure 4.4: Attitude and Power Reference

4.5 Controller

The central "brain" of the control system is the controller. The crux of the developed theory directly relates to the logic employed in the controller (see 4.5 and 4.6). The controller uses the vehicle configuration mentioned in the previous sections along with the desired attitude and power profiles to determine stable actuator torques that will steer the vehicle to the desired attitude while simultaneously meeting the power tracking requirements and heeding the torque amplification constraint.

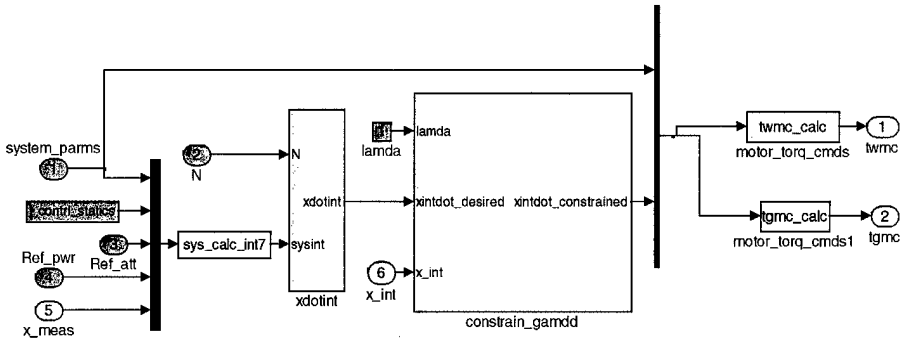

Figure 4.5: Controller Overview

4.6 Actuators Module

The commanded vehicle torque is generated by the actuators shown in figure 4.7. The actuators are divided into two major portions: the wheel motors and the gimbal motors. Both systems (the wheels and the gimbals) turn commanded motor torque voltages into actuated motor torques. These torques are used to calculate the actuated torque about the combined system center of mass (point O as described in Chapter 3). As in several of the other modules, this module has been designed to allow future designers to add model fidelity. This way, more realistic models of the actuator motors can be added to the simulation in order to analyze different actuator behaviors and concepts of control.

4.7 Plant Module

The plant houses the modeled vehicle inertias, the disturbance model inputs, the actuated torque computation function, and the integrated vehicle state equations

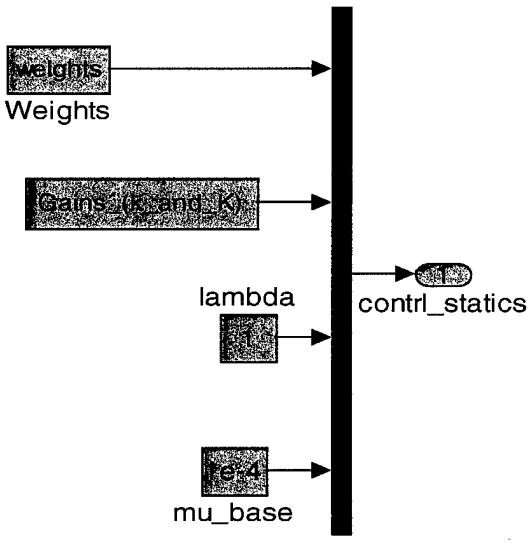

Figure 4.6: Controller Parameters Overview

(i.e. for vehicle rate and vehicle acceleration given the torques acting on the vehicle).

4.8 Sensors Module

Like the actuators module, the sensor module allows much room for the user to add more realistic, higher-fidelity models. Such models may include typical sensor

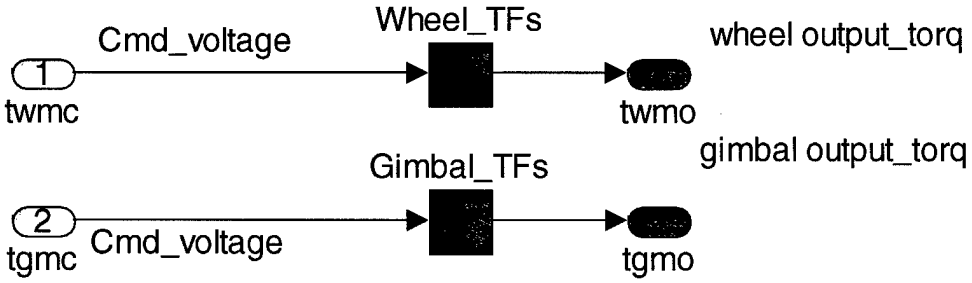

Figure 4.7: Actuator Motor Transfer Functions

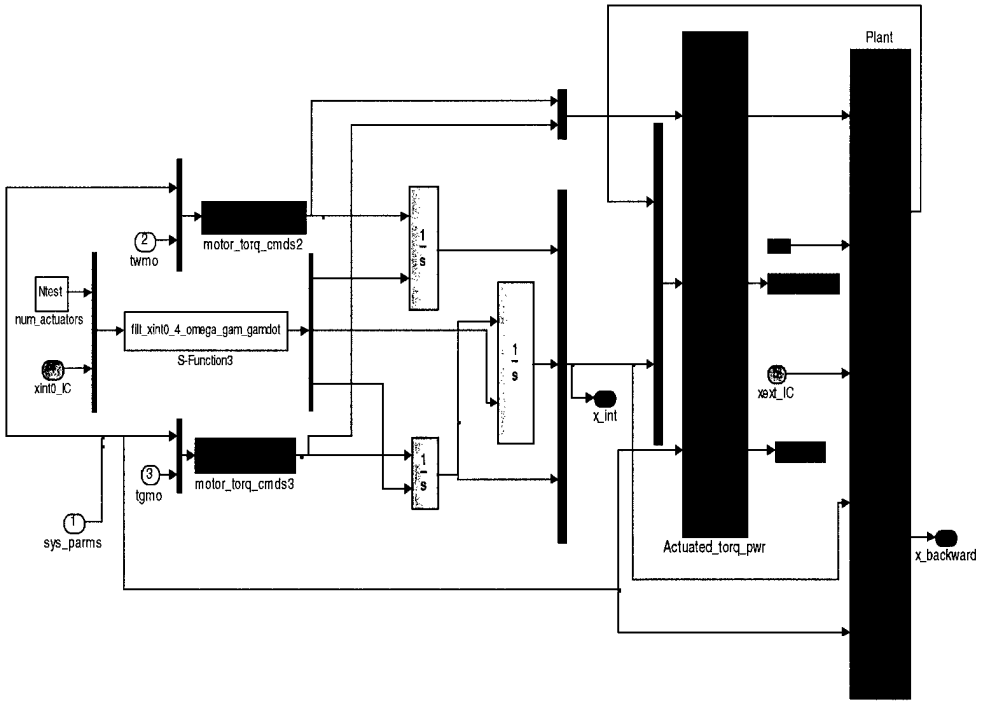

Figure 4.8: Plant Overview

inefficiencies, sensor data non-linear sensor phenomena (such as saturation, hysteresis, and backlash), and sensor fusion/weighting algorithms. All these topics permit much further in-depth analysis of on-orbit spacecraft phenomena never before feasible.

4.9 Summary of Program Operation

In order to use these different modules, the must have a good idea of how the simulation works. As far as basic program operations, the user

1. Determines where the actuators are installed (i.e. where the initial gimbal reference axis for each VSCMG is located relative to the body reference frame).

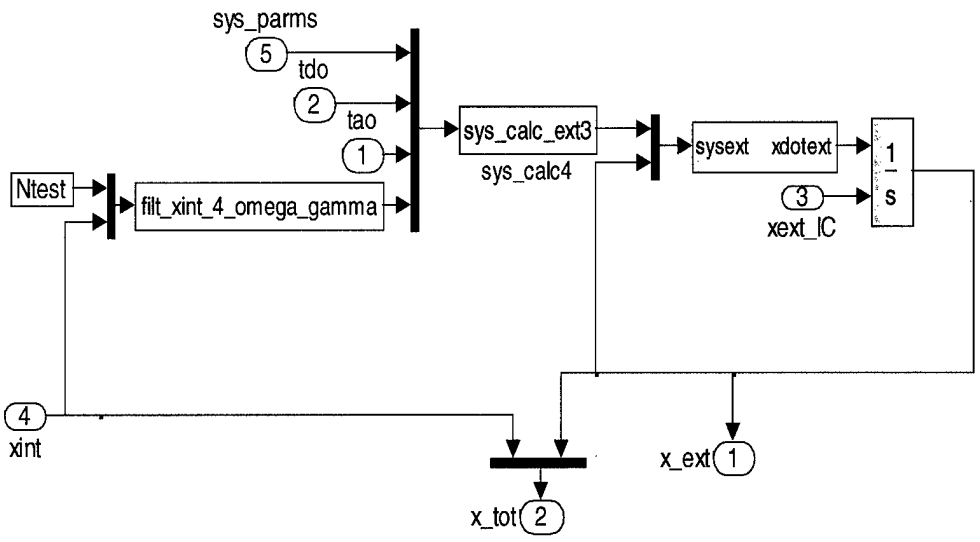

Figure 4.9: External System State Overview

2. Sets the vehicle platform plus actuator point-mass inertia matrix as well as the individual actuator inertia matrices (with respect to each $\mathcal{G}_i$ frame). These values are set in the system parameters module.

3. Configures the controller parameters (as appropriate) in the controller subsystem module.

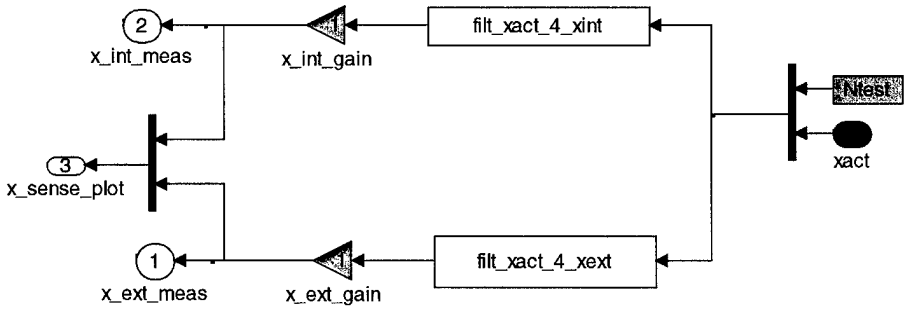

Figure 4.10: Sensor System

4. Sets the desired actuator model in the actuators system module according to the desired fidelity/response of the actuated system.

5. Runs the `load ref` function which will load reference data according to the desired scenario.

6. Starts the simulation in the Master program module by selecting the `play` button.

7. Selects `generate plots` in order to create MATLAB output plots, if desired, when the simulation is done. Note that the`load ref` and `generate plots` functions should be tailored according to the purpose to which this program is applied.

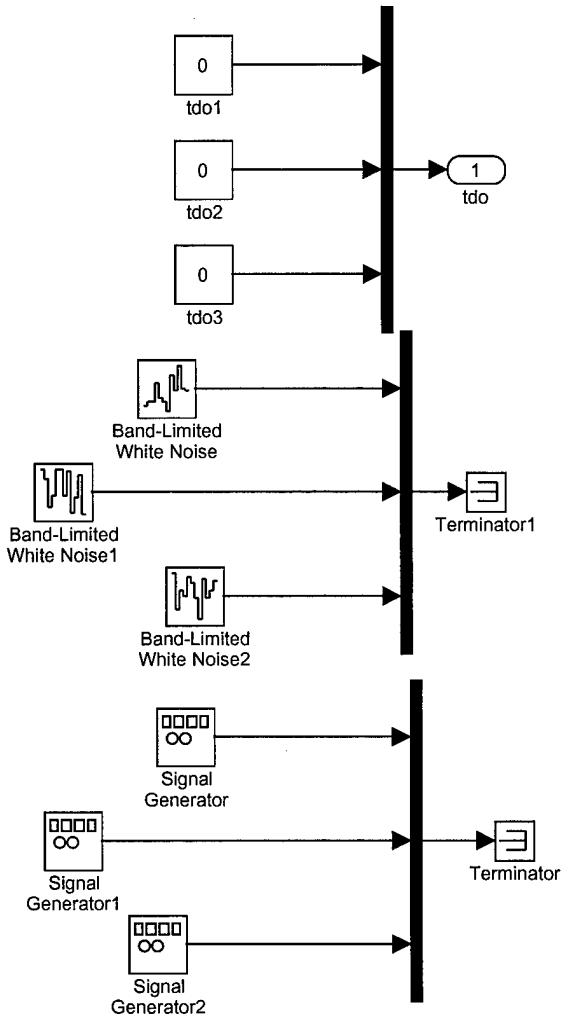

Figure 4.11: Disturbance Torque Inputs

CHAPTER 5

SIMULATION TESTS

Several different simulation tests were performed in order to study simultaneous spacecraft attitude control and power tracking. These tests can be broken down into several key areas: controller comparison tests, controller parameter tests, system parameter tests, simulation parameter tests, and actuator model tests.

Before describing these tests in more detail, one must first review some preliminary information on control mode weighting and singularity avoidance and then outline the scenarios used for attitude regulation and attitude tracking. Note that in this chapter, only the test scenarios and parameters are presented - analysis of the tests' results follows in the ensuing chapter. Furthermore, it is important to understand that the baseline tests described for each test group essentially serve as the "experimental control" variables and thus allows one to compare different parameter changes with the baseline in order to evaluate a parameter's impact on the system performance.

5.1 Weighting and Singularity Avoidance

Define the weighted generalized inverse $\boldsymbol{C}_1^{\dagger}$ identical to that used in [40]

$$\boldsymbol{C}_1^{\dagger} = \boldsymbol{W}\boldsymbol{C}_1{}^T \left(\boldsymbol{C}_1\boldsymbol{W}\boldsymbol{C}_1{}^T\right)^{-1} \tag{5.1}$$

where $\boldsymbol{W}$ is a diagonal RW/CMG mode weighting matrix such that W_{gj0} represents weighting the predominant CMG mode (to capitalize on its torque amplification property) and is constant throughout a maneuver. W_{sj} is the RW mode weight that comes into play near a CMG singularity. W_{sj} is given by

$$W_{sj} = W_{sj0} \exp^{-\mu\delta} \tag{5.2}$$

in which μ and W_{sj0} are chosen by the control system designer to elicit the desired performance. δ is a parameter that describes the proximity to a CMG singularity [37, 32, 39, 40]. The expression for δ used here is different from that of [40] and is defined as the minimum singular value of $\boldsymbol{C}_1$. This is a more accurate way to describe the singularity of the matrix $\boldsymbol{C}_1$ [43].

5.2 Attitude Regulation Scenario

The attitude regulation scenario is based on the examples found in [32], [40], and [39]. Parameters for the baseline attitude regulation scenario, which uses controller I from Chapter 3, are included in table 5.1

Similarly to these references, a standard four VSCMG pyramid configuration is used here, which is one in which the VSCMGs are installed so that the four gimbal

Table 5.1: Regulation Scenario Parameter Settings

Symbol	Value	Units
N	4	unitless
θ	54.75	deg
$\omega(0)$	[0 0 0]	rad/sec
$\beta(0)$	[0.5 0.5 0.5 0.5]	unitless
ω_r	[0 0 0]	rad/sec
β_r	[1 0 0 0]	unitless
$\gamma(0)$	$[\frac{\pi}{4}\ -\frac{\pi}{4}\ -\frac{\pi}{4}\ \frac{\pi}{4}\ ]$	rad
$\dot{\gamma}(0)$	[0 0 0 0]	rad
$\Omega(0)$	[50000 60000 55000 65000]	RPM
W_{sj0}	40	unitless
W_{gj0}	1	unitless
$\boldsymbol{I}_{Wj}$	diag {0.70, 0.20, 0.20}	Kg m^2
$\boldsymbol{I}_{Gj}$	diag {0.10 0.10 ,0.10}	Kg m^2
$\boldsymbol{I}_{sc}$	diag {15053, 6510, 11122}	Kg m^2
$\boldsymbol{K}$	diag {700, 700, 700}	Kg m^2/sec
k	35.0	Kg m^2/sec
μ	10^-4	unitless
λ	1	unitless

axes form a pyramid with respect to the body. The pyramid configuration has been implemented here in order to facilitate comparisons with the related literature even though the theory applies generically to the n-actuator case. Figure 5.1 which was taken from reference [38] depicts a standard CMG/VSCMG pyramid configuration. Note that θ represents the pyramid angle of each VSCMG that is measured from the

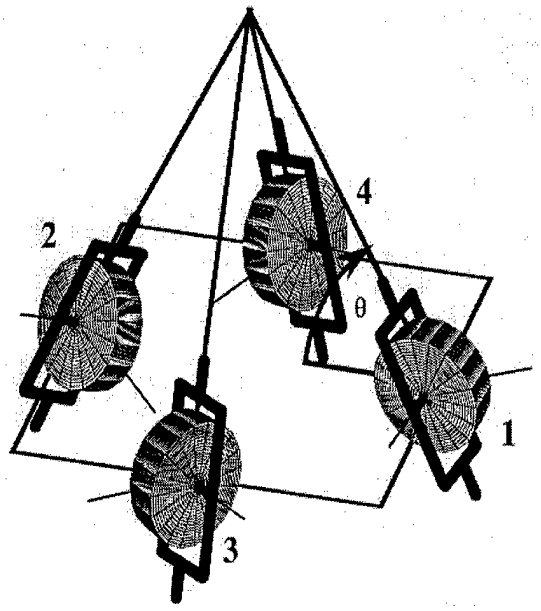

Figure 5.1: VSCMG Pyramid Configuration

vehicle's $b_1 - b_2$ plane to the VSCMG's gimbal axis.

In the regulation scenario, the goal is to bring the vehicle from some arbitrary attitude to the reference attitude while tracking a given power profile. The reference attitude in this case is assumed to be a fixed orientation with respect to frame $\mathcal{N}$. Without loss of generality, one can assume this orientation (in the regulation case) is

the origin as is done in [32] and [40] since one can always redefine the origin as being the desired inertial orientation.

5.3 Attitude Tracking Scenario

The tracking scenario is based on the example used in [4], which is briefly reviewed in Appendix E. Similar to the attitude regulation scenario presented in section 5.1, the goal in the attitude tracking case is to bring the vehicle from an undesired attitude to the reference attitude while tracking a given power profile. The given reference attitude position, velocity, and acceleration correspond to an on-orbit example similar to that used in [4] in which a near-polar orbital satellite has to meet specific sun and ground tracking requirements.

The parameters used in this scenario are virtually identical to that used for the regulation case (see table 5.1). The only difference is that instead of regulating about a fixed angular position, angular velocity, and angular acceleration, the Iridium 25578 orbital parameters are used to generate time varying reference values for angular position, angular velocity, and angular acceleration. The relevant parameters are summarized in table 5.2.

Table 5.2: Tracking Scenario Parameters Settings

Symbol	Value	Units
N	4	unitless
θ	54.75	deg
$\omega(0)$	[0 0 0]	rad/sec
$\beta(0)$	[0.5 0.5 0.5 0.5]	unitless
ω_r	Iridium 25578	rad/sec
β_r	Iridium 25578	unitless
$\gamma(0)$	$[\frac{\pi}{4}\ -\frac{\pi}{4}\ -\frac{\pi}{4}\ \frac{\pi}{4}\ ]$	rad
$\dot{\gamma}(0)$	[0 0 0 0]	rad
$\Omega(0)$	[50000 60000 55000 65000]	RPM
W_{sj0}	40	unitless
W_{gj0}	1	unitless
$\boldsymbol{I}_{Wj}$	diag {0.70, 0.20, 0.20}	Kg m^2
$\boldsymbol{I}_{Gj}$	diag {0.10 0.10 ,0.10}	Kg m^2
$\boldsymbol{I}_{sc}$	diag {15053, 6510, 11122}	Kg m^2
$\boldsymbol{K}$	diag {700, 700, 700}	Kg m^2/sec
k	35.0	Kg m^2/sec
μ	10^-4	unitless
λ	1	unitless

5.4 Significant Tests

The first set of tests compares the responses of the two controllers presented in chapter 3 for both scenarios, regulation and tracking. From it, one can see how effective each controller is for each scenario.

Next, there are a few controller parameters one has the freedom to select when using one of the presented control laws. This set of tests outlines the effects that these parameters, the matrix gain, $\boldsymbol{K}$, the scalar gain k, the reaction wheel mode weighting, W_{s0}, and the singularity scaling variable, μ, have on the response of the system.

Third, in order to best understand the spacecraft system, one needs a grasp of how the different system variables affect the system response. The primary system parameters tested here are the vehicle body and actuator inertias. These inertias have differing affects on the controlled system response. One might note that another big factor affecting the system is the location of the actuators (i.e. the actuator configuration). A study of the actuator locations is beyond the scope of this research but the possibilities are endless.

Fourth, the simulation of a large space structure of this magnitude and complexity obviously has several parameters related to the simulation design and performance that impact the realism of the simulation. In this set of tests, one is able to get a feel for how simulation parameters such as integration method, time step, and run time affect the realism of the simulation.

Finally, tests were performed to examine the effects of modeling the actuators.

The actuators were modeled in both as identity gain and as non-identity gain models. As in the other tests, the results are presented in chapter 6.

5.5 Other Tests Considered

Several other tests were run during this research effort. However, many of them did not appreciably affect the outcome of the simulations and have thus been left out of this analysis.

This includes issues such as disturbance torque effects, non-diagonal actuator and plant inertia matrices, and gimbal structure inertia changes. The latter of these was tested but there were very minor affects on the overall system. The disturbance torques were only initially tested and a full study of system disturbance rejection could be done in the future. Third, incorporating non-diagonal inertias was not fully modeled in the plant. It, too, could be examined in future research.

5.6 Test Chapter Summary

This chapter introduced several simulation tests carried out during this research. Although intended to cover a large portion of the satellite system envelope, this set of tests is by no means a completely exhaustive suite of tests. Its intention is to give the satellite control system designer more examples of different system effects. The results analysis of this battery of tests is presented in chapter 6.

CHAPTER 6

ANALYSIS OF TEST RESULTS

Once the simulation tests run for this research are understood, one can examine the test results. As was true of the test descriptions (see chapter 5), the test results can be broken down into several key areas: controller comparison results, control parameter effects, system parameter effects, simulation parameter effects, and actuator test results.

6.1 Controller Comparison Results

In this section, one is able to see the basic simulation output of the scenarios described in chapter 5 and the scenario data tables, tables 5.1 and 5.2.

6.1.1 Regulation

The first series of plots illustrates the regulation scenario output. Figures 6.1 and 6.2 show the results of using controller I and controller II, respectively, which were introduced in chapter 3.

These plots (from left to right starting at the top) show time histories of the vehicle angular position (in terms of the Euler parameter representation), angular position error, angular velocity, angular velocity error, the actuator wheel speeds, actuator gimbal angles, actuator gimbal rates, and the singularity parameter for controller I. A similar set of plots shows the time response of controller II.

Figure 6.1 provides a good demonstration of the typical system behavior based on the given initial conditions. This plot shows the system going to the desired attitude and regulating motion about it while simultaneously tracking the given power profile (shown in figure 6.5). One can see from these baseline plots the similarities in the controllers.

However, figures 6.3 and 6.4 show a more direct comparison of the controllers in terms of the different components of the angular velocity error, angular position error, and the control inputs. Note that this channel-by-channel plotting format is used extensively throughout the remainder of this chapter in order to present the effects that multiple parameters have on the system output. The results are further broken down by vehicle response (i.e. the components of the angular velocity error, $\omega - \omega_r$ for controller I and $\delta\omega$ for controller II - and the angular position error - $\beta - \beta_r$ for controller I and $\delta\beta$ for controller II) This presentation method permits helpful insight into the effects that certain parameters have on the overall system over time.

Figures 6.1 and 6.2 show that controller I and controller II are very similar in terms of speed of response. The primary difference appears to be that the stabilizing

vehicle trajectory path is different for each controller.

In figures 6.3 and 6.4, the blue line for each plot represents the controller I time response for each channel. The first column of sub plots in figure 6.3 contains the angular velocity sub-component error time histories and the second column contains the angular position error time response. In figure 6.4, the actuator responses given for each controller scenario are further broken down into three columns corresponding to the respective wheel speed, gimbal angle, and gimbal rate histories of each VSCMG. In the cases of both plots, the blue line is the controller I response and the green line is the controller II response.

Thus, it is clear from this plot that although the response performance is comparable between the two controllers, in terms of vehicle response, controller II provides a smoother, more even result. Likewise, in comparing the actuator responses displayed in 6.4, it is evident that the only difference in the resulting vehicle motion is reflected in the gimbal angles. It appears in this plot that controller II provides a less oscillatory result. Since highly oscillatory motion usually has negative impacts on a structure's lifetime and effectiveness, for this scenario controller II is more favorable than controller I.

In addition, one can see in figure 6.5 the power tracking response based on the power profile given in section 5.2. As the power tracking response is identical for both controllers, only one actual power output versus required power profile plot is included.

Note that it is difficult to distinguish the actual response from the desired profile. This makes sense as for these test runs, it was assumed that the actuator motors produce exactly the desired motor output torque. Obviously, as one adds fidelity to the actuator models and these models become more realistic, there will be some minor differences in the desired and output power as no actuator system is completely perfect. Actuator modeling affects are mentioned later in this chapter.

6.1.2 Tracking

One can see the baseline tracking scenario output histories for the two controllers in figures 6.6 and 6.7 based on the tracking scenario mentioned in chapter 5 and appendix E. The same power profile as that used for regulation is also used here.

The plots in figures 6.6 and 6.7 help one gain a feel for how the controllers perform as far as attitude tracking is concerned. As before, both controllers track the desired attitude in about the same amount of time. However, these plots indicate that controller II provides a slightly more damped response.

The next figures (6.8 and 6.9) show the direct comparison of these two controllers. The results of this scenario are very much like those of the regulation scenario as is amplified in these plots. In other words, the tracking scenario seems to bring out the smoother response of controller II over controller I. Hence, for similar reasons as before, it is clear that controller II is better in this situation.

6.2 Control Parameter Effects

Next, the effects that the controller parameters, i.e. the matrix gain $\boldsymbol{K}$, the scalar gain, k, the momentum wheel/control moment gyroscope weighting, W_{s0}, and the singularity parameter scaling constant, μ, have on the system can be examined.

Figure 6.10 includes the vehicle response to changes in the mentioned control parameters. In this figure, the dark green line in the subfigures represents the vehicle response with a large change in the scalar gain, k. Figure 6.11 reflects the impact perturbations in the control parameters have on the actuators.

In these two figures (6.10 and 6.11), the forest green line represents a large change in the scalar gain, k. The magenta line is the system response to a large change in the norm of $\boldsymbol{K}$. The red line relates to a vehicle simulation with a large decrease in the singularity parameter scaling constant μ (which the control designer selects based on the desired performance), the light blue line represents an increase in the norm of the momentum wheel spin weighting $\boldsymbol{W}_{s0}$, and the blue line is the regulation controller I comparison baseline. Here, the blue, light blue, and red lines in the sub figures are extremely close and therefore difficult to discriminate. On the other hand, the forest green line is clearly much more oscillatory than the other responses. This yields the slightly exaggerated but none the less instructive effect of increasing k. It was increased by an order of magnitude, from a value of 35 to 350 in this example. On the other hand, increasing the norm of $\boldsymbol{K}$ resulted in a more damped response that is centered about the baseline response (i.e. the blue line). This shows that as

this gain matrix's norm is increased, the result is a more damped response. Thus, as is common in a feedback control system, one can manipulate the system performance speed and damping through selection of the feedback gains (k and $\boldsymbol{K}$).

6.3 System Parameter Effects

Similar to studying the control parameters, one can analyze the impact that system parameters (i.e. system inertias) have on the resulting vehicle motion. These effects are given in figures 6.12 and 6.13.

In these plots, the blue line is again the baseline controller I during regulation response and the forest green line the vehicle response due to an increase in vehicle platform inertia plus actuator point-mass inertia. The red line represents increasing the norm of all the wheel inertia matrices; the light blue line represents increasing all the wheel spin axis inertia values; and the magenta line reflects increasing only one of the wheel spin axis inertias. It should be noted here that three of the five compared runs were only simulated from 0 to 500 seconds, so this is the region of primary interest on these plots. Here, one can see a large spike in the magenta response where that wheel's motion was adjusted due to the larger inertia. These results show the vehicle going to the target state but at the cost of some excessive wheel motion as compared to the baseline case. It should be noted, though, that this result mainly occurs when modifying any and all of the wheel spin-axis inertia. As these inertia values are much higher than the other axis inertia or the gimbal structure inertia (this is clearly due

to the assumed circular disk wheel shape for the flywheels). One can also see in the actuator plots that wheel spin-axis inertia changes result in more oscillatory actuator (and thus vehicle) motion as compared to the baseline. Interestingly, as reflected in the red line's performance, if all the wheel inertias are changed (e.g. scaled sizing along all axes of the wheel system), then the resulting motion is more favorable. Also interesting is that increasing the platform inertia did not seem to have as great an impact as increasing wheel spin-axis inertia.

6.4 Simulation Parameter Effects

The simulation parameters also affect the system response and realism. Although one might think using the smallest time step is the best solution (it can help precision), it is well known that decreasing the time step can also introduce numerical errors [44] as well greatly increase the run time. Figure 6.14 shows the results of different test runs with different fixed integration step sizes.

This plot shows that smaller time steps are more accurate. In this example, the angular momentum magnitude (which is required to be constant as energy is conserved) is compared at three time steps, $ts = 0.1$ sec, $ts = 0.001$ sec, and $ts = 0.00001$ sec with a Runge-Kuttam 45 solution method (using ode45 in MATLAB) with a variable step size. The result is that the 0.00001 sec step size yields an accuracy in angular momentum of about $1.8 \times 10^{(} - 6)$. For these test cases, the angular momentum was on the order of 7470.0 kg $m^2/$ sec. On the other hand, the

run time for these runs was greatly increased (for 10 seconds of simulation time run using 0.1 sec took less than 5 minutes whereas a 0.2 second run of the 0.00001 sec time step took over 2 hours to run). Thus, a simple cost benefit analysis shows that there is a balance between accuracy and run time. One should also note that lower time steps do not always yield more accuracy as round-off errors can greatly limit the stability/performance of a simulation run. So, for this case, a time step of 0.1 seconds is adequate for the purpose of the simulation.

In addition, different integration methods were tested using variable time steps. As far as using ode45 (Runge-Kutta), it appears to only affect the result a little but wastes much more state storage space and processing time. Thus, for this case, Bogacki-Shampine seems to be the best method to use in terms of finding a middle ground between storage space, run time, and numerical accuracy/stability.

6.5 Actuator Test Results

The last primary test results are those of the different actuator modeling tests. Figure 6.15 is a power actuated versus power required plot combining results from both the case of modeling the actuators as identity gain and as uniform scalar gain. The momentum wheel actuators were assumed to apply torque through standard DC motors and the CMG actuators were assumed torque the gimbals via geared DC motors. Figure 6.16 shows the results of applying three actuators aligned along the $\mathcal{B}$ axes instead of the pyramid configuration.

The next plot shows the impact of power tracking when using the different actuator models. Since there are only slight changes in the actuator models, as shown in the preceeding figures, the power tracking results seem to be very close. But, when the models are not as close (e.g. if one sets the scalar gain model much lower than 0.9), then the result is a not-so-perfect power output track. It will still track the desired power, just not as quickly.

Finally, the following illustrates the use of three actuators instead of four for the simultaneous attitude control/energy storage system.

One can see from this result that the system performs the dual functions marvelously in the three actuator case. However, this case is intended to verify the flexibility of the simulation model design and thus, further investigation into using three actuators versus four should be accomplished in terms of singularities, performance degradation, etc.

6.6 Summary of Results

This chapter presented the tests results of those tests described in the preceding chapter. One must realize that a large number of simulation tests were completed in this research and only a handful of these tests are described here. Since well over 100 different simulations were run during this research, it is hard to include plots of all the effects. The only important effect that was not plotted for this report relates to the wheel speeds. It should be noted that initial conditions seem to impact

the simulation results. Namely, the initial wheel speeds appear to impact the power tracking profile and thus the simultaneous solution. It was observed that if the initial wheel speeds are too small as compared to the peak power magnitude and duration, then the simulation will take a long time generating the required power and torque when the power profile goes through a peak power incident. This gives some slightly undesirable results in the simulation. Even though the required power is tracked through the wheel acceleration and not the wheel speed, the wheel speeds do have an effect on the total output power magnitude since wheel speeds are contained in the power tracking equation. The cases where the norm of the wheel speed initial conditions were small was that there seemed to be a slight discontinuity at the end of the peak power profile, so the simulation slowed down. This problem was rectified by increasing the initial wheel speed. This issue seems to be more of a simulation result and should not be a problem in reality as the wheels will work in a normal operating range that can be determined from the anticipated peak power requirement.

In order to recap, the results here were broken down into controller comparison results, system parameter results, integration method/time step results, validation results, and actuator modeling tests. From these tests, one can gain a very good understanding of the effects that different parameters have on the system and its control. This rewards users with an increased ability to tailor the system to their own needs.

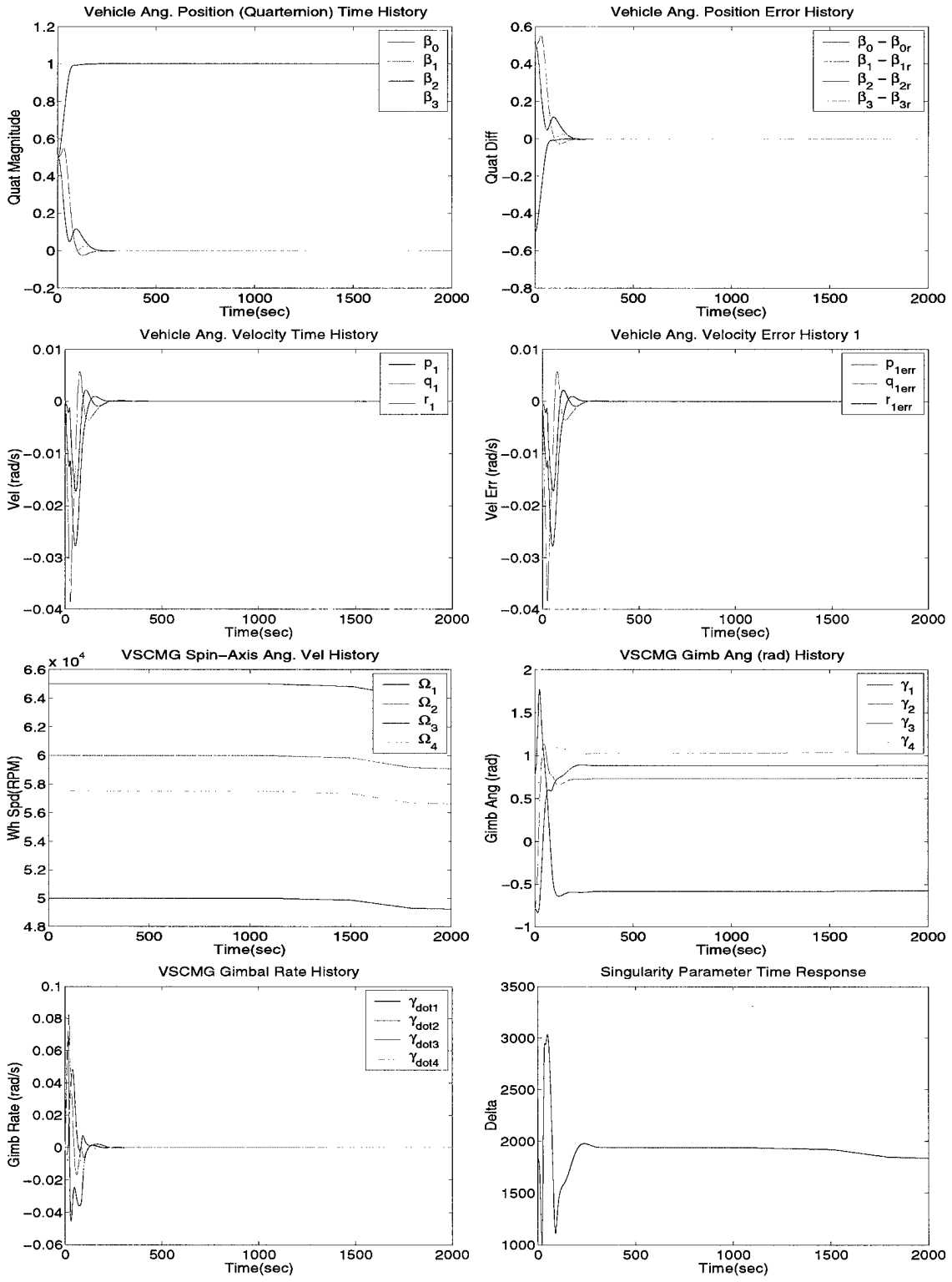

Figure 6.1: Regulation Controller I Time Response

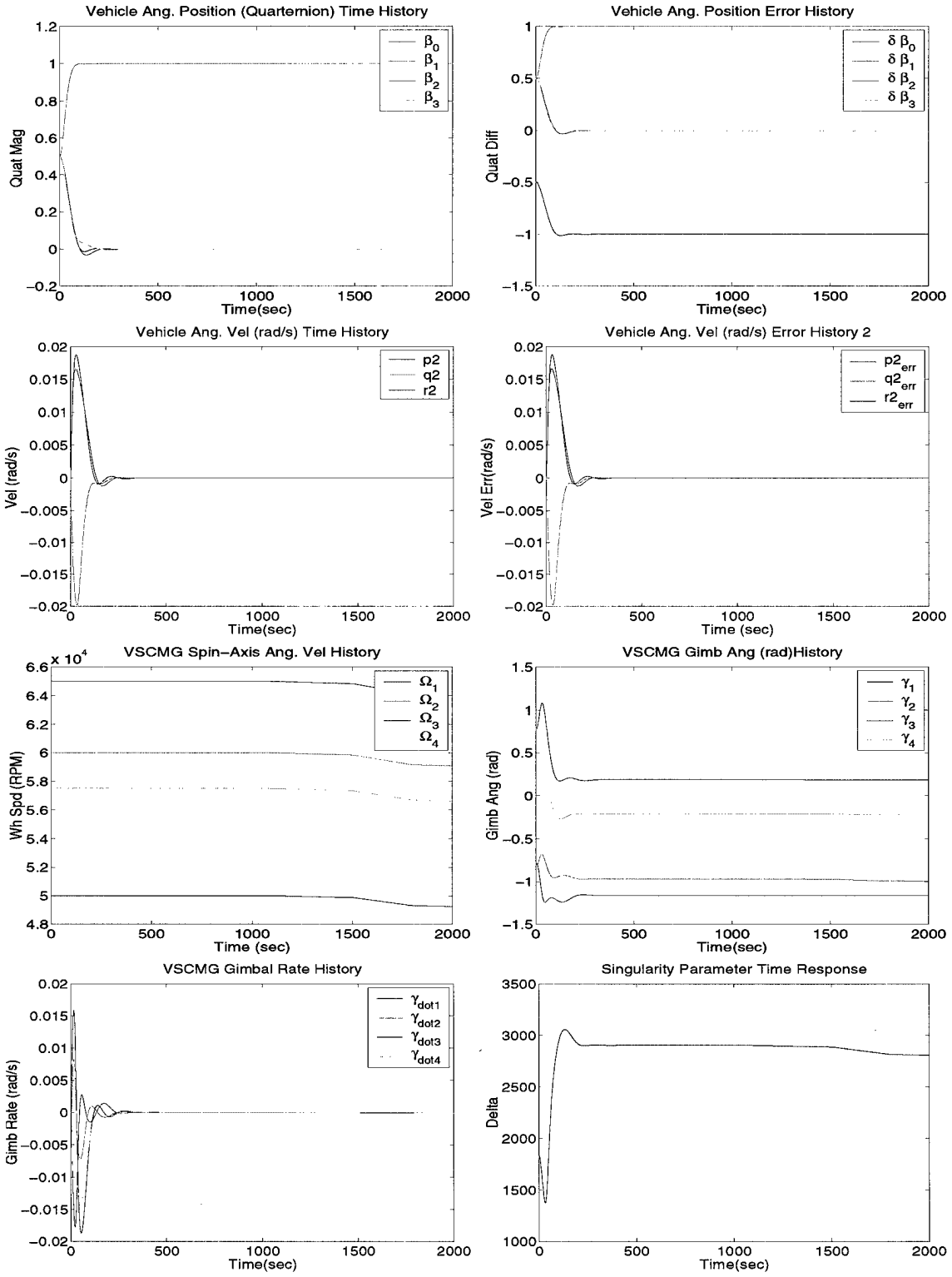

Figure 6.2: Regulation Controller II Time Response

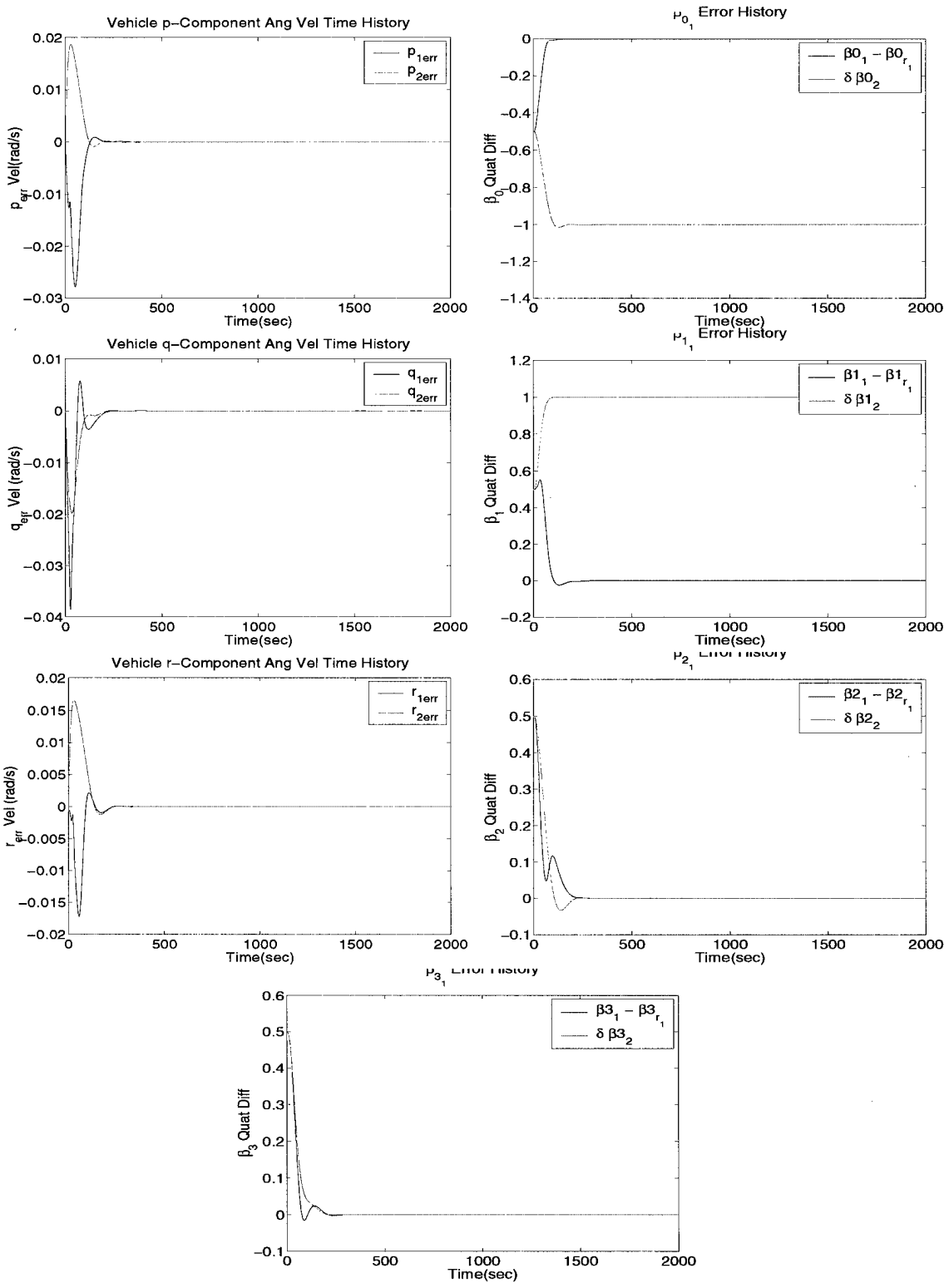

Figure 6.3: Regulation Controller Comparison Vehicle Time Response

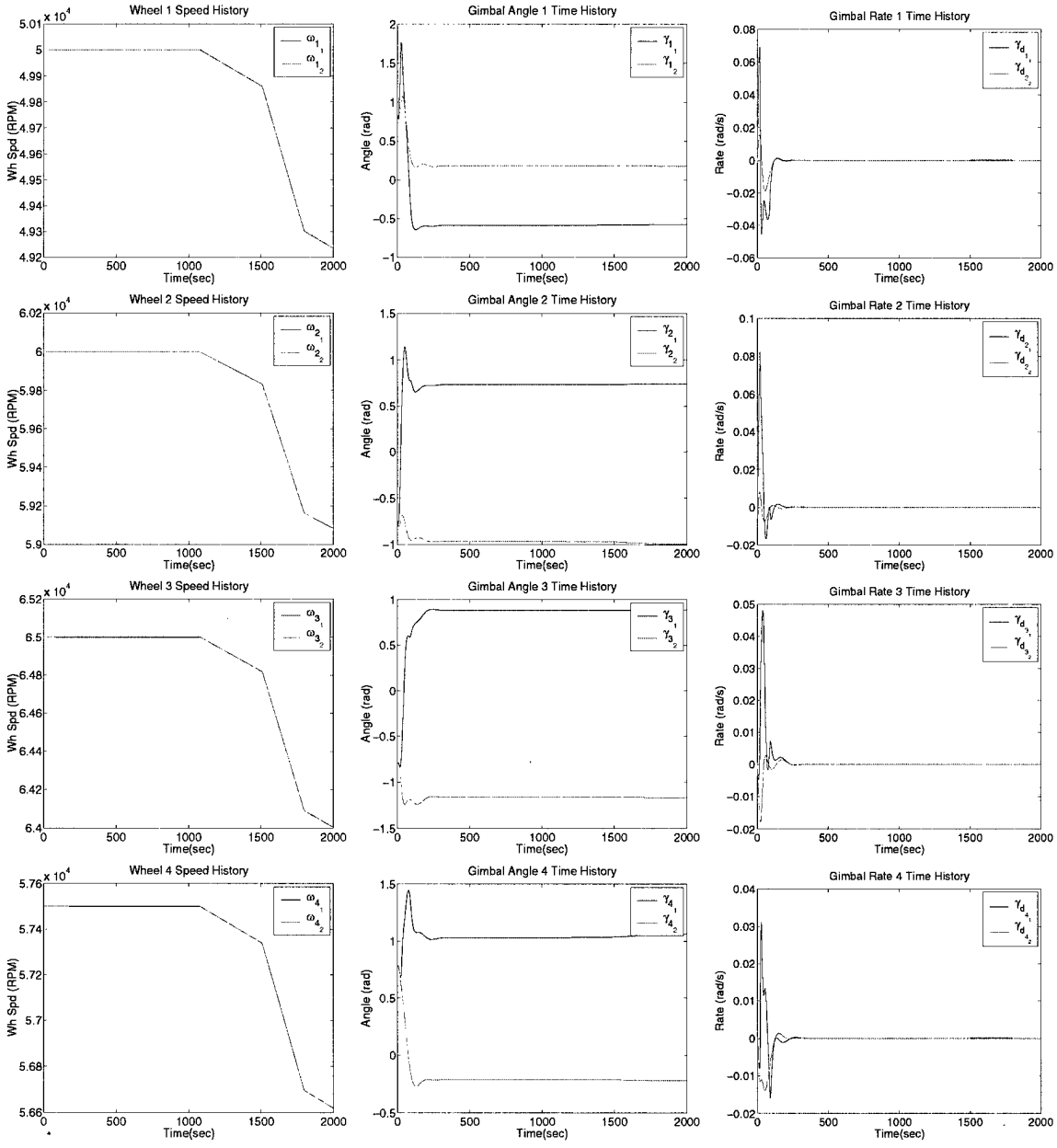

Figure 6.4: Regulation Controller Comparison Actuators Time Response

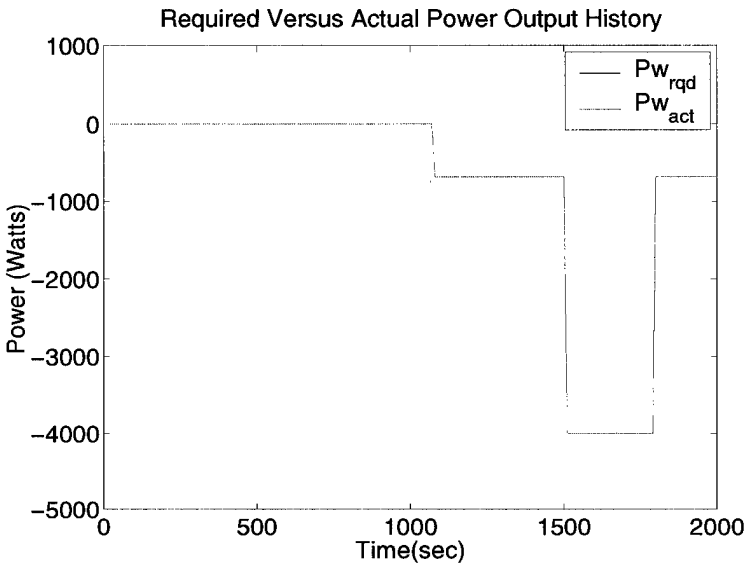

Figure 6.5: Power Tracking Actual Response Versus Profile

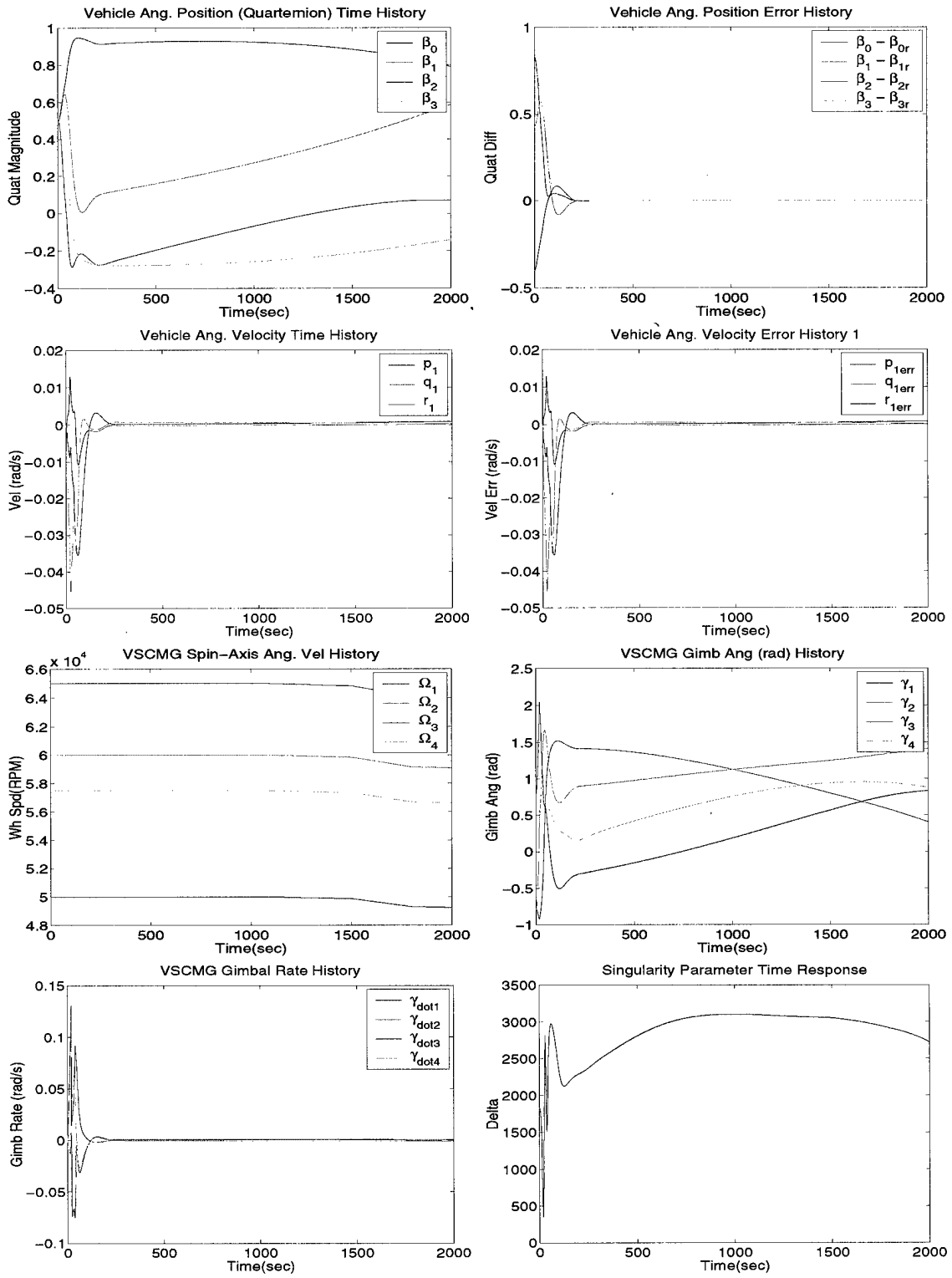

Figure 6.6: Tracking with Controller I Time Response

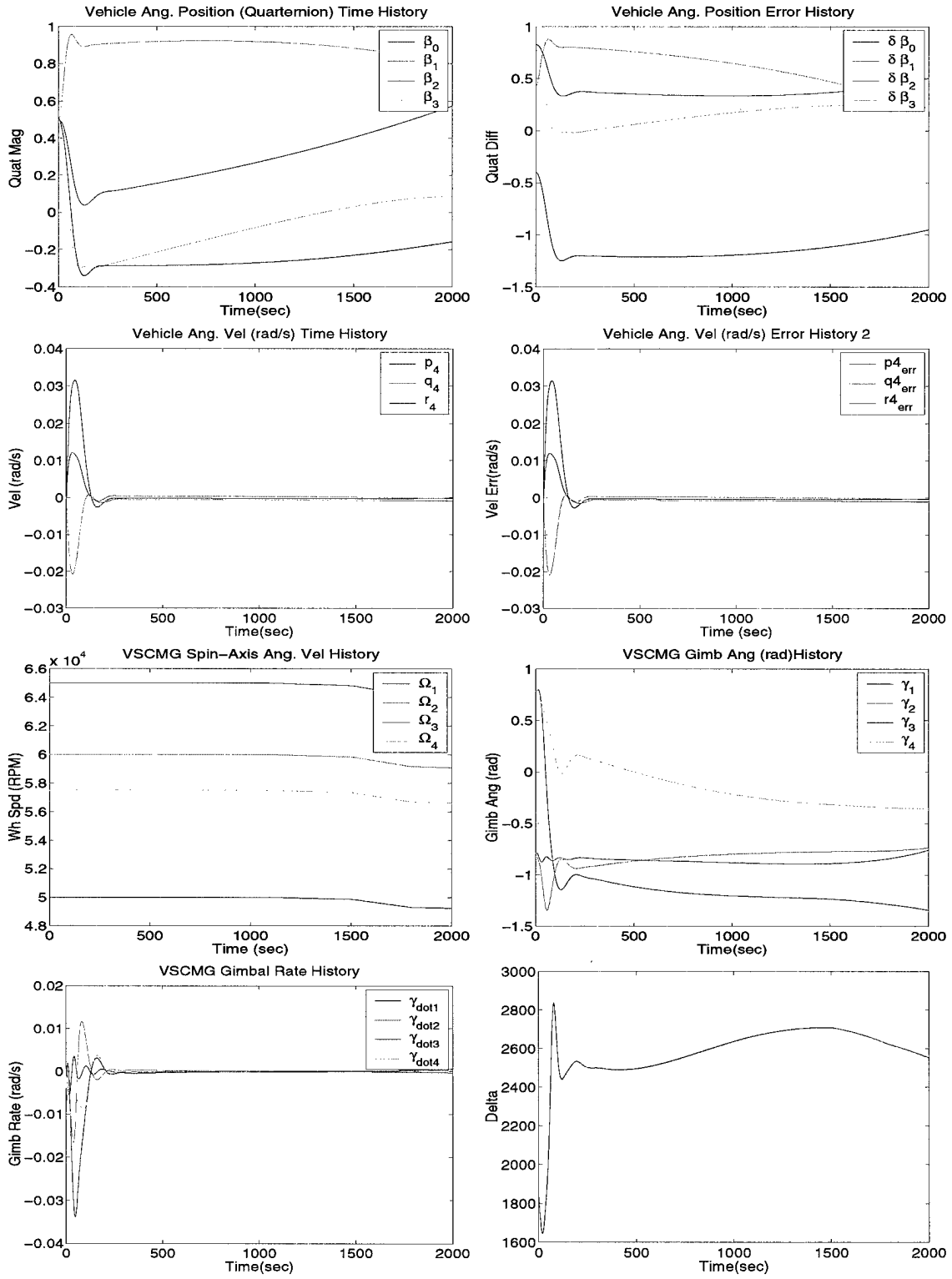

Figure 6.7: Tracking with Controller II Time Response

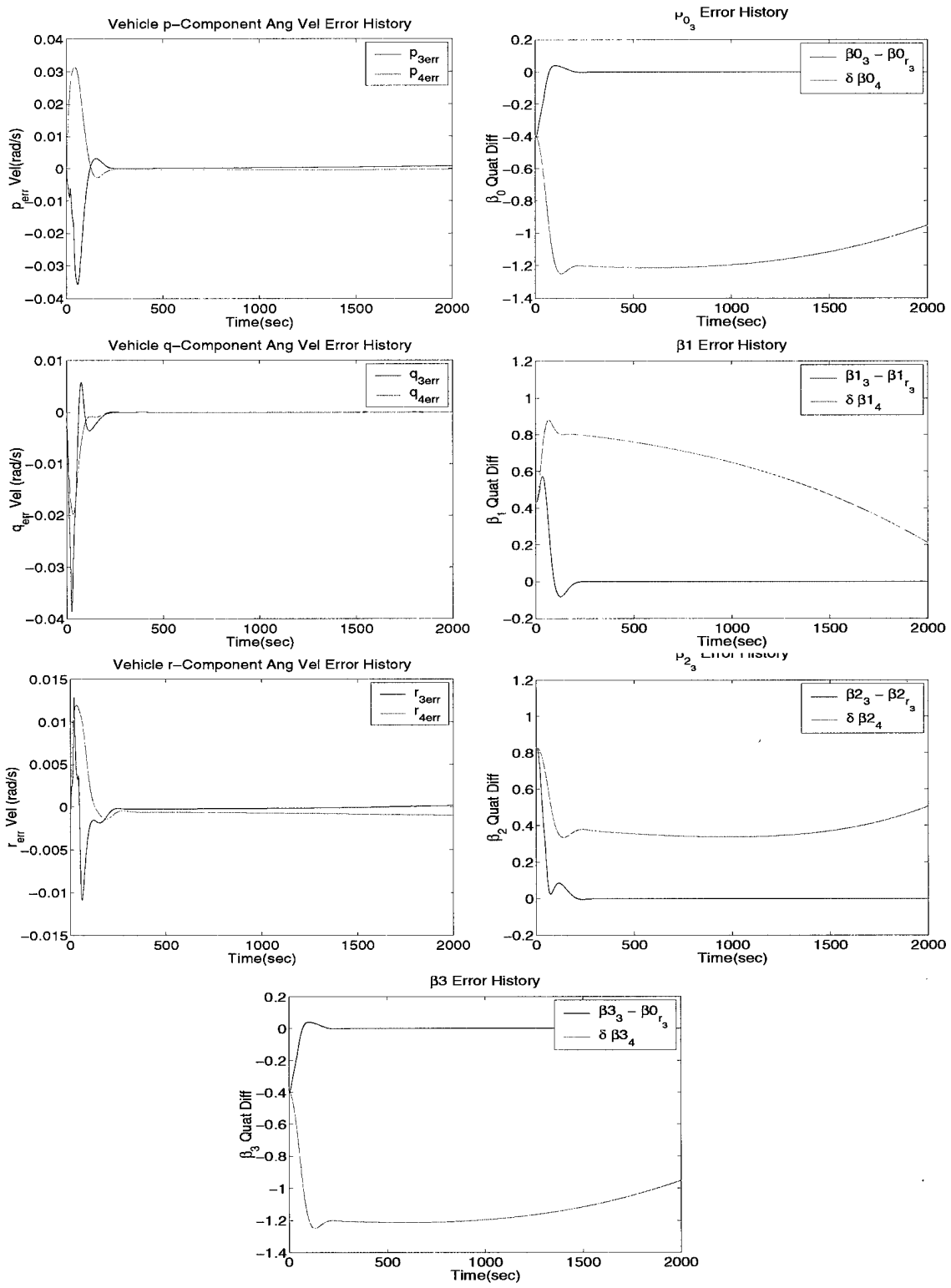

Figure 6.8: Tracking Controller Comparison Vehicle Time Response

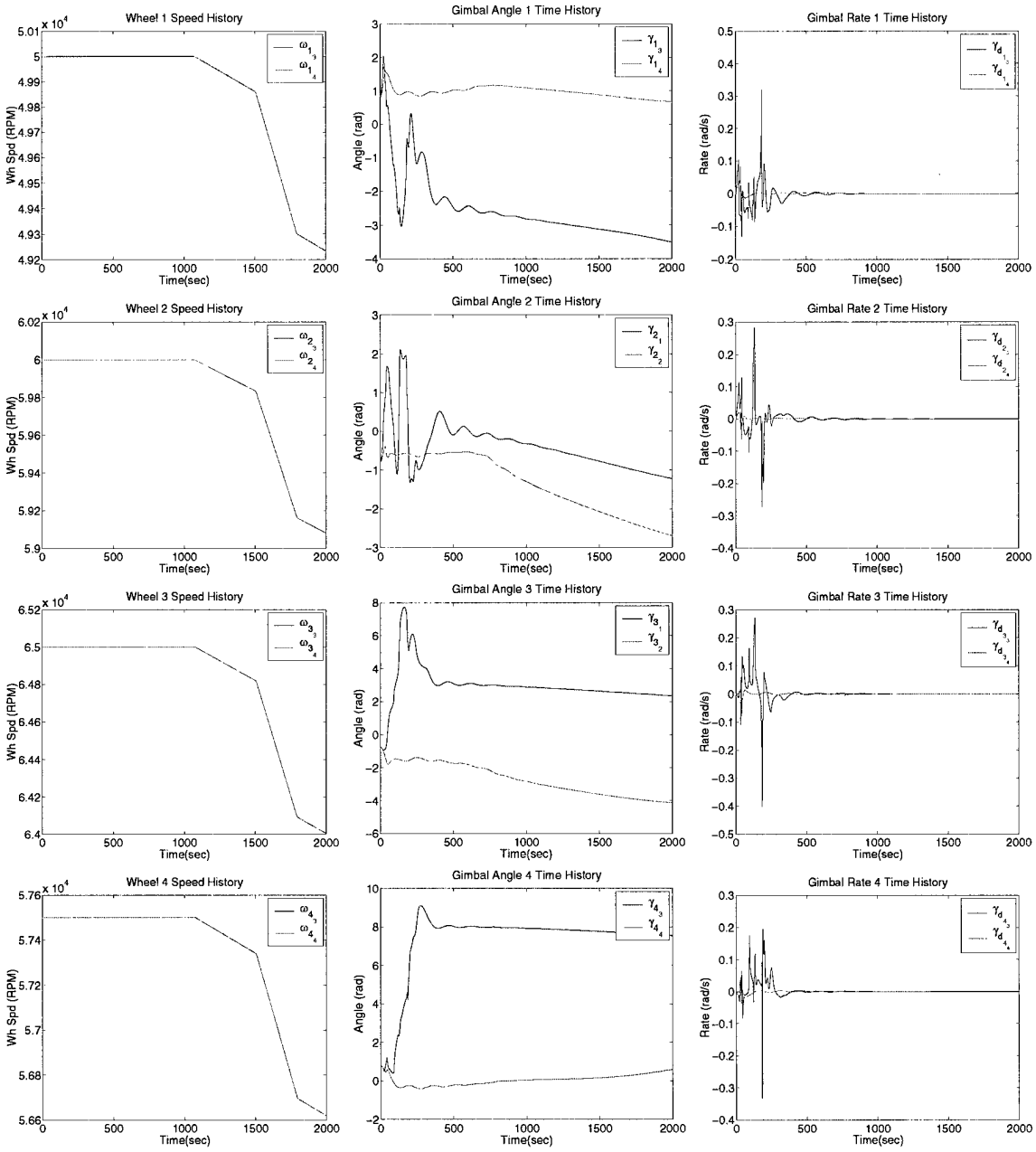

Figure 6.9: Tracking Controller Comparison Actuators Time Response

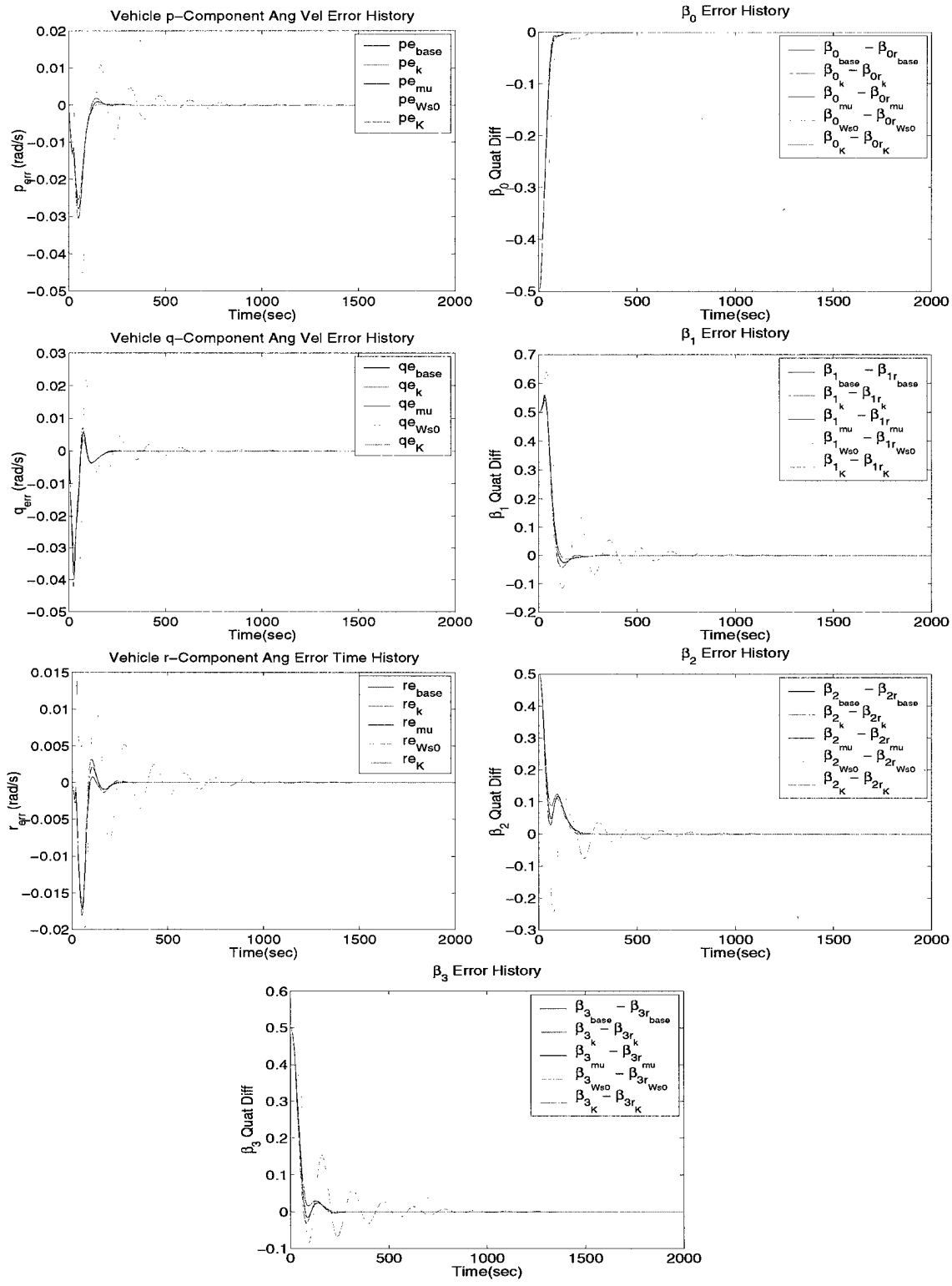

Figure 6.10: Control Parameter Vehicle Time Response Test Results

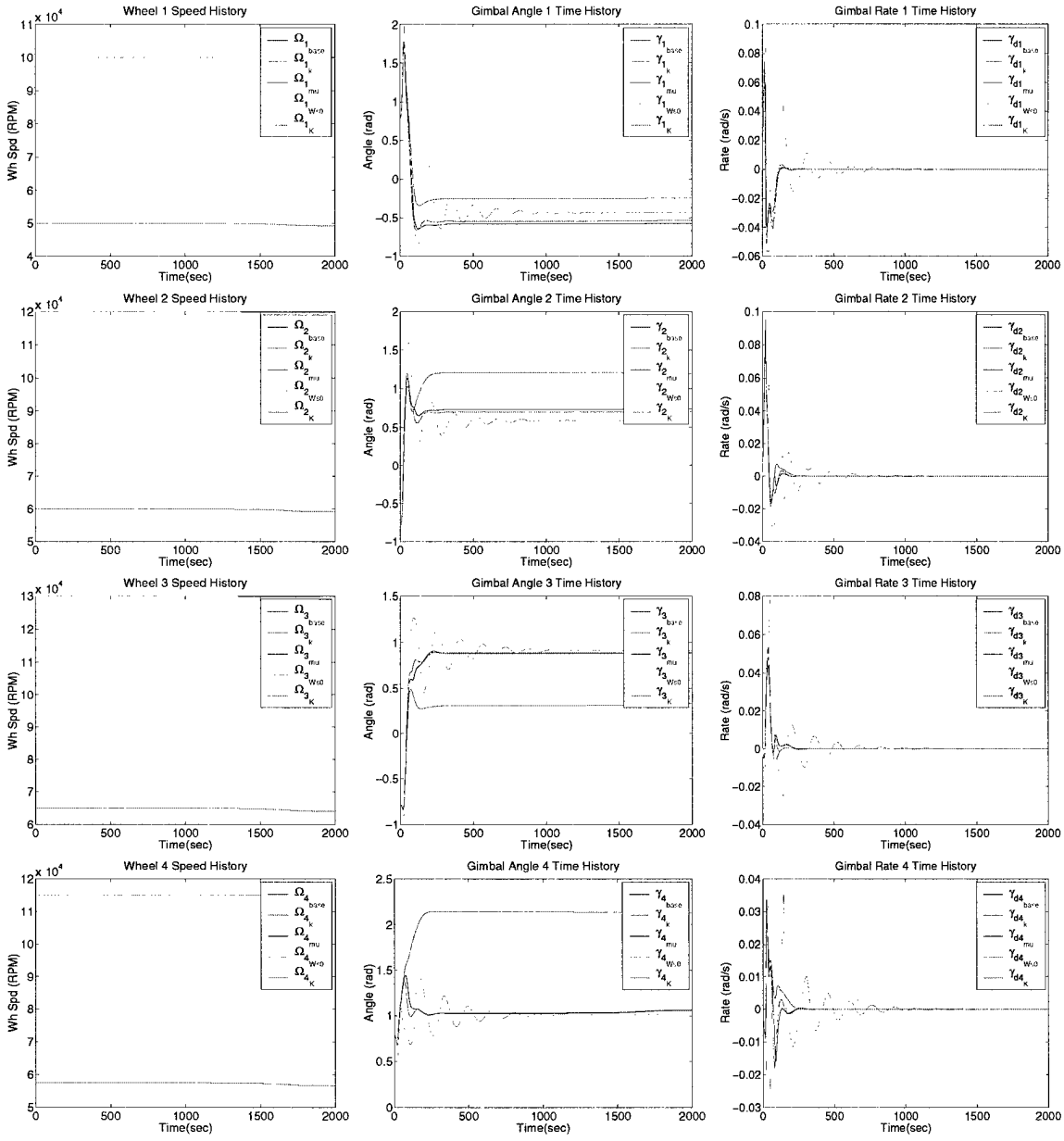

Figure 6.11: Control Parameter Actuators Time Response Test Results

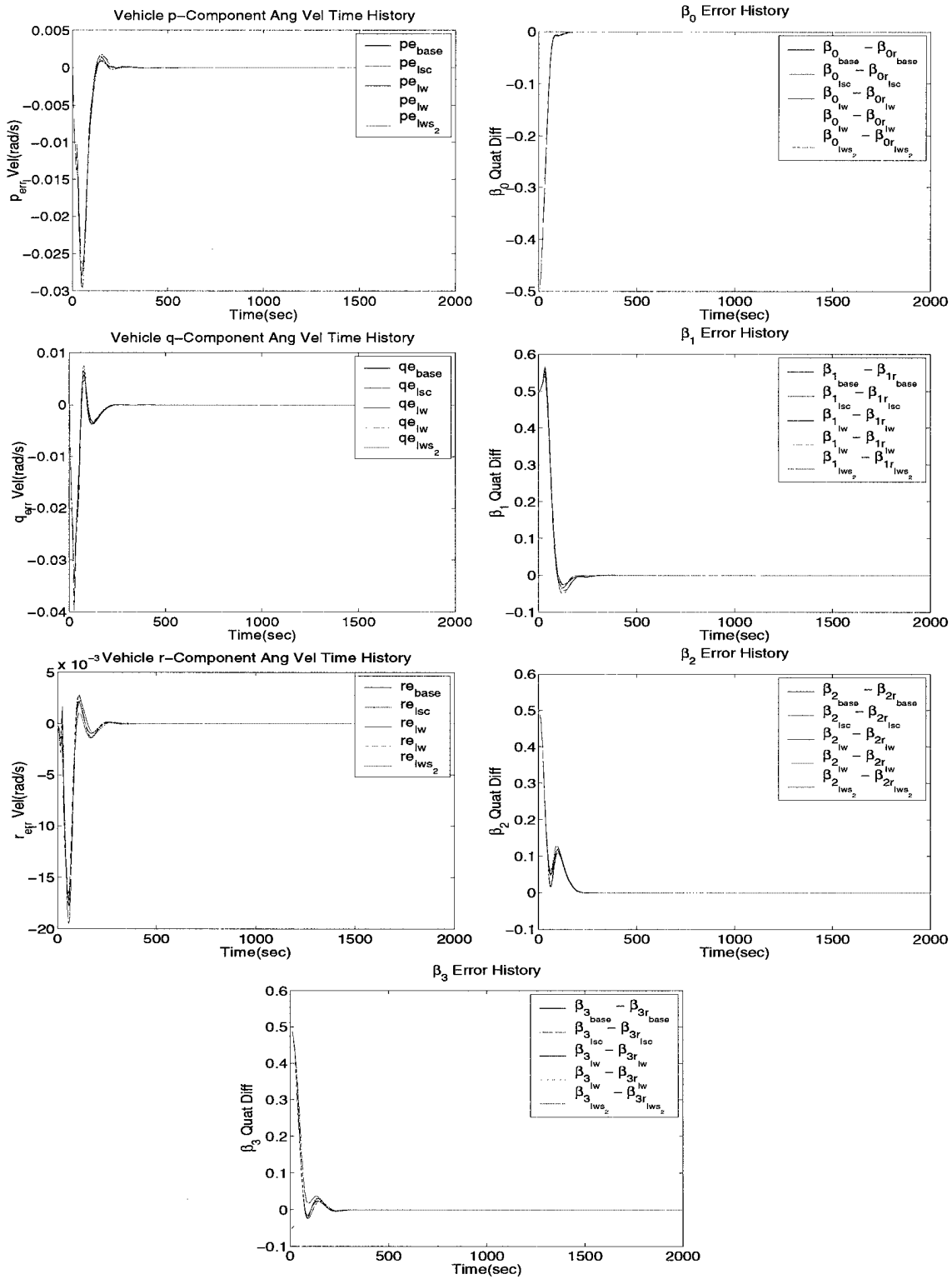

Figure 6.12: System Parameters Vehicle Time Response

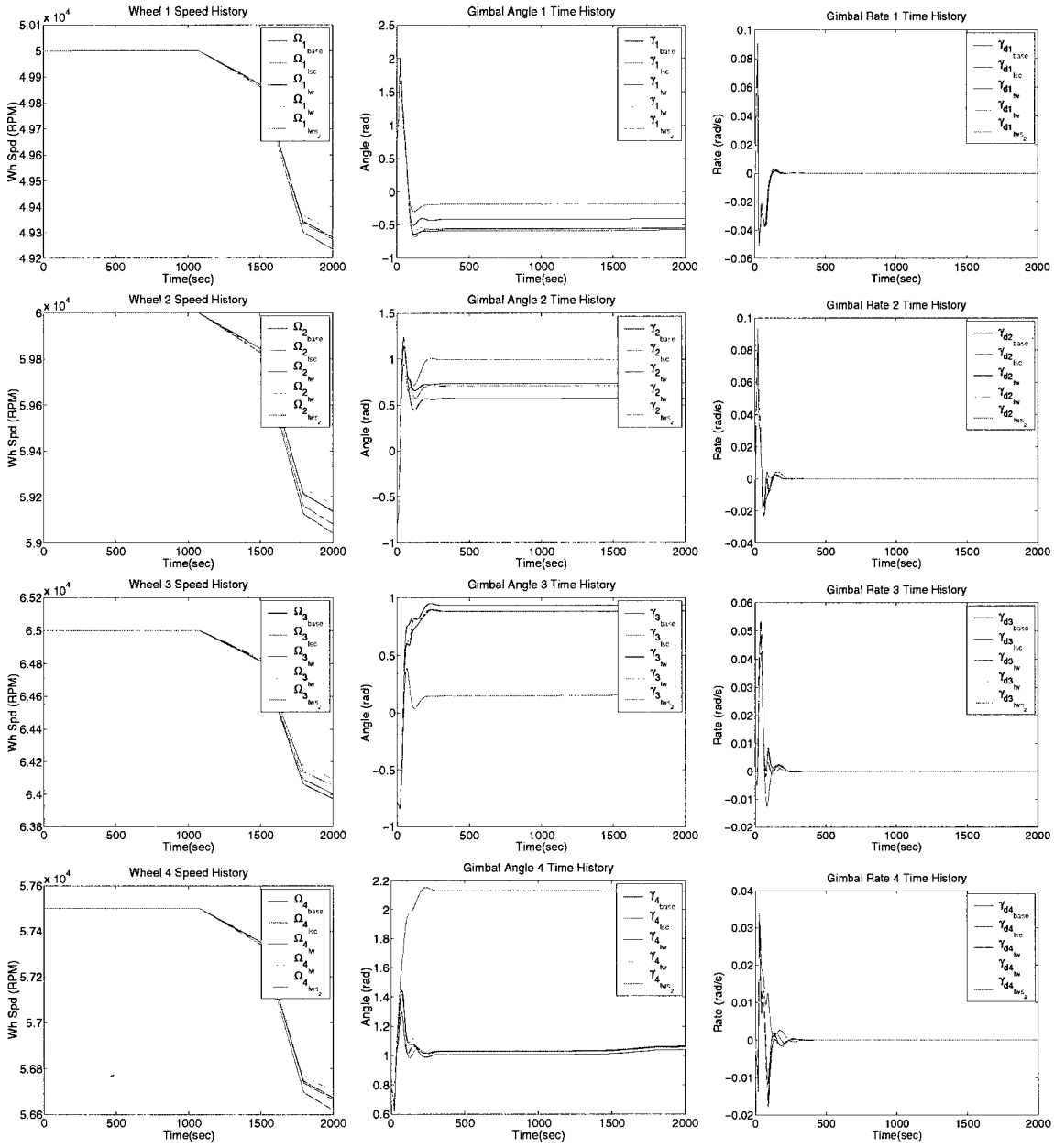

Figure 6.13: System Parameters Actuators Time Response

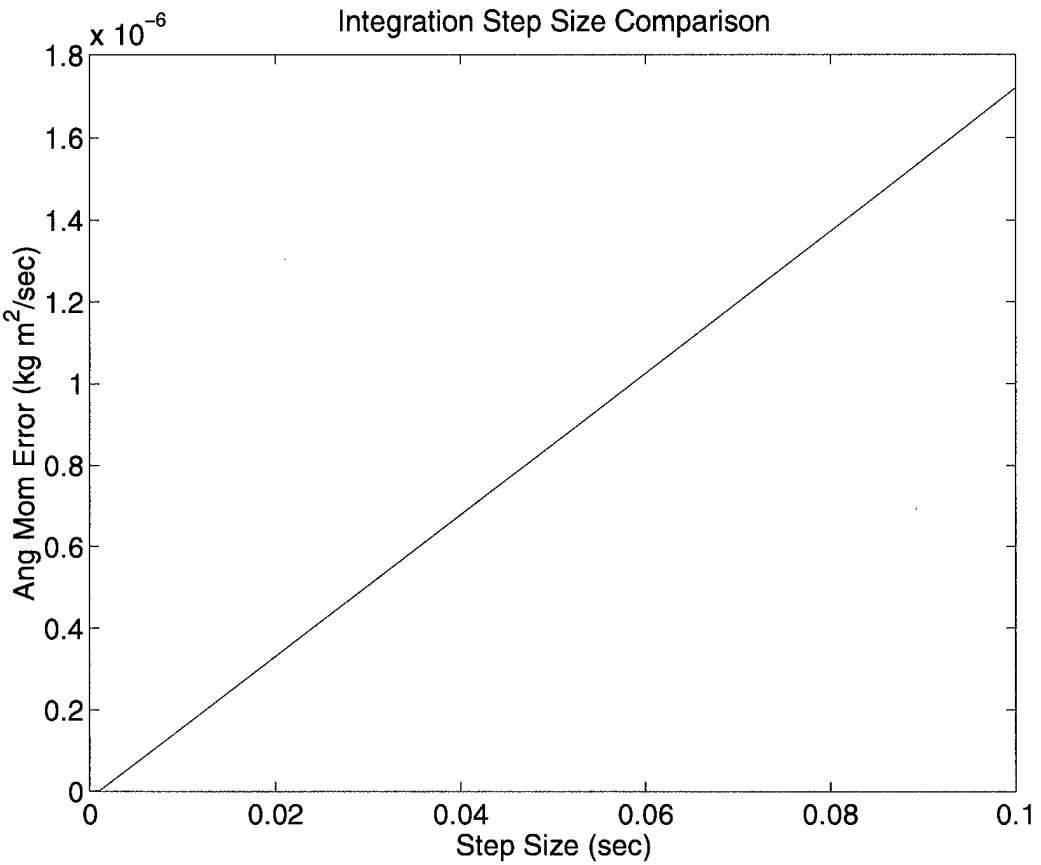

Figure 6.14: Integration Parameter Comparison Actuators Time Response

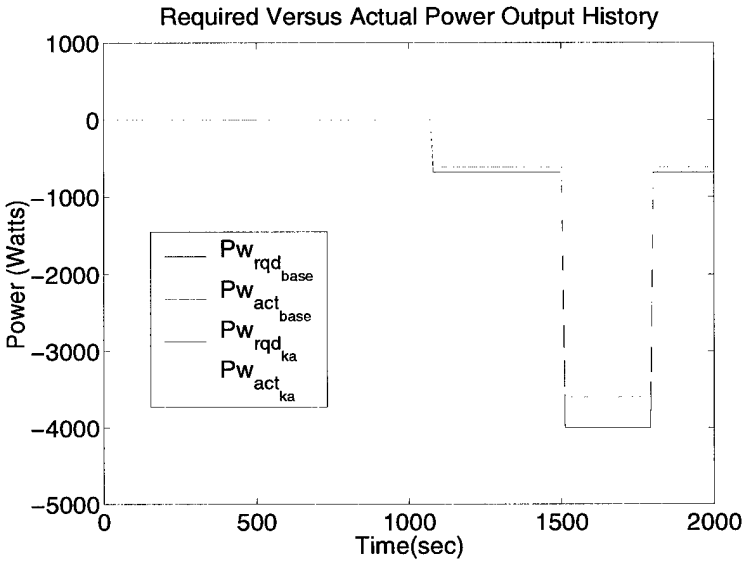

Figure 6.15: Actuator Power Time Response

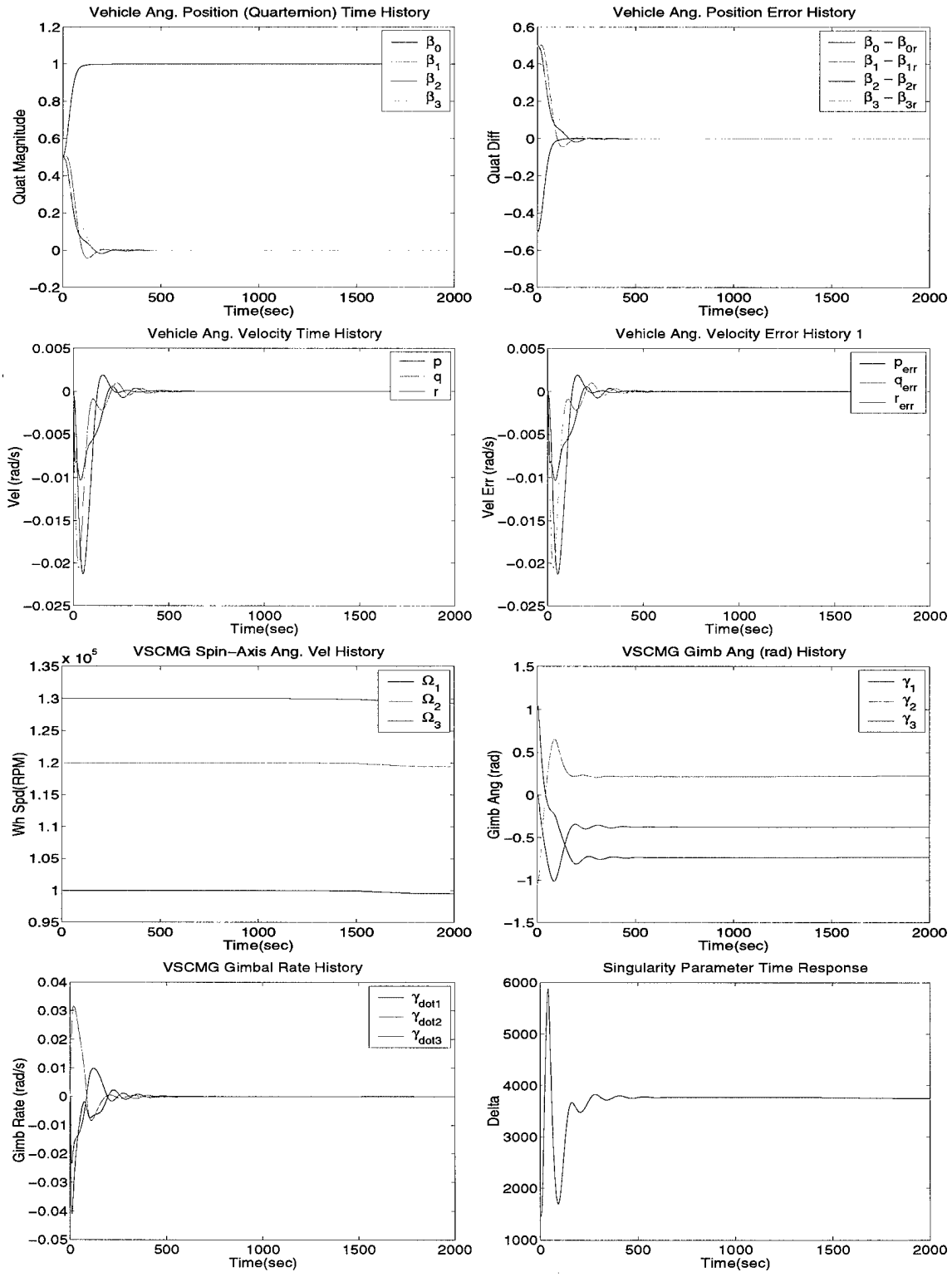

Figure 6.16: 3-Actuator Time Response

CHAPTER 7

CONCLUSIONS

This report has investigated the challenge of using Variable Speed Control Moment Gyroscopes as actuators for simultaneous attitude control and energy storage for spacecraft. After stating the problem, the relevant literature was summarized. This work next recapped the theoretical development of an algorithm for doing simultaneous energy storage and spacecraft attitude control as well as two different control laws for implementing the theory. Then, the design of the VSCMG Workbench, a software tool for implementing this methodology was presented. Fifth, overall system and specific controller parameter tests for analyzing a system employing this system on satellites was described. Finally, several of these tests' results were examined in order to characterize parameter effects for an example simultaneous attitude control/energy storage system.

The resulting control schemes simultaneously provide attitude control torque and energy storage torque while not imparting adverse torques on the satellite. Although both controllers respond in roughly the same amount of time, Controller II seems to provide a much more desirable result as the vehicle and actuator motion

in order to achieved the desired attitude are much smoother than controller I. As stated in chapter 6, the control simulation depends greatly on the actuator initial conditions, primarily the initial wheel speeds. In real applications, there will be an operating range for the wheels which will ensure that the maximal power surge to be handled by the satellite during eclipse will be accommodated.

The test results indicate that some parameters affect the system much more than others. In particular, the gimbal inertias do not seem to have the same impact that the wheel inertias have, especially the wheel spin axis inertia. Also, it seems that the most relevant controller parameters are the control scalar gain, k, and the matrix gain, $\boldsymbol{K}$. The mode weights do not seem to have as much impact as the gains.

CHAPTER 8

RECOMMENDATIONS

This chapter looks at several different areas in which one can further the present research. First, one should look into characterizing simultaneous attitude control and energy storage singularity avoidance methods. Related to this, further research can examine the effects of wheel speeds on the resulting vehicle motion. Specifically, one can examine forcing the equalization of wheel speeds to make a more fault tolerant system. Equal wheel speed solutions would allow for smoother controller operation once a wheel fails (e.g. in a four wheel configuration).

Second, one should convert the user defined SIMULINK S-functions from MATLAB *.m files to C code. This would allow faster simulations that can more accurately be used with Digital Sequence Processing tools for real-time implementation of the simulation.

Third, instituting more realistic inertia scalar matrices should be included in the simulation model and perhaps accounted for in the control law. This includes both the overall satellite inertia as well as the actuator (wheel and gimbal) inertias. This would allow one to study the effects of flywheel imbalance as well as allow the

control designer to assess the validity of assuming the diagonality of the wheel inertia matrices.

Fourth, characterizing different disturbances in the simulation should be done as well. The analysis done in this thesis only scratches the surface as far as disturbance rejection, instead primarily focusing on the problems of regulation and tracking. One could also look into loop shaping and other performance issues such that the control system provides the best system performance.

Fifth, further implementation of the power control loop which includes the power bus, its voltage regulation, and models the solar array power conversion method should be added to the VSCMG Workbench.

Sixth, one needs to investigate the minimal number of VSCMGs required for simultaneous attitude control and energy storage. This would relate to building more fault tolerant combined attitude control/energy storage systems.

Seventh, much more fidelity can be added to the simulation software to add realism. More realistic torque motor transfer functions can be added to make the system respond more like the true satellite system. In this vain, better models of sensors and even sensor data fusion can be added to the system. The simulation's modularity permits this model fidelity to be added in a somewhat straight-forward manner.

Eighth, many different nonlinear control laws such as adaptive control laws, neural networks, and robust control laws can be can be added to the system. This

will serve two purposes. First, it give one more insight into the use of the controllers in order to see which control laws work best with this system. Second, this will help make a great tool for inexperienced control system designers to learn the effects of these control laws and how to design them in a low-threat environment.

Ninth, system flexible modes can be modeled in the simulation as well as in the control. The system developed here was based on assuming all bodies in the system are rigid. Flexible analysis will permit more realistic assessment of the attitude control/energy storage system.

Such a system employing the derived methodology has several applications. Future work will implement this control methodology on a more realistic space vehicle simulation model to be used for controller design, hardware-in-the-loop testing, and vehicle plant modeling. This will allow a low cost attitude control and energy storage system design prior to implementing it on a real satellite. Finally, the culmination of this work will be a ground demonstration of flywheel hardware on a 3 degree-of-freedom spacecraft simulator at AFRL to validate combined attitude control and energy storage functionality.

APPENDIX A

DERIVATION OF THE ATTITUDE DYNAMIC EQUATIONS

In order to derive the dynamic equations of motion presented in chapter ch 3, one should first analyze the motion of a single VSCMG and then extend the results to the multiple VSCMG case. This is done by deriving the angular momentum first and then finding the torque acting on the spacecraft from the angular momentum.

A.1 Angular Momentum

Following [42], define the angular momentum for one VSCMG:

$$\vec{h}^{\text{sys/O}} = \vec{h}^{\text{P/O}} + \vec{h}^{\text{G/O}} + \vec{h}^{\text{W/O}}$$

Using the parallel axis theorem:

$$\vec{h}^{P/O} = \vec{h}^{P/P^*} + \vec{h}^{P^*/O}$$

$$\vec{h}^{G/O} = \vec{h}^{G/G^*} + \vec{h}^{G^*/O}$$

$$\vec{h}^{W/O} = \vec{h}^{W/W^*} + \vec{h}^{W^*/O}$$

Recall that W^* and G^* coincide by assumption. For the sake of completeness, these values have been left in the equations. This distinction is dropped later in this derivation.

Generally, as mentioned in [42],

$$\vec{h}^{X/O} \triangleq \sum_{i=1}^{v} m_i \vec{r}_{ox_i} \times \vec{v}_{x_i/N}$$

So, substitute body X's mass and treat it as a particle. Then, at point X^*:

$$\vec{h}^{X^*/O} \triangleq \sum_{i=1}^{v} m_i \left(\vec{r}_{ox} \times {}^N\vec{v}^x\right) = m_x \left(\vec{r}_{ox} \times {}^N\vec{v}^x\right)$$

$${}^N\vec{v}^x \triangleq \left(\vec{\omega}_{x/N} \times \vec{r}_{ox^*}\right)$$

Assume there's no translational motion and point O is constant in $\mathcal{N}$.

Now,

$$\vec{h}^{X^*/O} = m_x \left(\vec{r}_{ox^*} \times \vec{\omega}_{x/N} \times \vec{r}_{ox^*}\right)$$

Using this fact, the angular momenta of the particles about become

$$\vec{h}^{P^*/O} = m_P\left(\vec{r}_{op^*} \times {}^N\vec{v}^{P^*}\right) = m_P\left(\vec{r}_{op^*} \times \vec{\omega}_{B/N} \times \vec{r}_{op^*}\right)$$

$$\vec{h}^{G^*/O} = m_G\left(\vec{r}_{og^*} \times {}^N\vec{v}^{G^*}\right) = m_G\left(\vec{r}_{og^*} \times \vec{\omega}_{B/N} \times \vec{r}_{og^*}\right)$$

$$\vec{h}^{W^*/O} = m_W\left(\vec{r}_{ow^*} \times {}^N\vec{v}^{W^*}\right) = m_W\left(\vec{r}_{ow^*} \times \vec{\omega}_{B/N} \times \vec{r}_{ow^*}\right) = m_W\left(\vec{r}_{og^*} \times \vec{\omega}_{B/N} \times \vec{r}_{og^*}\right)$$

Since P^*, G^*, and W^* are fixed in $\mathcal{B}$, one can see that the angular velocity of each of the 3 points, expressed in $\mathcal{B}$, is $\vec{\omega}_{B/N}$.

Next, note that

$$\vec{h}^{X^*/O} = m_x\left(\vec{r}_{ox^*} \times \vec{\omega}_{X/N} \times \vec{r}_{ox^*}\right) = \underline{\underline{I}}^{x^*/O} \cdot \vec{\omega}_{Y/N}$$

where $\vec{\omega}_{Y/N}$ is the inertial angular velocity of point - mass X^* and $\underline{\underline{I}}^{X^*/O}$ is the inertia dyadic for a point mass X* with respect to point O, as used by [42]. This is defined as

$$\underline{\underline{I}}^{X^*/O} = m_x\left(\underline{\underline{U}}(\vec{r}^*_{ox} \cdot \vec{r}_{ox^*}) - \vec{r}_{ox^*}\vec{r}_{ox^*}\right)$$

Thus,

$$\underline{\underline{I}}^{x^*/O} \cdot \vec{\omega}_{Y/N} = m_x(\underline{\underline{U}}(\vec{r}_{ox^*} \cdot \vec{r}_{ox^*}) - \vec{r}_{ox^*}\vec{r}_{ox^*}) \cdot \vec{\omega}_{Y/N} = m_x((\vec{r}_{ox^*} \cdot \vec{r}_{ox^*})\underline{\underline{U}} \cdot \vec{\omega}_{Y/N} - \vec{r}_{ox^*}\vec{r}_{ox^*} \cdot \vec{\omega}_{Y/N})$$

$$\underline{\underline{I}}^{x^*/O} \cdot \vec{\omega}_{Y/N} = m_x((\vec{r}_{ox^*} \cdot \vec{r}_{ox^*})\vec{\omega}_{Y/N} - \vec{r}_{ox^*}(\vec{r}_{ox^*} \cdot \vec{\omega}_{Y/N})) = m_x((\vec{r}_{ox^*} \cdot \vec{r}_{ox^*})\vec{\omega}_{Y/N} - (\vec{r}_{ox^*} \cdot \vec{\omega}_{Y/N})\vec{r}_{ox^*})$$

$$\underline{\underline{I}}^{x^*/O} \cdot \vec{\omega}_{Y/N} = m_x(\vec{r}_{ox^*} \times \vec{\omega}_{Y/N} \times \cdot\vec{r}_{ox^*})$$

Now,

$$\vec{h}^{X^*/O} = \underline{\underline{I}}^{x^*/O} \cdot \vec{\omega}_{Y/N}$$

Therefore,

$$\vec{h}^{P^*/O} = \underline{\underline{I}}^{P^*/O} \cdot \vec{\omega}_{B/N}$$

$$\vec{h}^{G^*/O} = \underline{\underline{I}}^{G^*/O} \cdot \vec{\omega}_{B/N}$$

$$\vec{h}^{W^*/O} = \underline{\underline{I}}^{W^*/O} \cdot \vec{\omega}_{B/N}$$

Furthermore, the Central Angular Momentum of a body Z about its own center of mass is defined as

$$\vec{h}^{Z/Z^*} = \underline{\underline{I}}^{Z/Z^*} \cdot \vec{\omega}_{Z/N}$$

So,

$$\vec{h}^{P/P^*} = \underline{\underline{I}}^{P/P^*} \cdot \vec{\omega}_{B/N}$$

$$\vec{h}^{G/G^*} = \underline{\underline{I}}^{G/G^*} \cdot \vec{\omega}_{G/N}$$

$$\vec{h}^{W/W^*} = \underline{\underline{I}}^{W/W^*} \cdot \vec{\omega}_{W/N}$$

Now, calculate the system angular momentum with respect to point O

$$\vec{h}^{sys/O} = \vec{h}^{P/O} + \vec{h}^{G/O} + \vec{h}^{W/O} = \vec{h}^{P/P^*} + \vec{h}^{P^*/O} + \vec{h}^{G/G^*} + \vec{h}^{G^*/O} + \vec{h}^{W/W^*} + \vec{h}^{W^*/O}$$

$$\vec{h}^{sys/O} = \underline{\underline{I}}^{P/P^*} \cdot \vec{\omega}_{B/N} + \underline{\underline{I}}^{P^*/O} \cdot \vec{\omega}_{B/N} + \underline{\underline{I}}^{G^*/O} \cdot \vec{\omega}_{B/N} + \underline{\underline{I}}^{W^*/O} \cdot \vec{\omega}_{B/N} + \underline{\underline{I}}^{G/G^*} \cdot \vec{\omega}_{G/N} + \underline{\underline{I}}^{W/W^*} \cdot \vec{\omega}_{W/N}$$

Re-grouping terms gives

$$\vec{h}^{sys/O} = \left(\underline{\underline{I}}^{P/P^*} + \underline{\underline{I}}^{P^*/O} + \underline{\underline{I}}^{G^*/O} + \underline{\underline{I}}^{W^*/O}\right) \cdot \vec{\omega}_{B/N} + \underline{\underline{I}}^{G/G^*} \cdot \vec{\omega}_{G/N} + \underline{\underline{I}}^{W/G^*} \cdot \vec{\omega}_{W/N}$$

Next, define

$$\underline{\underline{I}}^{SC/O} \triangleq \underline{\underline{I}}^{P/P^*} + \underline{\underline{I}}^{P^*/O} + \underline{\underline{I}}^{G^*/O} + \underline{\underline{I}}^{W^*/O}$$

Note that $\underline{\underline{I}}^{SC/O}$ is the inertia dyadic of all inertia that remains constant in $\mathcal{B}$ over time, it includes the platform inertia with respect to its own center of mass plus the point-mass inertias of bodies P,G,W since they are not located at the system center of mass.

Rewriting the angular momentum, one obtains

$$\vec{h}^{sys/O} = \underline{\underline{I}}^{SC/O} \cdot \vec{\omega}_{B/N} + \underline{\underline{I}}^{G/G^*} \cdot \vec{\omega}_{G/N} + \underline{\underline{I}}^{W/G^*} \cdot \vec{\omega}_{W/N}$$

Next, express the system angular momentum about point O in terms of components in $\mathcal{B}$ as

$$\left(\vec{h}^{sys/O}\right)_B = [I^{SC/O}]_B \left(\vec{\omega}_{B/N}\right)_B + [I^{G/G^*}]_B \left(\vec{\omega}_{G/N}\right)_B + [I^{W/W^*}]_B \left(\vec{\omega}_{W/N}\right)_B$$

Assume $\hat{g}_s, \hat{g}_t, \hat{g}_g$ are central principal axes of bodies W and G for point O. Then the inertia matrices of body G about G^* and body W about G^*, both written as

components in $\mathcal{G}$ are

$$[\mathrm{I}^{G/G^*}]_G = \begin{bmatrix} \mathrm{I}_{G_s} & 0 & 0 \\ 0 & \mathrm{I}_{G_t} & 0 \\ 0 & 0 & \mathrm{I}_{G_g} \end{bmatrix}$$

$$[\mathrm{I}^{W/G^*}]_G = \begin{bmatrix} \mathrm{I}_{W_s} & 0 & 0 \\ 0 & \mathrm{I}_{W_t} & 0 \\ 0 & 0 & \mathrm{I}_{W_g} \end{bmatrix}$$

Now, let $\boldsymbol{L}_{BG}$ represent the coordinate transformation from $\mathcal{G}$ to $\mathcal{B}$ and $\boldsymbol{L}_{GB} = \boldsymbol{L}_{BG}^T$ be the coordinate transformation from $\mathcal{B}$ to $\mathcal{G}$. Additionally, per the angular velocity addition theorem

$$\vec{\omega}_{G/N} = \vec{\omega}_{G/B} + \vec{\omega}_{B/N}$$

and

$$\vec{\omega}_{W/N} = \vec{\omega}_{W/G} + \vec{\omega}_{G/B} + \vec{\omega}_{B/N}$$

where the gimbal structure rotates about G^* and the $\hat{g}_g-$ axis with angular speed $\dot{\gamma}$. The wheel rotates about $\hat{g}_s$ with angular speed Ω. Thus,

$$\begin{aligned} \vec{\omega}_{G/B} &= \dot{\gamma}\hat{g}_g \\ \vec{\omega}_{W/G} &= \Omega\hat{g}_s \end{aligned} \qquad \text{(A.0)}$$

Expressing these two quantities in $\mathcal{G}$

$$\left(\vec{\omega}_{G/B}\right)_G = \begin{bmatrix} 0 \\ 0 \\ \dot{\gamma} \end{bmatrix}$$

$$\left(\vec{\omega}_{W/G}\right)_G = \begin{bmatrix} \Omega \\ 0 \\ 0 \end{bmatrix} \Rightarrow \left(\vec{\omega}_{W/B}\right)_G = \begin{bmatrix} \Omega \\ 0 \\ \dot{\gamma} \end{bmatrix}$$

Next,

$$\left(\vec{\omega}_{W/N}\right)_B = L_{BG}\left(\vec{\omega}_{W/B}\right)_G + \left(\vec{\omega}_{B/N}\right)_B$$

$$\left(\vec{\omega}_{G/N}\right)_B = L_{BG}\left(\vec{\omega}_{G/B}\right)_G + \left(\vec{\omega}_{B/N}\right)_B$$

Thus,

$$\left(\vec{\omega}_{W/N}\right)_B = L_{BG}\left(\vec{\omega}_{W/B}\right)_G + \left(\vec{\omega}_{B/N}\right)_B = L_{BG}\begin{bmatrix} \Omega \\ 0 \\ \dot{\gamma} \end{bmatrix} + \left(\vec{\omega}_{B/N}\right)_B$$

$$\left(\vec{\omega}_{G/B}\right)_B = L_{BG}\left(\vec{\omega}_{G/B}\right)_G + \left(\vec{\omega}_{B/N}\right)_B = L_{BG}\begin{bmatrix} 0 \\ 0 \\ \dot{\gamma} \end{bmatrix} + \left(\vec{\omega}_{B/N}\right)_B$$

Now,

$$[\mathrm{I}^{G/G^*}]]_B = L_{BG}\,[\mathrm{I}^{G/G^*}]_G\,L_{BG}^T$$

$$[\mathrm{I}^{W/G^*}]_B = L_{BG}\,[\mathrm{I}^{W/G^*}]_G\,L_{BG}^T$$

Here note two (out of many) different ways to express the total inertial angular momentum of the system about its center of mass written in terms of components in $\mathcal{B}$, $\left(\tilde{\mathrm{h}}^{\mathrm{sys/O}}\right)_B$, i) Oh/Vidali's method [32] and ii) Schaub's method [40].

Restate the angular momentum equation just derived

$$\left(\vec{h}^{\mathrm{sys/O}}\right) = [\mathrm{I}^{\mathrm{SC/O}}]_B\left(\vec{\omega}_{B/N}\right)_B + [\mathrm{I}^{G/G^*}]_B\left(\vec{\omega}_{G/N}\right)_B + [\mathrm{I}^{W/W^*}]_B\left(\vec{\omega}_{W/N}\right)_B$$

This can also be written as:

$$\left(\vec{h}^{\mathrm{sys/O}}\right)_B = [\mathrm{I}^{\mathrm{SC/O}}]_B\left(\vec{\omega}_{B/N}\right)_B + L_{BG}\,[\mathrm{I}^{G/G^*}]_G\,L_{BG}^T\left(L_{BG}\begin{bmatrix}0\\0\\\dot{\gamma}\end{bmatrix} + \left(\vec{\omega}_{B/N}\right)_B\right)$$

$$+L_{BG}\,[\mathrm{I}^{W/G^*}]_G\,L_{BG}^T\left(L_{BG}\begin{bmatrix}\Omega\\0\\\dot{\gamma}\end{bmatrix} + \left(\vec{\omega}_{B/N}\right)_B\right)$$

Simplifying:

$$\left(\vec{h}^{\text{sys/o}}\right)_B = \left[\mathrm{I}^{\text{sc/o}}\right]_B \left(\vec{\omega}_{B/N}\right)_B + L_{BG}\left[\mathrm{I}^{\text{G/G*}}\right]_G \left(\begin{bmatrix} 0 \\ 0 \\ \dot{\gamma} \end{bmatrix} + L_{BG}^T \left(\vec{\omega}_{B/N}\right)_B\right)$$

$$+L_{BG}\left[\mathrm{I}^{\text{W/G*}}\right]_G \left(\begin{bmatrix} \Omega \\ 0 \\ \dot{\gamma} \end{bmatrix} + L_{BG}^T \left(\vec{\omega}_{B/N}\right)_B\right)$$

Further simplifying yields

$$\left(\vec{h}^{\text{sys/o}}\right)_B = \left[\mathrm{I}^{\text{sc/o}}\right]_B \left(\vec{\omega}_{B/N}\right)_B + L_{BG} \begin{bmatrix} \mathrm{I}_{\mathrm{G_s}} & 0 & 0 \\ 0 & \mathrm{I}_{\mathrm{G_t}} & 0 \\ 0 & 0 & \mathrm{I}_{\mathrm{G_g}} \end{bmatrix} \left(\begin{bmatrix} 0 \\ 0 \\ \dot{\gamma} \end{bmatrix} + L_{BG}^T \left(\vec{\omega}_{B/N}\right)_B\right)$$

$$+L_{BG} \begin{bmatrix} \mathrm{I}_{\mathrm{W_s}} & 0 & 0 \\ 0 & \mathrm{I}_{\mathrm{W_t}} & 0 \\ 0 & 0 & \mathrm{I}_{\mathrm{W_g}} \end{bmatrix} \left(\begin{bmatrix} \Omega \\ 0 \\ \dot{\gamma} \end{bmatrix} + L_{BG}^T \left(\vec{\omega}_{B/N}\right)_B\right)$$

Now, let

$$L_{BG} \triangleq \begin{bmatrix} g_s & g_t & g_g \end{bmatrix}$$

and

$$\left(\vec{\omega}_{B/N}\right)_G = L_{GB}\left(\vec{\omega}_{B/N}\right)_B \triangleq \begin{bmatrix} \omega_s \\ \omega_t \\ \omega_g \end{bmatrix} = \begin{bmatrix} g_s^T\left(\vec{\omega}_{B/N}\right)_B \\ g_t^T\left(\vec{\omega}_{B/N}\right)_B \\ g_g^T\left(\vec{\omega}_{B/N}\right)_B \end{bmatrix}$$

Then let $\left(\vec{h}^{\text{sys/o}}\right)_B = z_1 + z_2 + z_3$ where z_1 is equal to $\left[\text{I}^{\text{sc/o}}\right]_B\left(\vec{\omega}_{B/N}\right)_B$

Deriving z_2

$$z_2 = L_{BG}\begin{bmatrix} \text{I}_{\text{G}_\text{s}} & 0 & 0 \\ 0 & \text{I}_{\text{G}_\text{t}} & 0 \\ 0 & 0 & \text{I}_{\text{G}_\text{g}} \end{bmatrix}\left(\begin{bmatrix} 0 \\ 0 \\ \dot{\gamma} \end{bmatrix} + L_{BG}^T\left(\vec{\omega}_{B/N}\right)_B\right)$$

$$= \begin{bmatrix} g_s & g_t & g_g \end{bmatrix}\begin{bmatrix} \text{I}_{\text{G}_\text{s}} & 0 & 0 \\ 0 & \text{I}_{\text{G}_\text{t}} & 0 \\ 0 & 0 & \text{I}_{\text{G}_\text{g}} \end{bmatrix}\left(\begin{bmatrix} 0 \\ 0 \\ \dot{\gamma} \end{bmatrix} + \begin{bmatrix} g_s^T\left(\vec{\omega}_{B/N}\right)_B \\ g_t^T\left(\vec{\omega}_{B/N}\right)_B \\ g_g^T\left(\vec{\omega}_{B/N}\right)_B \end{bmatrix}\right)$$

$$z_2 = \begin{bmatrix} \text{I}_{\text{G}_\text{s}} g_s & \text{I}_{\text{G}_\text{t}} g_t & \text{I}_{\text{G}_\text{g}} g_g \end{bmatrix}\begin{bmatrix} g_s^T\left(\vec{\omega}_{B/N}\right)_B \\ g_t^T\left(\vec{\omega}_{B/N}\right)_B \\ \dot{\gamma} + g_g^T\left(\vec{\omega}_{B/N}\right)_B \end{bmatrix}$$

$$= \text{I}_{\text{G}_\text{s}} g_s g_s^T\left(\vec{\omega}_{B/N}\right)_B + \text{I}_{\text{G}_\text{t}} g_t g_t^T\left(\vec{\omega}_{B/N}\right)_B + \text{I}_{\text{G}_\text{g}} g_g g_g^T\left(\vec{\omega}_{B/N}\right)_B + \dot{\gamma}\text{I}_{\text{G}_\text{g}} g_g$$

Next, z_3 becomes:

$$z_3 = \boldsymbol{L}_{BG} \begin{bmatrix} \mathrm{I}_{\mathrm{W_s}} & 0 & 0 \\ 0 & \mathrm{I}_{\mathrm{W_t}} & 0 \\ 0 & 0 & \mathrm{I}_{\mathrm{W_g}} \end{bmatrix} \left(\left[\begin{pmatrix} \Omega \\ 0 \\ \dot{\gamma} \end{pmatrix} \right] + \boldsymbol{L}_{BG}^T \left(\vec{\omega}_{B/N} \right)_B \right)$$

$$= \left[\begin{pmatrix} g_s & g_t & g_g \end{pmatrix} \right] \left[\begin{pmatrix} \mathrm{I}_{\mathrm{W_s}} & 0 & 0 \\ 0 & \mathrm{I}_{\mathrm{W_t}} & 0 \\ 0 & 0 & \mathrm{I}_{\mathrm{W_g}} \end{pmatrix} \right] \left(\begin{bmatrix} \Omega \\ 0 \\ \dot{\gamma} \end{bmatrix} + \begin{bmatrix} g_s^T \left(\vec{\omega}_{B/N} \right)_B \\ g_t^T \left(\vec{\omega}_{B/N} \right)_B \\ g_g^T \left(\vec{\omega}_{B/N} \right)_B \end{bmatrix} \right)$$

$$z_3 = \begin{bmatrix} \mathrm{I}_{\mathrm{W_s}} g_s & \mathrm{I}_{\mathrm{W_t}} g_t & \mathrm{I}_{\mathrm{W_g}} g_g \end{bmatrix} \begin{bmatrix} \Omega + g_s^T \left(\vec{\omega}_{B/N} \right)_B \\ g_t^T \left(\vec{\omega}_{B/N} \right)_B \\ \dot{\gamma} + g_g^T \left(\vec{\omega}_{B/N} \right)_B \end{bmatrix}$$

$$= \mathrm{I}_{\mathrm{W_s}} g_s g_s^T \left(\vec{\omega}_{B/N} \right)_B + \mathrm{I}_{\mathrm{W_t}} \hat{g}_t \hat{g}_t^T \left(\vec{\omega}_{B/N} \right)_B + \mathrm{I}_{\mathrm{W_g}} g_g \, g_g^T \left(\vec{\omega}_{B/N} \right)_B$$

$$+ \Omega \mathrm{I}_{\mathrm{W_s}} g_s + \dot{\gamma} \mathrm{I}_{\mathrm{W_g}} g_g$$

From this one can write the angular momentum equation for one VSCMG in a different way [40]

$$\left(\vec{h}^{\mathrm{sys/o}} \right)_B = \left[\mathrm{I}^{\mathrm{SC/o}} \right]_B \left(\vec{\omega}_{B/N} \right)_B + \left(\mathrm{I}_{\mathrm{G_s}} + \mathrm{I}_{\mathrm{W_s}} \right) \hat{g}_s \hat{g}_s^T \left(\vec{\omega}_{B/N} \right)_B + \left(\mathrm{I}_{\mathrm{G_t}} + \mathrm{I}_{\mathrm{W_t}} \right) g_t g_t^T \left(\vec{\omega}_{B/N} \right)_B$$
$$+ \left(\mathrm{I}_{\mathrm{G_g}} + \mathrm{I}_{\mathrm{W_g}} \right) g_g g_g^T \left(\vec{\omega}_{B/N} \right)_B$$
$$+ \dot{\gamma} \left(\mathrm{I}_{\mathrm{G_g}} + \mathrm{I}_{\mathrm{W_g}} \right) g_g + \Omega \mathrm{I}_{\mathrm{W_s}} g_s$$

A.2 Torque

Now, find the total external torque of the system about point O with one VSCMG:

$$\vec{T}^{\text{SYS/O}} = {}^{N}\frac{d}{dt}\left(\vec{h}^{\text{SYS/O}}\right) = {}^{B}\frac{d}{dt}\left(\vec{h}^{\text{SYS/O}}\right) + \left(\vec{\omega}_{B/N}\right)_{B} \times \vec{h}^{\text{SYS/O}}$$

Next, break up this value into 2 terms. The first term is given by:

$${}^{B}\frac{d}{dt}\left(\vec{h}^{\text{SYS/O}}\right) = {}^{B}\frac{d}{dt}\left(\left[\text{I}^{\text{SC/O}}\right]_{B}\left(\vec{\omega}_{B/N}\right)_{B}\right) + {}^{B}\frac{d}{dt}\left[\text{I}^{\text{G/G*}}\right]_{B}\left(\vec{\omega}_{G/N}\right)_{B} + {}^{B}\frac{d}{dt}\left[\text{I}^{\text{W/W*}}\right]_{B}\left(\vec{\omega}_{W/N}\right)_{B}$$

and the second term is calculated as

$$\begin{aligned}
\left(\vec{\omega}_{B/N}\right)_{B} \times \vec{h}^{\text{SYS/O}} = {} & \tilde{\vec{\omega}}_{B/N}\left[\boldsymbol{I}_{sc}\right]_{B}\left(\vec{\omega_{B/N}}\right)_{B} + \tilde{\vec{\omega}}_{B/N}\boldsymbol{L}_{BG}\begin{pmatrix} I_{G_s} & 0 & 0 \\ 0 & I_{G_t} & 0 \\ 0 & 0 & I_{G_g} \end{pmatrix}\begin{pmatrix} 0 \\ 0 \\ \dot{\gamma} \end{pmatrix} \\
& + \tilde{\vec{\omega}}_{B/N}\boldsymbol{L}_{BG}\begin{pmatrix} I_{G_s} & 0 & 0 \\ 0 & I_{G_t} & 0 \\ 0 & 0 & I_{G_g} \end{pmatrix}\boldsymbol{L}_{BG}^{T}\tilde{\vec{\omega}}_{B/N} + \tilde{\vec{\omega}}_{B/N}\boldsymbol{L}_{BG}\begin{pmatrix} I_{W_s} & 0 & 0 \\ 0 & I_{W_t} & 0 \\ 0 & 0 & I_{W_g} \end{pmatrix}\begin{pmatrix} \Omega \\ 0 \\ \dot{\gamma} \end{pmatrix} \\
& + \tilde{\vec{\omega}}_{B/N}\boldsymbol{L}_{BG}\begin{pmatrix} I_{W_s} & 0 & 0 \\ 0 & I_{W_t} & 0 \\ 0 & 0 & I_{W_g} \end{pmatrix}\boldsymbol{L}_{BG}^{T}\tilde{\vec{\omega}}_{B/N}
\end{aligned}$$

Returning to the first term, one can substitute in the angular velocity terms:

$$
{}^{B}\frac{d}{dt}\left(\vec{h}^{\text{SYS/O}}\right) = {}^{B}\frac{d}{dt}\left[\text{I}^{\text{SC/O}}\right]_{B}\left(\vec{\omega}_{B/N}\right)_{B} + {}^{B}\frac{d}{dt}\left(L_{BG}\left[\text{I}^{\text{G/G*}}\right]_{G}L_{BG}^{T}\left(L_{BG}\begin{bmatrix}0\\0\\\dot{\gamma}\end{bmatrix} + \left(\vec{\omega}_{B/N}\right)_{B}\right)\right)
$$

$$
+{}^{B}\frac{d}{dt}\left(L_{BG}\left[\text{I}^{\text{W/G*}}\right]_{G}L_{BG}^{T}\left(L_{BG}\begin{bmatrix}\Omega\\0\\\dot{\gamma}\end{bmatrix} + \left(\vec{\omega}_{B/N}\right)_{B}\right)\right)
$$

The above equation reduces to:

$$
{}^{B}\frac{d}{dt}\left(\vec{h}^{\text{SYS/O}}\right) = {}^{B}\frac{d}{dt}\left[\text{I}^{\text{SC/O}}\right]_{B}\left(\vec{\omega}_{B/N}\right)_{B} + {}^{B}\frac{d}{dt}\left(L_{BG}\left[\text{I}^{\text{G/G*}}\right]_{G}\begin{bmatrix}0\\0\\\dot{\gamma}\end{bmatrix}\right) + {}^{B}\frac{d}{dt}\left(L_{BG}\left[\text{I}^{\text{G/G*}}\right]_{G}L_{BG}^{T}\left(\vec{\omega}_{B/N}\right)_{B}\right)
$$

$$
+{}^{B}\frac{d}{dt}\left(L_{BG}\left[\text{I}^{\text{W/G*}}\right]_{G}\begin{bmatrix}\Omega\\0\\\dot{\gamma}\end{bmatrix}\right) + {}^{B}\frac{d}{dt}\left(L_{BG}\left[\text{I}^{\text{W/G*}}\right]_{G}L_{BG}^{T}\left(\vec{\omega}_{B/N}\right)_{B}\right)
$$

Next, take the derivatives (note: a single dot over a vector epresents its time derivative taken in frame $\mathcal{B}$. A single dot over a scalar represents, of course, its scalar time

derivative):

$$
\begin{aligned}
{}^{B}\frac{d}{dt}\left(\vec{h}^{\text{SYS/O}}\right) &= \left[\text{I}^{\text{SC/O}}\right]_B \left(\dot{\vec{\omega}}_{B/N}\right)_B + \left[\dot{\text{I}}^{\text{SC/O}}\right]_B \left(\vec{\omega}_{B/N}\right)_B + \left(\dot{L}_{BG} \left[\text{I}^{\text{G/G}^*}\right]_G \begin{bmatrix} 0 \\ 0 \\ \dot{\gamma} \end{bmatrix} \right) \\
&+ \left(L_{BG} \left[\dot{\text{I}}^{\text{G/G}^*}\right]_G \begin{bmatrix} 0 \\ 0 \\ \dot{\gamma} \end{bmatrix} \right) + \left(L_{BG} \left[\text{I}^{\text{G/G}^*}\right]_G \begin{bmatrix} 0 \\ 0 \\ \ddot{\gamma} \end{bmatrix} \right) + \left(\dot{L}_{BG} \left[\text{I}^{\text{G/G}^*}\right]_G L_{BG}^T \left(\vec{\omega}_{B/N}\right)_B \right) \\
&+ \left(L_{BG} \left[\dot{\text{I}}^{\text{G/G}^*}\right]_G L_{BG}^T \left(\vec{\omega}_{B/N}\right)_B \right) + \left(L_{BG} \left[\text{I}^{\text{G/G}^*}\right]_G \dot{L}_{BG}^T \left(\vec{\omega}_{B/N}\right)_B \right) + \left(L_{BG} \left[\text{I}^{\text{G/G}^*}\right]_G L_{BG}^T \left(\dot{\vec{\omega}}_{B/N}\right)_B \right) \\
&+ \left(\dot{L}_{BG} \left[\text{I}^{\text{W/G}^*}\right]_G \begin{bmatrix} \Omega \\ 0 \\ \dot{\gamma} \end{bmatrix} \right) + \left(L_{BG} \left[\dot{\text{I}}^{\text{W/G}^*}\right]_G \begin{bmatrix} \Omega \\ 0 \\ \dot{\gamma} \end{bmatrix} \right) + \left(L_{BG} \left[\text{I}^{\text{W/G}^*}\right]_G \begin{bmatrix} \dot{\Omega} \\ 0 \\ \ddot{\gamma} \end{bmatrix} \right) \\
&+ \left(\dot{L}_{BG} \left[\text{I}^{\text{W/G}^*}\right]_G L_{BG}^T \left(\vec{\omega}_{B/N}\right)_B \right) + \left(L_{BG} \left[\dot{\text{I}}^{\text{W/G}^*}\right]_G L_{BG}^T \left(\vec{\omega}_{B/N}\right)_B \right) + \left(L_{BG} \left[\text{I}^{\text{W/G}^*}\right]_G \dot{L}_{BG}^T \left(\vec{\omega}_{B/N}\right)_B \right) \\
&+ \left(L_{BG} \left[\text{I}^{\text{W/G}^*}\right]_G L_{BG}^T \left(\dot{\vec{\omega}}_{B/N}\right)_B \right)
\end{aligned}
$$

Now, substitute the inertia scalar matrices into the equation for I^{G/G^*} and I^{W/G^*}:

$$
\begin{aligned}
{}^{B}\frac{d}{dt}\left(\vec{h}^{\,sys/O}\right) = {}&[I^{SC/O}]_B\left(\dot{\vec{\omega}}_{B/N}\right)_B + \left[\dot{I}^{SC/O}\right]_B\left(\vec{\omega}_{B/N}\right)_B + \left(\dot{L}_{BG}\begin{bmatrix} I_{G_s} & 0 & 0 \\ 0 & I_{G_t} & 0 \\ 0 & 0 & I_{G_g} \end{bmatrix}\begin{bmatrix} 0 \\ 0 \\ \dot{\gamma} \end{bmatrix}\right) \\
&+ \left(L_{BG}\begin{bmatrix} \dot{I}_{G_s} & 0 & 0 \\ 0 & \dot{I}_{G_t} & 0 \\ 0 & 0 & \dot{I}_{G_g} \end{bmatrix}\begin{bmatrix} 0 \\ 0 \\ \dot{\gamma} \end{bmatrix}\right) + \left(L_{BG}\begin{bmatrix} I_{G_s} & 0 & 0 \\ 0 & I_{G_t} & 0 \\ 0 & 0 & I_{G_g} \end{bmatrix}\begin{bmatrix} 0 \\ 0 \\ \ddot{\gamma} \end{bmatrix}\right) \\
&+ \left(\dot{L}_{BG}\begin{bmatrix} I_{G_s} & 0 & 0 \\ 0 & I_{G_t} & 0 \\ 0 & 0 & I_{G_g} \end{bmatrix} L_{BG}^T\left(\vec{\omega}_{B/N}\right)_B\right) + \left(L_{BG}\begin{bmatrix} \dot{I}_{G_s} & 0 & 0 \\ 0 & \dot{I}_{G_t} & 0 \\ 0 & 0 & \dot{I}_{G_g} \end{bmatrix} L_{BG}^T\left(\vec{\omega}_{B/N}\right)_B\right) \\
&+ \left(L_{BG}\begin{bmatrix} I_{G_s} & 0 & 0 \\ 0 & I_{G_t} & 0 \\ 0 & 0 & I_{G_g} \end{bmatrix} \dot{L}_{BG}^T\left(\vec{\omega}_{B/N}\right)_B\right) + \left(L_{BG}\begin{bmatrix} J_s & 0 & 0 \\ 0 & J_t & 0 \\ 0 & 0 & J_g \end{bmatrix} L_{BG}^T\left(\dot{\vec{\omega}}_{B/N}\right)_B\right) \\
&+ \left(\dot{L}_{BG}\begin{bmatrix} I_{W_s} & 0 & 0 \\ 0 & I_{W_t} & 0 \\ 0 & 0 & I_{W_g} \end{bmatrix}\begin{bmatrix} \Omega \\ 0 \\ \dot{\gamma} \end{bmatrix}\right) + \left(L_{BG}\begin{bmatrix} \dot{I}_{W_s} & 0 & 0 \\ 0 & \dot{I}_{W_t} & 0 \\ 0 & 0 & \dot{I}_{W_g} \end{bmatrix}\begin{bmatrix} \Omega \\ 0 \\ \dot{\gamma} \end{bmatrix}\right) \\
&+ \left(L_{BG}\begin{bmatrix} I_{W_s} & 0 & 0 \\ 0 & I_{W_t} & 0 \\ 0 & 0 & I_{W_g} \end{bmatrix}\begin{bmatrix} \dot{\Omega} \\ 0 \\ \ddot{\gamma} \end{bmatrix}\right) + \left(\dot{L}_{BG}\begin{bmatrix} I_{W_s} & 0 & 0 \\ 0 & I_{W_t} & 0 \\ 0 & 0 & I_{W_g} \end{bmatrix} L_{BG}^T\left(\vec{\omega}_{B/N}\right)_B\right) \\
&+ \left(L_{BG}\begin{bmatrix} \dot{I}_{W_s} & 0 & 0 \\ 0 & \dot{I}_{W_t} & 0 \\ 0 & 0 & \dot{I}_{W_g} \end{bmatrix} L_{BG}^T\left(\vec{\omega}_{B/N}\right)_B\right) + \left(L_{BG}\begin{bmatrix} I_{W_s} & 0 & 0 \\ 0 & I_{W_t} & 0 \\ 0 & 0 & I_{W_g} \end{bmatrix} \dot{L}_{BG}^T\left(\vec{\omega}_{B/N}\right)_B\right)
\end{aligned}
$$

Next, we use fact that $\mathrm{I}^{\mathrm{SC/O}}$, $\mathrm{I}^{\mathrm{G/G^*}}$, and $\mathrm{I}^{\mathrm{W/G^*}}$ are constant with respect to $\mathcal{B}$, $\mathcal{G}$, and $\mathcal{G}$, respectively. Thus, the listed inertia derivative terms are zero, so:

$$
\begin{aligned}
{}^{B}\frac{d}{dt}\left(\vec{h}^{\mathrm{sys/O}}\right) &= \left[\mathrm{I}^{\mathrm{SC/O}}\right]_B \left(\dot{\vec{\omega}}_{B/N}\right)_B + \left(\dot{L}_{BG} \begin{bmatrix} I_{G_s} & 0 & 0 \\ 0 & I_{G_t} & 0 \\ 0 & 0 & I_{G_g} \end{bmatrix} \begin{bmatrix} 0 \\ 0 \\ \dot{\gamma} \end{bmatrix} \right) \\
&+ \left(L_{BG} \begin{bmatrix} I_{G_s} & 0 & 0 \\ 0 & I_{G_t} & 0 \\ 0 & 0 & I_{G_g} \end{bmatrix} \begin{bmatrix} 0 \\ 0 \\ \ddot{\gamma} \end{bmatrix} \right) + \left(\dot{L}_{BG} \begin{bmatrix} I_{G_s} & 0 & 0 \\ 0 & I_{G_t} & 0 \\ 0 & 0 & I_{G_g} \end{bmatrix} L_{BG}^T \left(\vec{\omega}_{B/N}\right)_B \right) \\
&+ \left(L_{BG} \begin{bmatrix} I_{G_s} & 0 & 0 \\ 0 & I_{G_t} & 0 \\ 0 & 0 & I_{G_g} \end{bmatrix} \dot{L}_{BG}^T \left(\vec{\omega}_{B/N}\right)_B \right) + \left(\dot{L}_{BG} \begin{bmatrix} I_{W_s} & 0 & 0 \\ 0 & I_{W_t} & 0 \\ 0 & 0 & I_{W_g} \end{bmatrix} \begin{bmatrix} \Omega \\ 0 \\ \dot{\gamma} \end{bmatrix} \right) \\
&+ \left(L_{BG} \begin{bmatrix} I_{W_s} & 0 & 0 \\ 0 & I_{W_t} & 0 \\ 0 & 0 & I_{W_g} \end{bmatrix} \begin{bmatrix} \dot{\Omega} \\ 0 \\ \ddot{\gamma} \end{bmatrix} \right) + \left(\dot{L}_{BG} \begin{bmatrix} I_{W_s} & 0 & 0 \\ 0 & I_{W_t} & 0 \\ 0 & 0 & I_{W_g} \end{bmatrix} L_{BG}^T \left(\vec{\omega}_{B/N}\right)_B \right) \\
&+ \left(L_{BG} \begin{bmatrix} I_{W_s} & 0 & 0 \\ 0 & I_{W_t} & 0 \\ 0 & 0 & I_{W_g} \end{bmatrix} \dot{L}_{BG}^T \left(\vec{\omega}_{B/N}\right)_B \right) + \left(L_{BG} \begin{bmatrix} J_s & 0 & 0 \\ 0 & J_t & 0 \\ 0 & 0 & J_g \end{bmatrix} L_{BG}^T \left(\dot{\vec{\omega}}_{B/N}\right)_B \right)
\end{aligned}
$$

Substituting the fact that $\dot{L}_{BG} = L_{BG}\tilde{\dot{\gamma}}$ and $\dot{L}_{BG}^T = -\tilde{\dot{\gamma}} L_{BG}^T$, where:

$$
\tilde{\dot{\gamma}} = \begin{bmatrix} 0 & -(\dot{\gamma}) & 0 \\ \dot{\gamma} & 0 & 0 \\ 0 & 0 & 0 \end{bmatrix} \tag{A.1}
$$

and also noting that:

$$\tilde{\dot{\gamma}} \begin{bmatrix} I_{G_s} & 0 & 0 \\ 0 & I_{G_t} & 0 \\ 0 & 0 & I_{G_g} \end{bmatrix} \begin{bmatrix} 0 \\ 0 \\ \dot{\gamma} \end{bmatrix} = \begin{bmatrix} 0 & -\dot{\gamma} & 0 \\ \dot{\gamma} & 0 & 0 \\ 0 & 0 & 0 \end{bmatrix} \begin{bmatrix} 0 \\ 0 \\ I_{G_g}\dot{\gamma} \end{bmatrix} = \begin{bmatrix} 0 \\ 0 \\ 0 \end{bmatrix} \tag{A.2}$$

then we are left with:

$$\begin{aligned}
{}^{B}\frac{d}{dt}\left(\vec{h}^{\text{sys/O}}\right) &= [\text{I}^{\text{SC/O}}]_B \left(\dot{\vec{\omega}}_{B/N}\right)_B + \left(L_{BG} \begin{bmatrix} I_{G_s} & 0 & 0 \\ 0 & I_{G_t} & 0 \\ 0 & 0 & I_{G_g} \end{bmatrix} \begin{bmatrix} 0 \\ 0 \\ \ddot{\gamma} \end{bmatrix} \right) \\
&+ \left(L_{BG}(\tilde{\dot{\gamma}}) \begin{bmatrix} I_{G_s} & 0 & 0 \\ 0 & I_{G_t} & 0 \\ 0 & 0 & I_{G_g} \end{bmatrix} L_{BG}^T \left(\vec{\omega}_{B/N}\right)_B \right) + \left(L_{BG} \begin{bmatrix} I_{G_s} & 0 & 0 \\ 0 & I_{G_t} & 0 \\ 0 & 0 & I_{G_g} \end{bmatrix} (-\tilde{\dot{\gamma}}) L_{BG}^T \left(\vec{\omega}_{B/N}\right)_B \right) \\
&+ \left(L_{BG} \begin{bmatrix} I_{G_s} & 0 & 0 \\ 0 & I_{G_t} & 0 \\ 0 & 0 & I_{G_g} \end{bmatrix} L_{BG}^T \left(\dot{\vec{\omega}}_{B/N}\right)_B \right) + \left(L_{BG}(\tilde{\dot{\gamma}}) \begin{bmatrix} I_{W_s} & 0 & 0 \\ 0 & I_{W_t} & 0 \\ 0 & 0 & I_{W_g} \end{bmatrix} \begin{bmatrix} \Omega \\ 0 \\ \dot{\gamma} \end{bmatrix} \right) \\
&+ \left(L_{BG} \begin{bmatrix} I_{W_s} & 0 & 0 \\ 0 & I_{W_t} & 0 \\ 0 & 0 & I_{W_g} \end{bmatrix} \begin{bmatrix} \dot{\Omega} \\ 0 \\ \ddot{\gamma} \end{bmatrix} \right) + \left(L_{BG}(\tilde{\dot{\gamma}}) \begin{bmatrix} I_{W_s} & 0 & 0 \\ 0 & I_{W_t} & 0 \\ 0 & 0 & I_{W_g} \end{bmatrix} L_{BG}^T \left(\vec{\omega}_{B/N}\right)_B \right) \\
&+ \left(L_{BG} \begin{bmatrix} I_{W_s} & 0 & 0 \\ 0 & I_{W_t} & 0 \\ 0 & 0 & I_{W_g} \end{bmatrix} (-\tilde{\dot{\gamma}}) L_{BG}^T \left(\vec{\omega}_{B/N}\right)_B \right) + \left(L_{BG} \begin{bmatrix} I_{W_s} & 0 & 0 \\ 0 & I_{W_t} & 0 \\ 0 & 0 & I_{W_g} \end{bmatrix} L_{BG}^T \left(\dot{\vec{\omega}}_{B/N}\right)_B \right)
\end{aligned}$$

Combining term 1 and term 2 yields:

$$\vec{\tau}^{\text{sys/O}} = {}^{N}\frac{d}{dt}\left(\vec{h}^{\text{sys/O}}\right) = {}^{B}\frac{d}{dt}\left(\vec{h}^{\text{sys/O}}\right) + \left(\vec{\omega}_{B/N}\right)_B \times \vec{h}^{\text{sys/O}} = \left[\text{I}^{\text{SC/O}}\right]_B \left(\dot{\vec{\omega}}_{B/N}\right)_B$$

$$+ \left(L_{BG} \begin{bmatrix} I_{G_s} & 0 & 0 \\ 0 & I_{G_t} & 0 \\ 0 & 0 & I_{G_g} \end{bmatrix} \begin{bmatrix} 0 \\ 0 \\ \ddot{\gamma} \end{bmatrix} \right) + \left(L_{BG}(\tilde{\dot{\gamma}}) \begin{bmatrix} I_{G_s} & 0 & 0 \\ 0 & I_{G_t} & 0 \\ 0 & 0 & I_{G_g} \end{bmatrix} L_{BG}^T \left(\vec{\omega}_{B/N}\right)_B \right)$$

$$+ \left(L_{BG} \begin{bmatrix} I_{G_s} & 0 & 0 \\ 0 & I_{G_t} & 0 \\ 0 & 0 & I_{G_g} \end{bmatrix} (-\tilde{\dot{\gamma}}) L_{BG}^T \left(\vec{\omega}_{B/N}\right)_B \right) + \left(L_{BG} \begin{bmatrix} I_{G_s} & 0 & 0 \\ 0 & I_{G_t} & 0 \\ 0 & 0 & I_{G_g} \end{bmatrix} L_{BG}^T \left(\dot{\vec{\omega}}_{B/N}\right)_B \right)$$

$$+ \left(L_{BG}(\tilde{\dot{\gamma}}) \begin{bmatrix} I_{W_s} & 0 & 0 \\ 0 & I_{W_t} & 0 \\ 0 & 0 & I_{W_g} \end{bmatrix} \begin{bmatrix} \Omega \\ 0 \\ \dot{\gamma} \end{bmatrix} \right) + \left(L_{BG} \begin{bmatrix} I_{W_s} & 0 & 0 \\ 0 & I_{W_t} & 0 \\ 0 & 0 & I_{W_g} \end{bmatrix} \begin{bmatrix} \dot{\Omega} \\ 0 \\ \ddot{\gamma} \end{bmatrix} \right)$$

$$+ \left(L_{BG}(\tilde{\dot{\gamma}}) \begin{bmatrix} I_{W_s} & 0 & 0 \\ 0 & I_{W_t} & 0 \\ 0 & 0 & I_{W_g} \end{bmatrix} L_{BG}^T \left(\vec{\omega}_{B/N}\right)_B \right) + \left(L_{BG} \begin{bmatrix} I_{W_s} & 0 & 0 \\ 0 & I_{W_t} & 0 \\ 0 & 0 & I_{W_g} \end{bmatrix} (-\tilde{\dot{\gamma}}) L_{BG}^T \left(\vec{\omega}_{B/N}\right)_B \right)$$

$$+ \left(L_{BG} \begin{bmatrix} I_{W_s} & 0 & 0 \\ 0 & I_{W_t} & 0 \\ 0 & 0 & I_{W_g} \end{bmatrix} L_{BG}^T \left(\dot{\vec{\omega}}_{B/N}\right)_B \right) + \tilde{\vec{\omega}}_{B/N} \boldsymbol{L}_{BG} \begin{bmatrix} I_{G_s} & 0 & 0 \\ 0 & I_{G_t} & 0 \\ 0 & 0 & I_{G_g} \end{bmatrix} \begin{bmatrix} 0 \\ 0 \\ \dot{\gamma} \end{bmatrix}$$

$$+ \tilde{\vec{\omega}}_{B/N} \boldsymbol{L}_{BG} \begin{bmatrix} J_s & 0 & 0 \\ 0 & J_t & 0 \\ 0 & 0 & J_g \end{bmatrix} \boldsymbol{L}_{BG}^T \tilde{\vec{\omega}}_{B/N} + \tilde{\vec{\omega}}_{B/N} \boldsymbol{L}_{BG} \begin{bmatrix} I_{W_s} & 0 & 0 \\ 0 & I_{W_t} & 0 \\ 0 & 0 & I_{W_g} \end{bmatrix} \begin{bmatrix} \Omega \\ 0 \\ \dot{\gamma} \end{bmatrix} + \tilde{\vec{\omega}}_{B/N} \left[\boldsymbol{I}_{sc}\right]_B \left(\vec{\omega}_{B/N}\right)_B$$

Note that the above equation refers to one VSCMG. We can extend this equation

to the multiple n-VSCMG case by summing all the contributions from the gimbal structures and wheels. If we define:

$$[\mathrm{I}^{\mathrm{TOT/O}}]_B = [\mathrm{I}^{\mathrm{SC/O}}]_B + \left(\sum_{i=1}^{n} L_{BG_i} \left([\mathrm{I}^{\mathrm{G_i/G_i^*}}]_{G_i} + [\mathrm{I}^{\mathrm{W_i/G_i^*}}]_{G_i} \right) L_{G_iB} \right)$$

and substitute $\mathrm{I}^{\mathrm{G/G^*}}$, and $\mathrm{I}^{\mathrm{W/G^*}}$ back into the equations, this can be written more compactly as:

$$\begin{aligned}
\left(\vec{\tau}^{\mathrm{sys/O}}\right)_B &= [I^{\mathrm{TOT/O}}]_B \left(\dot{\vec{\omega}}_{B/N}\right)_B + \left(\tilde{\vec{\omega}}_{B/N}\right)_B [\mathrm{I}^{\mathrm{TOT/O}}]_B \left(\vec{\omega}_{B/N}\right)_B \\
&+ \left(\sum_{i=1}^{n} L_{BG_i} \tilde{\dot{\gamma}}_i [\mathrm{I}^{\mathrm{W_i/G_i^*}}]_{G_i} \left(\begin{bmatrix} \Omega_i \\ 0 \\ \dot{\gamma}_i \end{bmatrix} \right) + \boldsymbol{L}_{G_iB} \left(\vec{\omega}_{B/N}\right)_B \right) \\
&+ \left(\tilde{\vec{\omega}}_{B/N}\right)_B \left(\sum_{i=1}^{n} L_{BG_i} \left([\mathrm{I}^{\mathrm{G_i/G_i^*}}]_{G_i} + [\mathrm{I}^{\mathrm{W_i/G_i^*}}]_{G_i} \right) \begin{bmatrix} 0 \\ 0 \\ \dot{\gamma}_i \end{bmatrix} \right) \\
&+ \left(\sum_{i=1}^{n} L_{BG_i} (\tilde{\dot{\gamma}}_i) [\mathrm{I}^{\mathrm{G_i/G_i^*}}]_{G_i} L_{G_iB} - L_{BG_i} \left([\mathrm{I}^{\mathrm{G_i/G_i^*}}]_{G_i} + [\mathrm{I}^{\mathrm{W_i/G_i^*}}]_{G_i} \right) (\tilde{\dot{\gamma}}_i) L_{G_iB} \right) \left(\vec{\omega}_{B/N}\right)_B \\
&+ \left(\sum_{i=1}^{n} L_{BG_i} [\mathrm{I}^{\mathrm{G_i/G_i^*}}]_{G_i} \begin{bmatrix} 0 \\ 0 \\ \ddot{\gamma}_i \end{bmatrix} \right) + \left(\sum_{i=1}^{n} L_{BG_i} [\mathrm{I}^{\mathrm{W_i/G_i^*}}]_{G_i} \begin{bmatrix} 0 \\ 0 \\ \ddot{\gamma}_i \end{bmatrix} \right) + \left(\sum_{i=1}^{n} L_{BG_i} [\mathrm{I}^{\mathrm{W_i/G_i^*}}]_{G_i} \begin{bmatrix} \dot{\Omega}_i \\ 0 \\ 0 \end{bmatrix} \right) \\
&+ \left(\tilde{\vec{\omega}}_{B/N}\right)_B \left(\sum_{i=1}^{n} L_{BG_i} [\mathrm{I}^{\mathrm{W_i/G_i^*}}]_{G_i} \begin{bmatrix} \Omega_i \\ 0 \\ 0 \end{bmatrix} \right)
\end{aligned}$$

A.3 Simplifying the Torque Equation

Next, let

$$\boldsymbol{D}_1 \begin{bmatrix} \dot{\gamma}_1 \\ \dot{\gamma}_2 \\ \cdots \\ \dot{\gamma}_n \end{bmatrix} \triangleq \left(\sum_{i=1}^{n} L_{BG_i}(\tilde{\dot{\gamma}}_i) \left[\mathrm{I}^{\mathrm{W_i/G_i^*}}\right]_{G_i} \left(\begin{bmatrix} \Omega_i \\ 0 \\ \dot{\gamma}_i \end{bmatrix} + L_{G_iB} \left(\vec{\omega}_{B/N}\right)_B \right) \right)$$

$$D_2 \begin{bmatrix} \dot{\gamma}_1 \\ \dot{\gamma}_2 \\ \cdots \\ \dot{\gamma}_n \end{bmatrix} \triangleq \left(\tilde{\vec{\omega}}_{B/N}\right)_B \left(\sum_{i=1}^{n} L_{BG_i} \left(\left[\mathrm{I}^{\mathrm{G_i/G_i^*}}\right]_{G_i} + \left[\mathrm{I}^{\mathrm{W_i/G_i^*}}\right]_{G_i} \right) \begin{bmatrix} 0 \\ 0 \\ \dot{\gamma}_i \end{bmatrix} \right)$$

$$D_3 \begin{bmatrix} \dot{\gamma}_1 \\ \dot{\gamma}_2 \\ \cdots \\ \dot{\gamma}_n \end{bmatrix} \triangleq \left(\sum_{i=1}^{n} L_{BG_i}(\tilde{\dot{\gamma}}_i) \left[\mathrm{I}^{\mathrm{G_i/G_i^*}}\right]_{G_i} L_{G_iB} - L_{BG_i} \left(\left[\mathrm{I}^{\mathrm{G_i/G_i^*}}\right]_{G_i} + \left[\mathrm{I}^{\mathrm{W_i/G_i^*}}\right]_{G_i} \right) (\tilde{\dot{\gamma}}_i) L_{G_iB} \right) \left(\vec{\omega}_{B/N}\right)_B$$

$$B_1 \begin{bmatrix} \ddot{\gamma}_1 \\ \ddot{\gamma}_2 \\ \cdots \\ \ddot{\gamma}_n \end{bmatrix} \triangleq \left(\sum_{i=1}^{n} L_{BG_i} \left[\mathrm{I}^{\mathrm{G_i/G_i^*}}\right]_{G_i} \begin{bmatrix} 0 \\ 0 \\ \ddot{\gamma}_i \end{bmatrix} \right)$$

$$B_2 \begin{bmatrix} \ddot{\gamma}_1 \\ \ddot{\gamma}_2 \\ \cdots \\ \ddot{\gamma}_n \end{bmatrix} \triangleq \left(\sum_{i=1}^{n} L_{BG_i} \left[\mathrm{I}^{\mathrm{W_i/G_i^*}}\right]_{G_i} \begin{bmatrix} 0 \\ 0 \\ \ddot{\gamma}_i \end{bmatrix} \right)$$

$$E\begin{bmatrix}\dot{\Omega}_1\\ \dot{\Omega}_2\\ \cdots\\ \dot{\Omega}_n\end{bmatrix} \triangleq \left(\sum_{i=1}^{n} L_{BG_i}\left[\mathrm{I}^{\mathrm{W_i/G_i^*}}\right]_{G_i}\begin{bmatrix}\dot{\Omega}_i\\ 0\\ 0\end{bmatrix}\right)$$

$$F\begin{bmatrix}\Omega_1\\ \Omega_2\\ \cdots\\ \Omega_n\end{bmatrix} \triangleq \left(\tilde{\vec{\omega}}_{B/N}\right)_B\left(\sum_{i=1}^{n} L_{BG_i}\left[\mathrm{I}^{\mathrm{W_i/G_i^*}}\right]_{G_i}\begin{bmatrix}\Omega_i\\ 0\\ 0\end{bmatrix}\right)$$

This yields the system dynamic motion equations (presented chapter 3

$$\left(\vec{\tau}^{\mathrm{sys/O}}\right)_B = \left[\mathrm{I}^{\mathrm{TOT/O}}\right]_B\left(\dot{\vec{\omega}}_{B/N}\right)_B + \left(\tilde{\vec{\omega}}_{B/N}\right)_B\left[\mathrm{I}^{\mathrm{TOT/O}}\right]_B\left(\vec{\omega}_{B/N}\right)_B$$

$$+(D_1+D_2+D_3)\begin{bmatrix}\dot{\gamma}_1\\ \dot{\gamma}_2\\ \cdots\\ \dot{\gamma}_n\end{bmatrix} + (B_1+B_2)\begin{bmatrix}\ddot{\gamma}_1\\ \ddot{\gamma}_2\\ \cdots\\ \ddot{\gamma}_n\end{bmatrix} + E\begin{bmatrix}\dot{\Omega}_1\\ \dot{\Omega}_2\\ \cdots\\ \dot{\Omega}_n\end{bmatrix} + F\begin{bmatrix}\Omega_1\\ \Omega_2\\ \cdots\\ \Omega_n\end{bmatrix}$$

APPENDIX B

SIMPLIFICATION OF THE ATTITUDE DYNAMICS – NOTATIONAL DERIVATIONS

This appendix presents the derived simplification of the dynamic equation of motion presented in chapter 3. In order to derive this result, one must first review the relevant matrices liberally used in this derivation.

$$G_g = \begin{bmatrix} g_{g_1} & \cdots & g_{g_n} \end{bmatrix}$$

$$G_{gm} = \begin{bmatrix} g_{g_1} & g_{g_1} & g_{g_1} & \cdots & g_{g_n} & g_{g_n} & g_{g_n} \end{bmatrix}$$

$$G_{gd} = \text{blockdiag}\left\{ \begin{bmatrix} g_{g_1} & \cdots & g_{g_n} \end{bmatrix} \right\}$$

$$I_{G_{gk}} = \begin{bmatrix} I_{G_{g1}} & \cdots & I_{G_{gn}} \end{bmatrix}$$

$$I_{G_{gd}} = \text{diag}\left\{ I_{G_{gk}} \right\}$$

These hold for the spin and transverse axes of the wheels and gimbals as well.

Since

$$J_{Gg} \triangleq I_{Gg} + I_{Wg}$$

one can define the following

$$J_{G_{gd}} = I_{G_{gd}} + I_{W_{gd}}$$

$$\omega_d = \text{blockdiag}\left\{\left[\left(\tilde{\vec{\omega}}_{B/N}\right)_B \left(\tilde{\vec{\omega}}_{B/N}\right)_B \left(\tilde{\vec{\omega}}_{B/N}\right)_B \cdots \left(\tilde{\vec{\omega}}_{B/N}\right)_B\right]\right\}$$

Now, derive explicit expressions for the B_1, B_2,E, F, D_1, D_2, and D_3 matrices:

$$B_1 \begin{bmatrix} \ddot{\gamma}_1 \\ \ddot{\gamma}_2 \\ \cdots \\ \ddot{\gamma}_n \end{bmatrix} \triangleq$$

$$\left(\sum_{i=1}^{n} L_{BG_i} \begin{bmatrix} \boldsymbol{I}_{\mathrm{I_{s_i}}} & 0 & 0 \\ 0 & \mathrm{I_{G_{t_i}}} & 0 \\ 0 & 0 & \mathrm{I_{G_{g_i}}} \end{bmatrix} \begin{bmatrix} 0 \\ 0 \\ \ddot{\gamma}_i \end{bmatrix} \right) = \left(\sum_{i=1}^{n} \begin{bmatrix} g_{s_i} & g_{t_i} & g_{g_i} \end{bmatrix} \begin{bmatrix} \mathrm{I_{G_{s_i}}} & 0 & 0 \\ 0 & \mathrm{I_{G_{t_i}}} & 0 \\ 0 & 0 & \mathrm{I_{G_{g_i}}} \end{bmatrix} \begin{bmatrix} 0 \\ 0 \\ \ddot{\gamma}_i \end{bmatrix} \right)$$

$$= \left(\sum_{i=1}^{n} \begin{bmatrix} g_{s_i} & g_{t_i} & g_{g_i} \end{bmatrix} \begin{bmatrix} 0 \\ 0 \\ \mathrm{I_{G_{g_i}}} \ddot{\gamma}_i \end{bmatrix} \right) = \left(\sum_{i=1}^{n} \mathrm{I_{G_{g_i}}} \ddot{\gamma}_i g_{g_i} \right) = \mathrm{I_{G_{g_1}}} g_{g_1} \ddot{\gamma}_1 + \mathrm{I_{G_{g_2}}} g_{g_2} \ddot{\gamma}_2 + \ldots + \mathrm{I_{G_{gn}}} g_{g_n} \ddot{\gamma}_n$$

$$= \begin{bmatrix} g_{g_1} & g_{g_2} & \cdots & g_{g_n} \end{bmatrix} \begin{bmatrix} \mathrm{I_{G_{g_1}}} & 0 & 0 & 0 \\ 0 & \mathrm{I_{G_{g_2}}} & 0 & 0 \\ 0 & 0 & \ddots & 0 \\ 0 & 0 & 0 & \mathrm{I_{G_{gn}}} \end{bmatrix} \begin{bmatrix} \ddot{\gamma}_1 \\ \ddot{\gamma}_2 \\ \ldots \\ \ddot{\gamma}_n \end{bmatrix}$$

$$\Rightarrow B_1 = G_g I_{G_{g_d}} = \begin{bmatrix} (g_{g_1} \otimes \mathrm{I_{G_{g_1}}}) & (g_{g_2} \otimes \mathrm{I_{G_{g_2}}}) & \cdots & (g_{g_n} \otimes \mathrm{I_{G_{gn}}}) \end{bmatrix}$$

The derivation is identical for B_2, E, and F except one uses $I_{W_{gd}}$, $I_{W_{sd}}$, G_s, and $I_{W_{sd}}$ plus G_s pre-multiplied by $\tilde{\omega}$ to find the respective matrices. Furthermore, D_2 is found similarly to B_4

The matrices derived are summarized as

$$B_1 = G_g I_{G_{gd}} = \left[\begin{array}{cccc} (g_{g1} \otimes \mathrm{I}_{\mathrm{G}_{\mathrm{g}_1}}) & (g_{g2} \otimes \mathrm{I}_{\mathrm{G}_{\mathrm{g}_2}}) & \cdots & (g_{gn} \otimes \mathrm{I}_{\mathrm{G}_{\mathrm{gn}}}) \end{array} \right]$$

$$B_2 = G_g I_{W_{gd}} = \left[\begin{array}{cccc} (g_{g1} \otimes \mathrm{I}_{\mathrm{W}_{\mathrm{g}_1}}) & (g_{g_2} \otimes \mathrm{I}_{\mathrm{W}_{\mathrm{g}_2}}) & \cdots & (g_{g_n} \otimes \mathrm{I}_{\mathrm{W}_{\mathrm{gn}}}) \end{array} \right]$$

$$E = G_s I_{W_{sd}} = \left[\begin{array}{cccc} (g_{s1} \otimes \mathrm{I}_{\mathrm{W}_{s_1}}) & (g_{s_2} \otimes \mathrm{I}_{\mathrm{W}_{s_2}}) & \cdots & (g_{s_n} \otimes \mathrm{I}_{\mathrm{W}_{s\mathrm{n}}}) \end{array} \right]$$

$$F = \left(\tilde{\vec{\omega}}_{B/N}\right)_B G_s I_{W_{sd}} = \left(\tilde{\vec{\omega}}_{B/N}\right)_B \left[\begin{array}{cccc} (g_{s1} \otimes \mathrm{I}_{\mathrm{W}_{s_1}}) & (g_{s_2} \otimes \mathrm{I}_{\mathrm{W}_{s_2}}) & \cdots & (g_{s_n} \otimes \mathrm{I}_{\mathrm{W}_{s\mathrm{n}}}) \end{array} \right]$$

$$D_2 = \left(\tilde{\vec{\omega}}_{B/N}\right)_B G_g J_{gd} = \left(\tilde{\vec{\omega}}_{B/N}\right)_B \left[\begin{array}{cccc} (g_{g_1} \otimes \mathrm{J}_{\mathrm{g}_1}) & (g_{g_2} \otimes \mathrm{J}_{\mathrm{g}_2}) & \cdots & (g_{g_n} \otimes \mathrm{J}_{\mathrm{g}_n}) \end{array} \right]$$

APPENDIX C

CONTROL LAW DERIVATION DETAILS

C.1 Controller I

In this section, support details in the derivation of the control law for controller I (derived in Chapter 3) is presented. Note that this control law is very similar to that used in references [37], [32], and [39]. It's main assumptions are that one is interested in regulation of the vehicle about some fixed inertial reference and can thus neglect orbital motion. Since most of the control law is derived in Chapter 3, only details not included earlier are described here.

First, note that

$$\hat{e}_1 = \beta - \beta_r \tag{C.1}$$

and

$$V_1 = k\hat{e}_1^T\hat{e}_1 \tag{C.2}$$

In addition, if one defines

$$\boldsymbol{Q}(\beta) \triangleq \begin{bmatrix} -\beta_1 & -\beta_2 & -\beta_3 \\ \beta_0 & -\beta_3 & \beta_2 \\ \beta_3 & \beta_0 & -\beta_1 \\ -\beta_2 & \beta_1 & \beta_0 \end{bmatrix} \tag{C.3}$$

where

$$\beta \triangleq \begin{bmatrix} \beta_0 \\ \beta_1 \\ \beta_2 \\ \beta_3 \end{bmatrix} \tag{C.4}$$

and

$$\beta_r \triangleq \begin{bmatrix} \beta_{r_0} \\ \beta_{r_1} \\ \beta_{r_2} \\ \beta_{r_3} \end{bmatrix} \tag{C.5}$$

results in

$$\boldsymbol{Q}(\beta_r) \triangleq \begin{bmatrix} -\beta_{r_1} & -\beta_{r_2} & -\beta_{r_3} \\ \beta_{r_0} & -\beta_{r_3} & \beta_{r_2} \\ \beta_{r_3} & \beta_{r_0} & -\beta_{r_1} \\ -\beta_{r_2} & \beta_{r_1} & \beta_{r_0} \end{bmatrix} \tag{C.6}$$

Then,

$$\boldsymbol{Q}^T(\beta_r)\,\beta = -\boldsymbol{Q}^T(\beta)\,\beta_r \tag{C.7}$$

This is true since the left hand side of the above equation is equal to:

$$\begin{bmatrix} -\beta_{r_1} & -\beta_{r_2} & -\beta_{r_3} \\ -\beta_{r_0} & -\beta_{r_3} & \beta_{r_2} \\ \beta_{r_3} & \beta_{r_0} & -\beta_{r_1} \\ -\beta_{r_2} & \beta_{r_1} & \beta_{r_0} \end{bmatrix}^T \begin{bmatrix} \beta_0 \\ \beta_1 \\ \beta_2 \\ \beta_3 \end{bmatrix} = \begin{bmatrix} -\beta_{r_1}\beta_0 + \beta_{r_0}\beta_1 + \beta_{r_3}\beta_2 - \beta_{r_2}\beta_3 \\ -\beta_{r_2}\beta_0 - \beta_{r_3}\beta_1 + \beta_{r_0}\beta_2 + \beta_{r_1}\beta_3 \\ -\beta_{r_3}\beta_0 + \beta_{r_2}\beta_1 - \beta_{r_1}\beta_2 + \beta_{r_0}\beta_3 \end{bmatrix} \tag{C.8}$$

Now, one computes the right hand side:

$$-\begin{bmatrix} -\beta_1 & \beta_0 & \beta_3 & -\beta_2 \\ -\beta_2 & -\beta_3 & \beta_0 & \beta_1 \\ -\beta_3 & \beta_2 & -\beta_1 & \beta_0 \end{bmatrix} \begin{bmatrix} \beta_{r_0} \\ \beta_{r_1} \\ \beta_{r_2} \\ \beta_{r_3} \end{bmatrix} = -\begin{bmatrix} -\beta_1\beta_{r_0} + \beta_0\beta_{r_1} + \beta_3\beta_{r_2} - \beta_2\beta_{r_3} \\ -\beta_2\beta_{r_0} - \beta_3\beta_{r_1} + \beta_0\beta_{r_2} + \beta_1\beta_{r_3} \\ -\beta_3\beta_{r_0} + \beta_2\beta_{r_1} - \beta_1\beta_{r_2} + \beta_0\beta_{r_3} \end{bmatrix} \tag{C.9}$$

Slightly rearranging this result yields:

$$\begin{bmatrix} -\beta_0\beta_{r_1} + \beta_1\beta_{r_0} - \beta_3\beta_{r_2} + \beta_2\beta_{r_3} \\ \beta_2\beta_{r_0} + \beta_3\beta_{r_1} - \beta_0\beta_{r_2} - \beta_1\beta_{r_3} \\ \beta_3\beta_{r_0} - \beta_2\beta_{r_1} + \beta_1\beta_{r_2} - \beta_0\beta_{r_3} \end{bmatrix} \tag{C.10}$$

Now, comparing the left hand side to the right hand side verifies that:

$$\boldsymbol{Q}^T(\beta_r)\,\beta = -\boldsymbol{Q}^T(\beta)\,\beta_r \tag{C.11}$$

These relationships are useful in the subsequent derivation. One should also note that since $\hat{e}_1^T\dot{\hat{e}}_1$ is a scalar, then its transpose is equal to $\dot{\hat{e}}_1^T\hat{e}_1$. This relationship will also be needed here.

C.1.1 Lyapunov Equation Analysis

Realize that

$$\dot{V}_1 = k\dot{\hat{e}}_1^T\hat{e}_1 + k\hat{e}_1^T\dot{\hat{e}}_1 \tag{C.12}$$

Simplifying this yields

$$\dot{V}_1 = 2k\hat{e_1}^T\dot{\hat{e}}_1 = 2k\left(\beta^T - \beta_r^T\right)\left(\dot{\beta} - \dot{\beta}_r\right) \tag{C.13}$$

Multiplying this term out becomes

$$\dot{V}_1 = 2k\left(\beta^T\dot{\beta} - \beta_r^T\dot{\beta} - \beta^T\dot{\beta}_r + \beta_r^T\dot{\beta}_r\right) \tag{C.14}$$

Next, note that:

$$\beta_r^T\beta_r = \|\beta_r\|^2 = 1 \tag{C.15}$$

and

$$\beta^T\beta = \|\beta\|^2 = 1 \tag{C.16}$$

Then, taking the derivatives of these terms yields:

$$\beta^T\dot{\beta} = \dot{\beta}^T\beta = \beta_r^T\dot{\beta}_r = \dot{\beta_r}^T\beta_r = 0 \tag{C.17}$$

Now, the $\dot{V}_1$ equation is:

$$\dot{V}_1 = 2k\left(-\beta_r^T\dot{\beta} - \beta^T\dot{\beta}_r\right) = 2k\left(-\dot{\beta_r}^T\beta - \dot{\beta}^T\beta_r\right) \tag{C.18}$$

As in [32], the Euler parameter formulation yields the kinematic differential equation

$$\dot{\beta} = \frac{1}{2}\boldsymbol{Q}(\beta)\omega \tag{C.19}$$

and similarly

$$\dot{\beta}_r = \frac{1}{2}\boldsymbol{Q}(\beta_r)\omega_r \tag{C.20}$$

Now, plug this into the $\dot{V}_1$ equation to get

$$\dot{V}_1 = 2k\left(-\frac{1}{2}\omega_r^T\boldsymbol{Q}^T(\beta_r)\beta - \frac{1}{2}\omega^T\boldsymbol{Q}^T(\beta)\beta_r\right) \tag{C.21}$$

plugging the earlier relationship that $\boldsymbol{Q}^T(\beta_r)\,\beta = -\boldsymbol{Q}^T(\beta)\,\beta_r$, yields

$$\dot{V}_1 = 2k\left(\frac{1}{2}\omega_r^T\boldsymbol{Q}^T(\beta)\beta_r - \frac{1}{2}\omega^T\boldsymbol{Q}^T(\beta)\beta_r\right) \tag{C.22}$$

Finally, this becomes:

$$\dot{V}_1 = -\left(\omega^T - \omega_r^T\right)\left(k\boldsymbol{Q}^T(\beta)\beta_r\right) \tag{C.23}$$

This completes the details that supplement the text in chapter 3.

C.2 Controller II

In several applications requiring three-axis attitude control, devices such as Reaction Wheel Assemblies and Control Moment Gyroscopes must not only provide the necessary torques but also precision is required. For this reason, a slightly more accurate control law is investigated here to yield different results for the simultaneous problem. The theory derived is similar to the one presented earlier [8].

First, as shown in [45], $\delta\dot{\omega}$ can be simplified. Use the strap-down equation to

show that $\dot{\boldsymbol{L}}_{BR} = \tilde{\boldsymbol{\omega}}\delta\omega$ as follows

$$\dot{\boldsymbol{L}}_{BN} = -\tilde{\boldsymbol{\omega}}\boldsymbol{L}_{BN} \tag{C.24}$$

$$\dot{\boldsymbol{L}}_{RN} = -\tilde{\boldsymbol{\omega}}_r\boldsymbol{L}_{RN} \tag{C.25}$$

$$\dot{\boldsymbol{L}}_{BR} = \boldsymbol{L}_{BN}\dot{\boldsymbol{L}}_{RN}^T + \dot{\boldsymbol{L}}_B N\boldsymbol{L}_{RN}^T \tag{C.26}$$

$$= \boldsymbol{L}_{BN}(-\tilde{\boldsymbol{\omega}}_r\boldsymbol{L}_{RN})^T + -(\tilde{\boldsymbol{\omega}}\boldsymbol{L}_{BN})\boldsymbol{L}_{RN}^T \tag{C.27}$$

$$= \boldsymbol{L}_{BN}\boldsymbol{L}_{RN}^T(-\tilde{\boldsymbol{\omega}}_r)^T + -(\tilde{\boldsymbol{\omega}})\boldsymbol{L}_{BN}\boldsymbol{L}_{RN}^T \tag{C.28}$$

$$= \boldsymbol{L}_{BR}(-\tilde{\boldsymbol{\omega}}_r)^T + -(\tilde{\boldsymbol{\omega}})\boldsymbol{L}_{BR} \tag{C.29}$$

$$= \boldsymbol{L}_{BR}\tilde{\boldsymbol{\omega}}_r + -\tilde{\boldsymbol{\omega}}\boldsymbol{L}_{BR} \tag{C.30}$$

Now,

$$\dot{\boldsymbol{L}}_{BR}\omega_r = \boldsymbol{L}_{BR}\tilde{\boldsymbol{\omega}}_r\omega_r - \tilde{\boldsymbol{\omega}}\boldsymbol{L}_{BR}\omega_r \tag{C.31}$$

$$= -\tilde{\boldsymbol{\omega}}\boldsymbol{L}_{BR}\omega_r \tag{C.32}$$

$$= -\tilde{\boldsymbol{\omega}}(\omega - \delta\omega) \tag{C.33}$$

$$= \tilde{\boldsymbol{\omega}}\delta\omega \tag{C.34}$$

Second, one can simplify $\delta\dot{\omega}$

$$\delta\dot{\omega} = \dot{\omega} - \boldsymbol{L}_{BR}\dot{\omega}_r - \tilde{\boldsymbol{\omega}}\delta\omega \tag{C.35}$$

$$= \dot{\omega} - \boldsymbol{L}_{BR}\dot{\omega}_r - \tilde{\boldsymbol{\omega}}(\omega - \boldsymbol{L}_{BR}\omega_r) \tag{C.36}$$

$$= \dot{\omega} - \boldsymbol{L}_{BR}\dot{\omega}_r + \tilde{\boldsymbol{\omega}}\boldsymbol{L}_{BR}\omega_r \tag{C.37}$$

$$\tag{C.38}$$

Note that this relationships will become important as the derivation unfolds.

C.2.1 Approach

Prior to solving for the control law, one can summarize the approach.

1. At time t, one is given given: β_r, ω_r, $\dot{\omega}_r$, β, ω, Ω, γ, and $\dot{\gamma}$.

2. Solve for τ_r to yield stable regulation/tracking (this solution is derived in the remainder of this Appendix).

3. Using τ_r, one finds $\dot{\Omega}$ and $\ddot{\gamma}$ to provide stable attitude control and power tracking.

4. Assuming less than perfect actuators, one actuates $\ddot{\gamma}$ and $\dot{\Omega}$ through $\tau_G mc$ and $\tau_W mc$, the motor command torques.

5. Use the motor output torques $\tau_G mo$ and $\tau_W mo$ to find the actuated $\ddot{\gamma}$ and $\dot{\Omega}$.

6. Integrate to get the new γ and Ω.

7. Repeat step 1 at $t = t + \Delta t$.

C.2.2 Stable Attitude Controller

Begin with the Lyapunov function candidate (where k > 0):

$$V = kV_q + V_\omega \tag{C.39}$$

where $V_q = \delta\beta_1^2 + \delta\beta_2^2 + \delta\beta_3^2 + (\delta\beta_0 - 1)^2$ and $V_w = \frac{1}{2}\delta\omega^T \boldsymbol{I}_T \delta\omega$.

One can see that this Lyapunov candidate is positive definite and radially unbounded. Thus, it is a valid Lyapunov function candidate. Next, find $\dot{V}$.

$$\dot{V} = k\dot{V}_q + \dot{V}_\omega \tag{C.40}$$

$$\dot{V}_q = 2(\delta\beta_1\delta\dot{\beta}_1 + \delta\beta_2\delta\dot{\beta}_2 + \delta\beta_3\delta\dot{\beta}_3 + 2(\delta\beta_0 - 1)(\delta\dot{\beta}_0)) \tag{C.41}$$

$$\dot{V}_q = 2\begin{bmatrix}\delta\beta_0 & \delta\beta_1 & \delta\beta_2 & \delta\beta_3\end{bmatrix}\begin{bmatrix}\delta\dot{\beta}_0 \\ \delta\dot{\beta}_1 \\ \delta\dot{\beta}_2 \\ \delta\dot{\beta}_3\end{bmatrix} - \delta\dot{\beta}_0 \tag{C.42}$$

$$\dot{V}_q = 2(\delta\beta^T\delta\dot{\beta} - \delta\dot{\beta}_0) \tag{C.43}$$

Also, one finds $\dot{V}_\omega$ as follows:

$$\dot{V}_\omega = \tfrac{1}{2}\delta\dot{\omega}^T\boldsymbol{I}_T\delta\omega + \tfrac{1}{2}\delta\omega^T\boldsymbol{I}_T\delta\dot{\omega} + \tfrac{1}{2}\delta\omega^T\dot{\boldsymbol{I}}_T\delta\omega \tag{C.44}$$

Note that $\frac{1}{2}\delta\dot{\omega}^T\boldsymbol{I}_T\delta\omega = \frac{1}{2}\delta\omega^T\boldsymbol{I}_T\delta\dot{\omega}$, so our equation is now

$$\dot{V}_\omega = \delta\omega^T\boldsymbol{I}_T\delta\dot{\omega} + \tfrac{1}{2}\delta\omega^T\dot{\boldsymbol{I}}_T\delta\omega \tag{C.45}$$

Thus,

$$\dot{V} = 2k(\delta\dot{\beta}^T\delta\beta - \delta\dot{\beta}_0) + \delta\omega^T\boldsymbol{I}_T\delta\dot{\omega} + \tfrac{1}{2}\delta\omega^T\dot{\boldsymbol{I}}_T\delta\omega \tag{C.46}$$

Page 418 of reference [8] gives

$$2\delta\dot{\beta}_0 = -\delta\omega^T\begin{bmatrix}\delta\beta_1 \\ \delta\beta_2 \\ \delta\beta_3\end{bmatrix} \tag{C.47}$$

This implies that

$$-\delta\dot{\beta}_0 = \tfrac{1}{2}\delta\omega^T \begin{bmatrix} \delta\beta_1 \\ \delta\beta_2 \\ \delta\beta_3 \end{bmatrix} \tag{C.48}$$

Also,

$$\delta\dot{\beta} = \tfrac{1}{2}\boldsymbol{Q}(\delta\beta)\delta\omega \tag{C.49}$$

And this implies that

$$\delta\dot{\beta}^T = \tfrac{1}{2}\delta\omega^T\boldsymbol{Q}^T(\delta\beta) \tag{C.50}$$

Next, substitute these relationships into the $\dot{V}$ equation, yielding

$$\dot{V} = 2k\left(\tfrac{1}{2}\delta\omega^T\boldsymbol{Q}^T(\delta\beta)\delta\beta + \tfrac{1}{2}\delta\omega^T\begin{bmatrix} \delta\beta_1 \\ \delta\beta_2 \\ \delta\beta_3 \end{bmatrix}\right) + \delta\omega^T\boldsymbol{I}_T\delta\dot{\omega} + \tfrac{1}{2}\delta\omega^T\dot{\boldsymbol{I}}_T\delta\omega \tag{C.51}$$

Then,

$$\dot{V} = k\delta\omega^T\boldsymbol{Q}^T(\delta\beta)\delta\beta + k\delta\omega^T\begin{bmatrix} \delta\beta_1 \\ \delta\beta_2 \\ \delta\beta_3 \end{bmatrix} + \delta\omega^T\boldsymbol{I}_T\delta\dot{\omega} + \tfrac{1}{2}\delta\omega^T\dot{\boldsymbol{I}}_T\delta\omega \tag{C.52}$$

And,

$$\dot{V} = \delta\omega^T\left(k\boldsymbol{Q}^T(\delta\beta)\delta\beta + k\begin{bmatrix} \delta\beta_1 \\ \delta\beta_2 \\ \delta\beta_3 \end{bmatrix} + \boldsymbol{I}_T\delta\dot{\omega} + \tfrac{1}{2}\dot{\boldsymbol{I}}_T\delta\omega\right) \tag{C.53}$$

Now, define a positive definite gain matrix, $\boldsymbol{K}$ so that:

$$-\boldsymbol{K}\delta\omega = k\boldsymbol{Q}^T(\delta\beta)\delta\beta + k\begin{bmatrix}\delta\beta_1\\ \delta\beta_2\\ \delta\beta_3\end{bmatrix} + \boldsymbol{I}_T\delta\dot{\omega} + \tfrac{1}{2}\dot{\boldsymbol{I}}_T\delta\omega \tag{C.54}$$

From this, one can see that

$$\dot{V} = -\delta\omega^T\boldsymbol{K}\delta\omega \leq 0 \tag{C.55}$$

This implies that the system is Lyapunov Stable since $\dot{V}$ is less than or equal to zero. In order to draw a conclusion about asymptotic stability, one must employ LaSalle's theorem by examining the largest invariant set contained within the set of all states where $\dot{V}$ is zero. Clearly, since $\boldsymbol{K}$ is positive definite, then for $\dot{V}$ to be zero, $\delta\omega$ must be zero. That is to say

$$-\boldsymbol{K}\delta\omega = k\boldsymbol{Q}^T(\delta\beta)\delta\beta + k\begin{bmatrix}\delta\beta_1\\ \delta\beta_2\\ \delta\beta_3\end{bmatrix} + \boldsymbol{I}_T\delta\dot{\omega} + \tfrac{1}{2}\dot{\boldsymbol{I}}_T\delta\omega = 0 \tag{C.56}$$

This further implies that

$$k\boldsymbol{Q}^T(\delta\beta)\delta\beta + k\begin{bmatrix}\delta\beta_1\\ \delta\beta_2\\ \delta\beta_3\end{bmatrix} + \boldsymbol{I}_T\delta\dot{\omega} = 0 \tag{C.57}$$

Additionally, within the largest invariant set where $\dot{V}$ is zero (which in turn implies that $\delta\omega$ is zero) necessitates that $\delta\omega$ is zero for all time. Obviously, for the

case where $\delta\omega$ is zero for all time, then most assuredly $\delta\dot{\omega}$ must also be zero for all time in order for $\delta\omega$ to be contained in the largest invariant set.

One must now identify where $\dot{V}$, $\delta\omega$, and $\delta\dot{\omega}$ equal zero. Here, the stability constraint addressed in (C.57) reduces to

$$k\boldsymbol{Q}^T(\delta\beta)\delta\beta + k\begin{bmatrix}\delta\beta_1\\ \delta\beta_2\\ \delta\beta_3\end{bmatrix} = 0 \tag{C.58}$$

This can be simplified even further when one examines $Q^T(\delta\beta)\delta\beta$:

$$\begin{bmatrix}-\delta\beta_1 & -\delta\beta_2 & -\delta\beta_3\\ -\delta\beta_0 & -\delta\beta_3 & \delta\beta_2\\ \delta\beta_3 & \delta\beta_0 & -\delta\beta_1\\ -\delta\beta_2 & \delta\beta_1 & \delta\beta_0\end{bmatrix}^T \begin{bmatrix}\delta\beta_0\\ \delta\beta_1\\ \delta\beta_2\\ \delta\beta_3\end{bmatrix} \tag{C.59}$$

This results in

$$\begin{bmatrix}-\delta\beta_1\delta\beta_0 + \delta\beta_0\delta\beta_1 + \delta\beta_3\delta\beta_2 - \delta\beta_2\delta\beta_3\\ -\delta\beta_2\delta\beta_0 - \delta\beta_3\delta\beta_1 + \delta\beta_0\delta\beta_2 + \delta\beta_1\delta\beta_3\\ -\delta\beta_3\delta\beta_0 + \delta\beta_2\delta\beta_1 - \delta\beta_1\delta\beta_2 + \delta\beta_0\delta\beta_3\end{bmatrix} = 0 \tag{C.60}$$

Now, one is left with a case where

$$k\begin{bmatrix}\delta\beta_1\\ \delta\beta_2\\ \delta\beta_3\end{bmatrix} = 0 \tag{C.61}$$

This implies that $\delta\beta_1 = \delta\beta_2 = \delta\beta_3 = 0$. Since $\delta\beta$ must have a norm of 1, then given that three of the 4×1 column matrices are zero, $\delta\beta_0$ must equal 1. So, the largest invariant set where $\dot{V}$ is zero contains

$$\delta\beta = \begin{bmatrix} 1 \\ 0 \\ 0 \\ 0 \end{bmatrix} \tag{C.62}$$

From this, one can see that $\delta\beta$ goes to the identity transformation over time, which implies that the orientation difference from the current angular position and the desired angular position is equal to identity. Thus, the body is at its desired angular position. To summarize the stability result, when equation (C.54) is satisfied, then the largest invariant set where the positive definite, radially unbounded function V's derivative is zero, the only states contained in this set are at the origin (i.e. the points where the attitude position, velocity, and acceleration errors are zero). This implies global asymptotic stability of the closed loop system.

Now that stability has been proven, one only now needs to find controls that satisfy (C.54). Recalling that

$$\delta\dot{\omega} = \dot{\omega} - \boldsymbol{L}_{BR}\dot{\omega}_r + \tilde{\boldsymbol{\omega}}\boldsymbol{L}_{BR}\omega_r \tag{C.63}$$

One needs

$$\boldsymbol{K}\delta\omega = -\left(k\boldsymbol{Q}^T(\delta\beta)\delta\beta + k\begin{bmatrix}\delta\beta_1\\ \delta\beta_2\\ \delta\beta_3\end{bmatrix} + \boldsymbol{I}_T(\dot{\omega} - \boldsymbol{L}_{BR}\dot{\omega}_r + \tilde{\boldsymbol{\omega}}\boldsymbol{L}_{BR}\omega_r) + \tfrac{1}{2}\dot{\boldsymbol{I}}_T\delta\omega \right) \tag{C.64}$$

This can be rearranged to

$$\boldsymbol{K}(\omega - \boldsymbol{L}_{BR}\omega_r) = -\boldsymbol{I}_T\dot{\omega} + \boldsymbol{I}_T\boldsymbol{L}_{BR}\dot{\omega}_r - \boldsymbol{I}_T\tilde{\omega}\boldsymbol{L}_{BR}\omega_r - \tfrac{1}{2}\dot{\boldsymbol{I}}_T\delta\omega - k\begin{bmatrix}\delta\beta_1\\ \delta\beta_2\\ \delta\beta_3\end{bmatrix} \tag{C.65}$$

Now note that

$$\boldsymbol{I}_T\dot{\omega} = \tau_D - \tilde{\omega}\boldsymbol{I}_T\omega - \boldsymbol{B}\ddot{\gamma} - \boldsymbol{D}_s\dot{\gamma} - \boldsymbol{E}\dot{\Omega} - \boldsymbol{F}\Omega \tag{C.66}$$

This yields

$$\boldsymbol{K}\omega - \boldsymbol{K}\boldsymbol{L}_{BR}\omega_r = -\tau_D + \tilde{\omega}\boldsymbol{I}_T\omega + \boldsymbol{B}\ddot{\gamma} + \boldsymbol{D}_s\dot{\gamma} + \boldsymbol{E}\dot{\Omega} + \boldsymbol{F}\Omega + \boldsymbol{I}_T\boldsymbol{L}_{BR}\dot{\omega}_r \tag{C.67}$$

$$\boldsymbol{I}_T\tilde{\omega}\boldsymbol{L}_{BR}\omega_r - \tfrac{1}{2}\dot{\boldsymbol{I}}_T(\omega - \boldsymbol{L}_{BR}\omega_r) - k\begin{bmatrix}\delta\beta_1\\ \delta\beta_2\\ \delta\beta_3\end{bmatrix} \tag{C.68}$$

Further rearranging, this becomes

$$\boldsymbol{K}\omega - \boldsymbol{K}\boldsymbol{L}_{BR}\omega_r + \tau_D - \tilde{\omega}\boldsymbol{I}_T\omega - \boldsymbol{I}_T\boldsymbol{L}_{BR}\dot{\omega}_r + \boldsymbol{I}_T\tilde{\omega}\boldsymbol{L}_{BR}\omega_r - k\begin{bmatrix}\delta\beta_1\\ \delta\beta_2\\ \delta\beta_3\end{bmatrix} = -\tfrac{1}{2}\dot{\boldsymbol{I}}_T(\omega - \boldsymbol{L}_{BR}\omega_r)$$
$$+\boldsymbol{B}\ddot{\gamma} + \boldsymbol{D}_s\dot{\gamma} + \boldsymbol{E}\dot{\Omega} + \boldsymbol{F}\Omega \tag{C.69}$$

Now, let

$$\tau_R = \boldsymbol{K}\omega - \boldsymbol{K}\boldsymbol{L}_{BR}\omega_r - \tilde{\omega}\boldsymbol{I}_T\omega - \boldsymbol{I}_T\boldsymbol{L}_{BR}\dot{\omega}_r + \boldsymbol{I}_T\tilde{\omega}\boldsymbol{L}_{BR}\omega_r - k\begin{bmatrix}\delta\beta_1\\ \delta\beta_2\\ \delta\beta_3\end{bmatrix} \tag{C.70}$$

Note that $-\frac{1}{2}\dot{\boldsymbol{I}}_T(\omega - \boldsymbol{L}_{BR}\omega_r) = R\dot{\gamma}$, so that

$$\tau_R + \tau_D = \tau_D + \boldsymbol{K}\omega - \boldsymbol{K}\boldsymbol{L}_{BR}\omega_r - \tilde{\omega}\boldsymbol{I}_T\omega - \boldsymbol{I}_T\boldsymbol{L}_{BR}\dot{\omega}_r + \boldsymbol{I}_T\tilde{\omega}\boldsymbol{L}_{BR}\omega_r - k\begin{bmatrix}\delta\beta_1\\ \delta\beta_2\\ \delta\beta_3\end{bmatrix} \tag{C.71}$$

which also gives

$$\tau_D + \tau_R = \boldsymbol{B}\ddot{\gamma} + (\boldsymbol{D}_s + \boldsymbol{R})\dot{\gamma} + \boldsymbol{E}\dot{\Omega} + \boldsymbol{F}\Omega \tag{C.72}$$

This is similar to the control law derived earlier. Therefore, the required torque is summarized as

$$\tau_R = \boldsymbol{K}\omega - \boldsymbol{K}\boldsymbol{L}_{BR}\omega_r - \tilde{\omega}\boldsymbol{I}_T\omega - \boldsymbol{I}_T\boldsymbol{L}_{BR}\dot{\omega}_r + \boldsymbol{I}_T\tilde{\omega}\boldsymbol{L}_{BR}\omega_r - k\begin{bmatrix}\delta\beta_1\\ \delta\beta_2\\ \delta\beta_3\end{bmatrix} \tag{C.73}$$

It should be pointed out that once one obtains the attitude error $\delta\beta$, then one can get the transformation $\boldsymbol{L}_{BR}$ (from $\mathcal{R}$ to $\mathcal{B}$) using

$$\boldsymbol{L}_{BR} = \begin{bmatrix} (\delta\beta_0^2 + \delta\beta_1^2 - \delta\beta_2^2 - \delta\beta_3^2) & 2(\delta\beta_1\delta\beta_2 + \delta\beta_0\delta\beta_3) & 2(\delta\beta_1\delta\beta_3 - \delta\beta_0\delta\beta_2) \\ 2(\delta\beta_1\delta\beta_2 - \delta\beta_0\delta\beta_3) & (\delta\beta_0^2 - \delta\beta_1^2 + \delta\beta_2^2 - \delta\beta_3^2) & 2(\delta\beta_2\delta\beta_3 + \delta\beta_0\delta\beta_1) \\ 2(\delta\beta_1\delta\beta_3 + \delta\beta_0\delta\beta_2) & 2(\delta\beta_1\delta\beta_3 - \delta\beta_0\delta\beta_1) & (\delta\beta_0^2 - \delta\beta_1^2 - \delta\beta_2^2 + \delta\beta_3^2) \end{bmatrix} \tag{C.74}$$

So, the question remains, how does one compute $\delta\beta_1$, $\delta\beta_2$, and $\delta\beta_3$ at any instant in time? From page 443 of reference [8], one finds that

$$\begin{bmatrix} \delta\beta_1 \\ \delta\beta_2 \\ \delta\beta_3 \\ \delta\beta_4 \end{bmatrix} = \begin{bmatrix} \beta_0 & \beta_3 & -\beta_2 & -\beta_1 \\ -\beta_3 & \beta_0 & \beta_1 & -\beta_2 \\ \beta_2 & -\beta_1 & \beta_0 & -\beta_3 \\ \beta_1 & \beta_2 & \beta_3 & \beta_0 \end{bmatrix} \begin{bmatrix} \beta_{1r} \\ \beta_{2r} \\ \beta_{3r} \\ \beta_{0r} \end{bmatrix} \tag{C.75}$$

Therefore, one is able to find the attitude error to compute the required torque from equation (C.73) for stable tracking of the vehicle reference attitude.

APPENDIX D

ACTUATOR CONFIGURATION

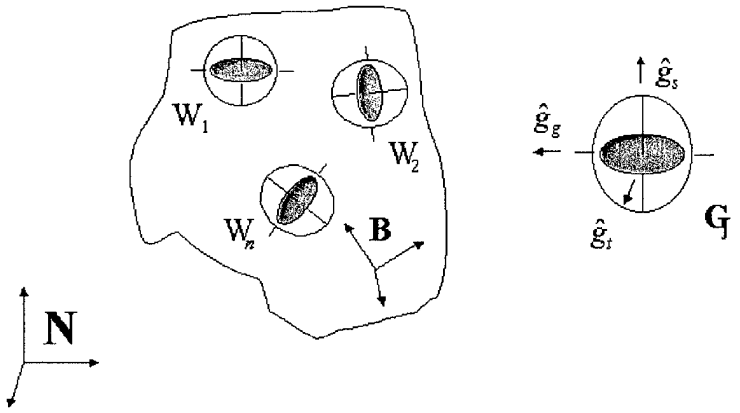

Figure D.1: Generic VSCMG Layout

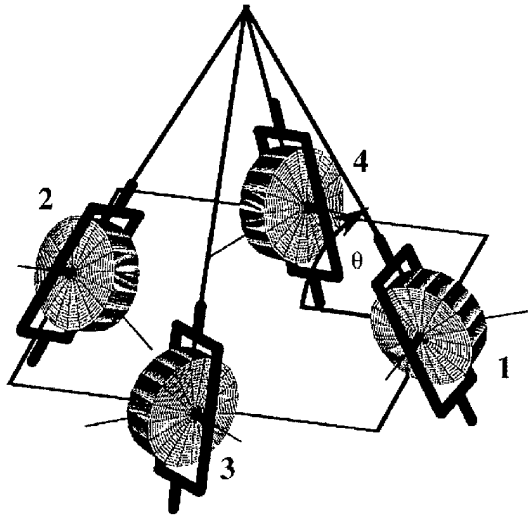

Figure D.2: VSCMG Pyramid Configuration

APPENDIX E

EXAMPLE COMBINED ATTITUDE/POWER TRACKING PROBLEM

Most of the orbital example is derived from Tsiotras, Shen, and Hall [5, 4]. This orbital example of a satellite, Iridium (spacecraft number 25578), provides a rigorous case study in the simultaneous attitude/power tracking control system under worst case polar orbit conditions. In this scenario, the flywheel energy storage function augments a satellite's solar array system. During sunlight, the solar array provides energy to the many spacecraft subsystems. Any excess power is used to charge the flywheels within the VSCMG suite. Then, during eclipse, the satellite uses the array to power its many subsystems. Since there is no back-up for the VSCMGs during eclipse, the system must be prepared to meet a peak power requirement.

Note that a few RWA control laws for this problem were developed in ([45]).

Figures (E.1) and (E.2) reflect the satellite with solar arrays deployed, the tracking scenario, the associated coordinate reference frames.

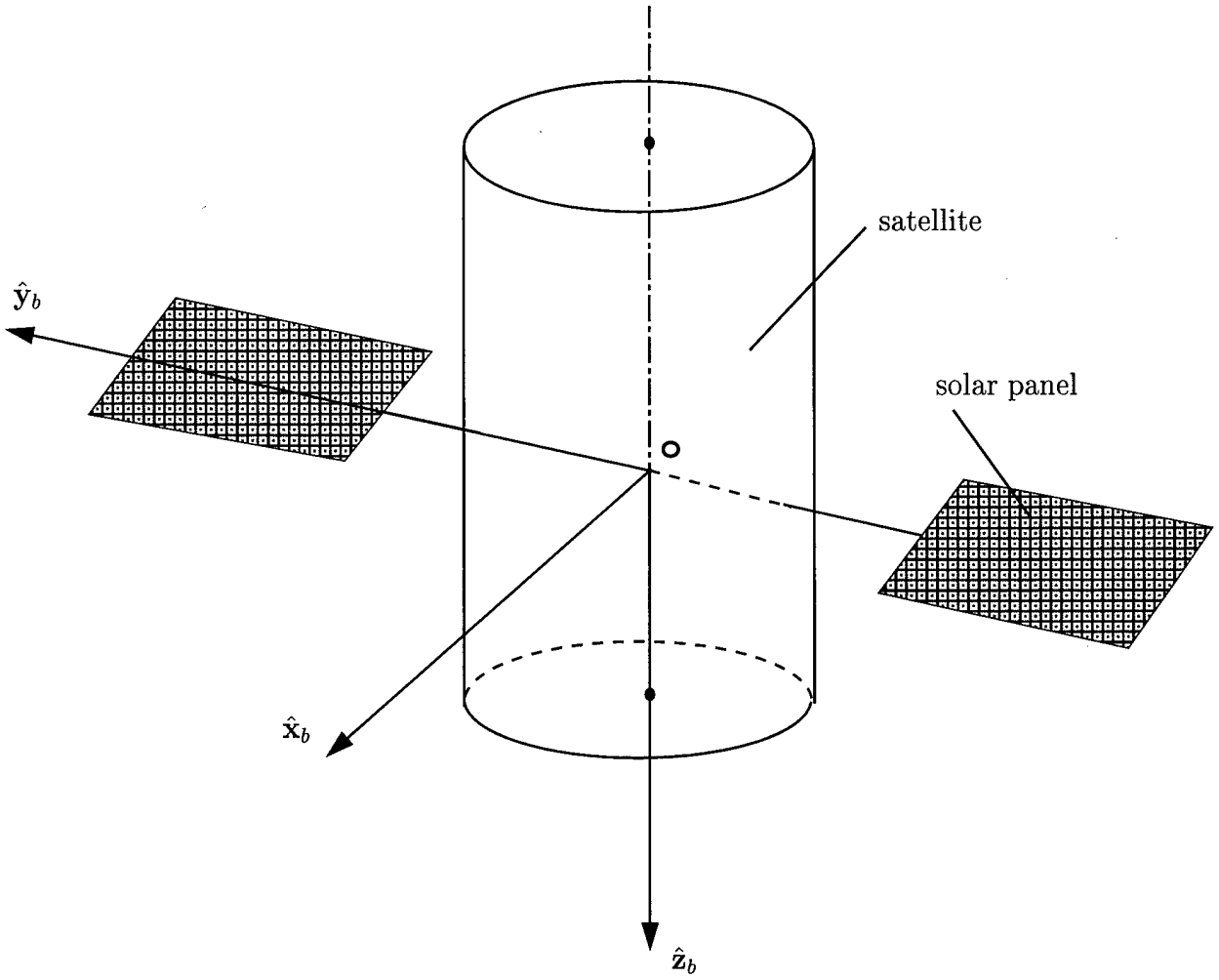

Figure E.1: Satellite

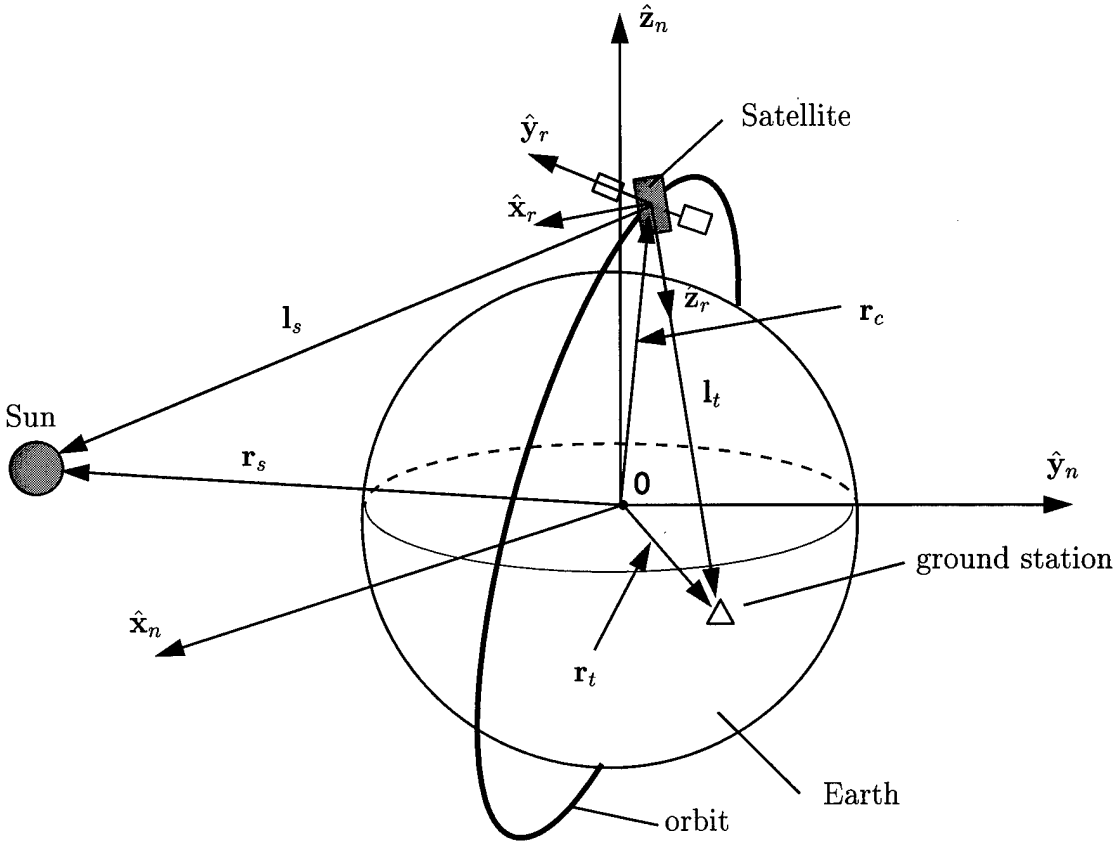

Figure E.2: Scenario Layout

APPENDIX F

VSCMG WORKBENCH:

SIMULATION DESIGN DETAILS

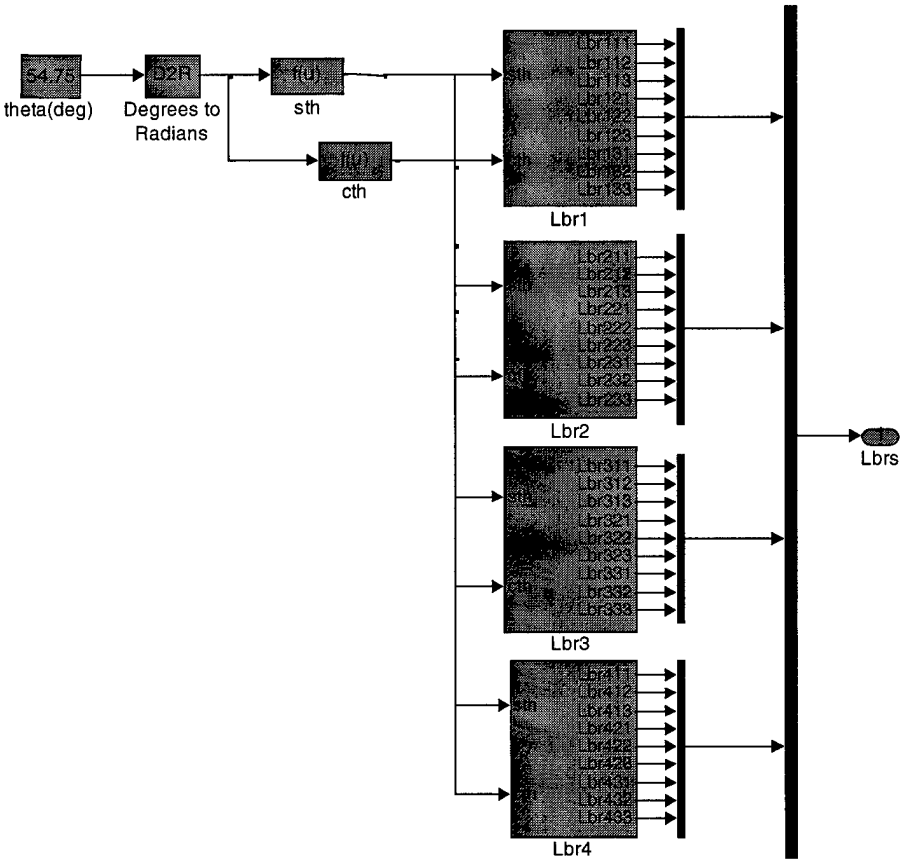

Figure F.1: Actuator Coordinate Transforms Overview

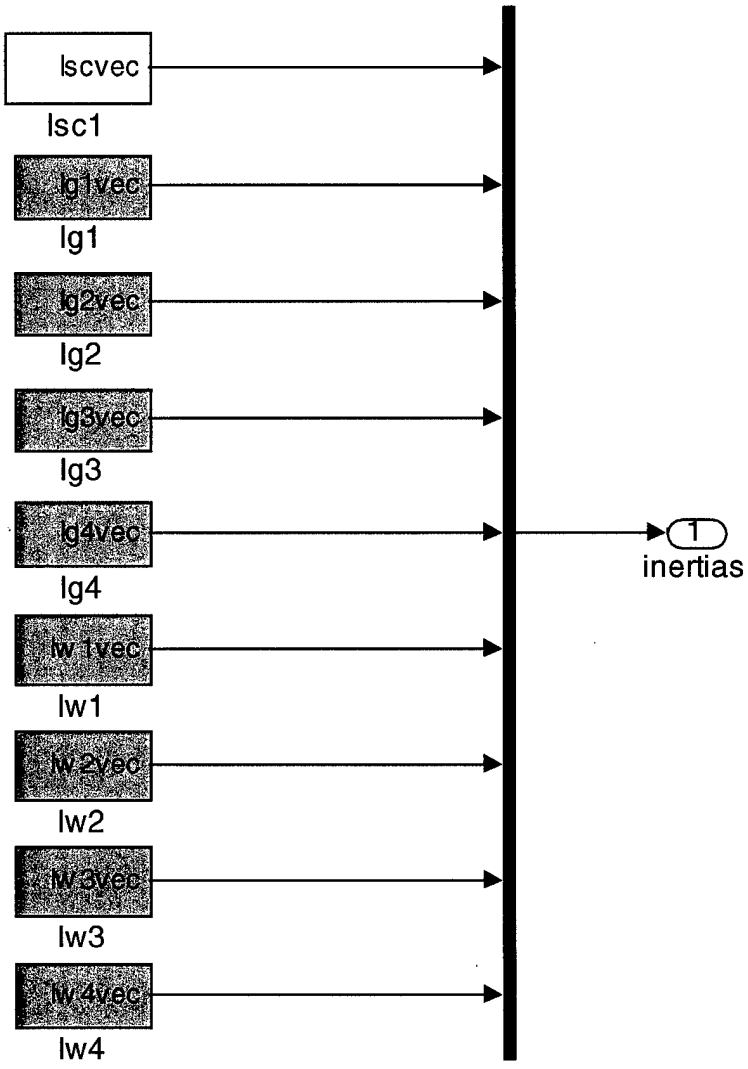

Figure F.2: System Inertia Overview

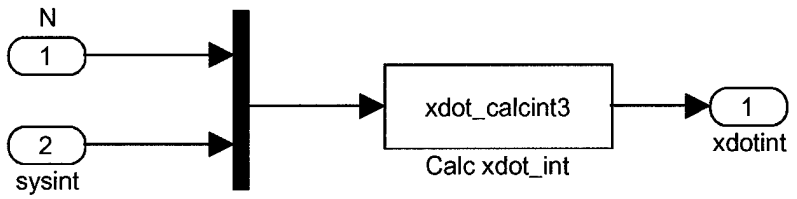

Figure F.3: Internal System State Derivative Computation Logic

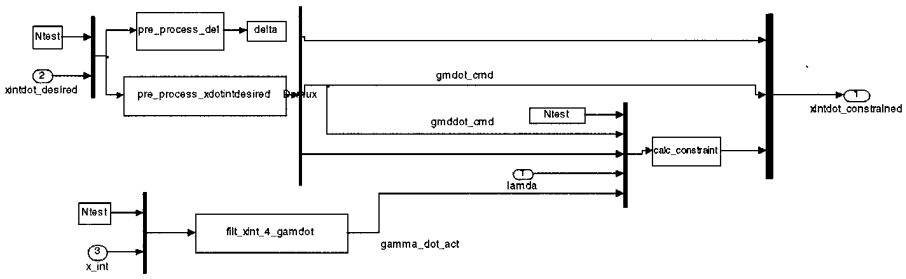

Figure F.4: Gimbal Rate Torque Amplification Constraint

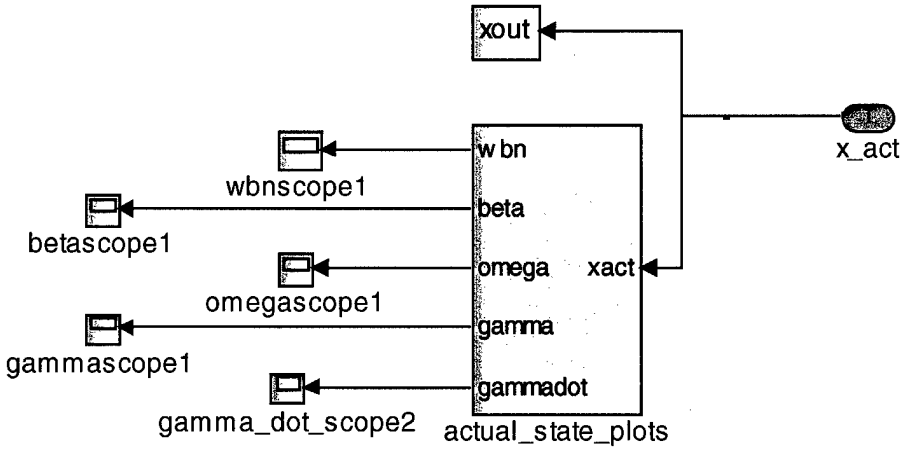

Figure F.5: Actual Plant Output States Oscilloscope

Bibliography

[1] J. Wertz and W. J. Larson, editors. *Space Mission Analysis and Design.* Kluwer Academic Publishers, Boston, 1999.

[2] J. Fausz and D. Richie. Flywheel simultaneous attitude control and energy storage using vscmgs. In *IEEE International Conference on Control Applications*, pages 991–995, Sept. 25–27 2000. Ancorage, AK.

[3] C. Hall. High-speed flywheels for integrated energy storage and attitude control. In *Proceedings of the American Control Conference*, pages 1894–1898, June 4–6 1997. Albuquerque, NM.

[4] P.Tsiotras, H.Shen, and C.D. Hall. Satellite attitude control and power tracking with energy/momentum wheels. *AIAA Journal of Guidance, Control, and Dynamics*, 24(1):23–34, 2001.

[5] H. Shen and P. Tsiotras. Satellite attitude control and power tracking with momentum wheels. In *AAS/AIAA Astrodynamics Specialist Conference, AAS Paper 99-317*, Aug. 16–18 1999. Girdwood, AK.

[6] Kevin A. Ford. *Reorientations of Flexible Spacecraft Using Momentum Exchange Devices.* PhD thesis, Air Force Institude of Technology, Wright-Patterson AFB, Ohio, September 1997.

[7] M. Kaplan. *Modern Spacecraft Dynamics and Control.* John Wiley and Sons, New York, 1976.

[8] B. Wie. *Space Vehicle Dynamics and Control.* American Institutde of Aeronautics and Astronautics, Reston, Virginia, 1998.

[9] D. Davis and A. Csomor. The new age of high performance kinetic energy storage systems. In *Proceedings of the 15th Intersociety Energy Conversion Engineering Conference*, volume 2, pages 1507–1512, 1980.

[10] J. A. Kirk. Flywheel energy storage part i: Basic concepts. *International Journal of Mechanical Sciences*, 19(4):223–231, 1977.

[11] J. A. Kirk and P.A. Studer. Flywheel energy storage part ii: Magnetically suspended superflywheel. *International Journal of Mechanical Science*, 19(4):233–245, 1977.

[12] J. B. Roes. An electro-mechanical energy storage system for space application. *Progress in Astronautics and Rocketry.*

[13] W.W. Anderson and C.R. Keckler. Integrated power/attitude control system (ipacs) for space application. In *Proceedings of the 5th IFAC Symposium on Automatic Control in Space*, 1973.

[14] A. Cormack III. Three axis flywheel energy and control systems. Technical Report NASA TN-73-G&C-8, North American Rockwell Corp., 1973.

[15] C. R. Keckler and K. L. Jacobs. A spacecraft integrated power/attitude control system,. In *9th Intersociety Energy Conversion Engineering Conference*, 1974.

[16] J. E. Notti, W.C. Schmill, W.J. Klein, and A. Cormack III. Integrated power/attitude control system (IPACS) study: Volume II–conceptual designs. Technical Report NASA CR-2384, Rockwell International Space Division, Downey, CA, 1974.

[17] R.W. Will, C.R. Keckler, and K.L. Jacobs. Description and simulation of an integrated power and attitude control system concept for space-vehicle application. Technical Report NASA TN-D-7459, NASA, 1974.

[18] D. Anand, J. A. Kirk, and D. A. Frommer. Design considerations for magnetically suspended flywheel systems. In *Proceedings of the 20th Intersociety Energy Conversion Engineering Conference*, volume 2, pages 449–453, 1985.

[19] J. Downer, D. Eisenhaure, R. Hockney, B. Johnson, and S. O'Dea. Magnetic suspension design options for satellite attitude control and energy storage. In

Proceedings of the 20st Intersociety Energy Conversion Engineering Conference, volume 2, pages 424–430, 1985.

[20] D.B. Eisenhaure, J.R. Downer, T.E. Bliamptis, and S.D. Hendrie. A low-authority control law for underactuated rigid spacecraft. In *22nd Aerospace Sciences Meeting*, pages 1–10, Reno, NV, Jan. 9-12, 1984. AIAA Paper 84-0565.

[21] T. Flatley. Tetrahedron array of reaction wheels for attitude control and energy storage. In *Proceedings of the 20st Intersociety Energy Conversion Engineering Conference*, volume 2, pages 2353–2360, 1985.

[22] S. O'Dea, P. Burdick, J. Downer, D. Eisenhaure, and L. Larkin. Design and development of a high efficiency effector for the control of attitude and power in space systems. In *Proceedings of the 20st Intersociety Energy Conversion Engineering Conference*, volume 2, pages 353–360, 1985.

[23] R. E. Oglevie and D. B. Eisenhaure. Integated power and attitude control system (IPACS) technology. In *Proceedings of the 21st Intersociety Energy Conversion Engineering Conference*, volume 3, pages 1834–1837, 1986.

[24] D. R. Olmsted. Feasibility of flywheel energy storage in spacecraft applications. In *Proceedings of the 20st Intersociety Energy Conversion Engineering Conference*, volume 2, pages 444–448, 1985.

[25] M. Olszewski and D. U. O'Kain. Advances in flywheel technology for space power applications. In *Proceedings of the 21st Intersociety Energy Conversion Engineering Conference*, volume 3, pages 1823–1828, 1986.

[26] W.E. Simon and K.E. Van Tassel. Inertial energy storage for advanced space station applications. In *Proceedings of the 20st Intersociety Energy Conversion Engineering Conference*, volume 2, pages 337–342, 1985.

[27] P. A. Studer and G. E. Rodriguez. High speed reaction wheels for satellite attitude control and energy storage. In *Proceedings of the 20th Intersociety Energy Conversion Engineering Conference*, volume 2, pages 349–352, 1985.

[28] M. Ahrens, L. Kucera, and R. Larsonneur. Performance of a magnetically suspended flywheel energy storage device. *IEEE Transactions on Control Systems Technology*, 4(5):494–502, 1996.

[29] D.T. Radzykewycz, J.L. Fausz, and W.R. James. Energy storage technology development at the air force research laboratory space vehicles directorate. In *Proceedings of the 1999 Space Technology Conference and Exposition*, pages 1–5, September 28–30 1999. Albuquerque, NM.

[30] A. D. Jacot and D. Liska. Control moment gyros in attitude control. *Journal of Spacecraft and Rockets*, 3(9):1313–1320, 1966.

[31] G. Margulies and J.N. Aubrun. Geometric theory of single-gimbal control moment gyro systems. *Journal of the Astronautical Sciences*, 26(2):159–191, 1978.

[32] H.S. Oh and S.R. Vadali. Feedback control and steering laws for spacecraft using single gimbal control moment gyros. *Journal of the Astronautical Sciences*, 39(2):183–203, 1994.

[33] N.S. Bedrossian, J. Paradiso, E.V. Bergmann, and D. Rowell. Redundant single gimbal control moment gyroscope singularity analysis. *Journal of Guidance*, 13(6), 1989.

[34] B.R. Hoelscher and S.R. Vadali. Optimal open-loop and feedback control using single gimbal control moment gyroscopes. *Journal of the Astronautical Sciences*, 42(2):189–206, 1994.

[35] S.R. Vadali and S. Krishnan. suboptimal command generation for control moment gyroscopes and feedback control of spacecraft. *Journal of Guidance, Control, and Dynamics*, 18(6):1350–1354, 1995.

[36] S.R. Vadali, H.S. Oh, and S.R. Walker. Preferred gimbal angles for single gimbal control moment gyros. *Journal of Guidance*, 13(6):1090–1095, 1989.

[37] K. A. Ford and C. D. Hall. Singular direction avoidance steering for control-moment gyros. *AIAA Journal of Guidance, Control, and Dynamics*, 23(4):648–656, 2000.

[38] Hanspeter Schaub. *Novel Coordinates For Nonlinear Multibody Motion with Applications to Spacecraft Dynamics and Control.* PhD thesis, Texas A and M University, Arlington, TX, May 1998.

[39] H. Schaub and J. L. Junkins. Singularity avoidance using null motion and variable-speed control moment gyros. *AIAA Journal of Guidance, Control, and Dynamics*, 23(1):11–16, 2000.

[40] H. Schaub, S. R. Vadali, and J. L. Junkins. Feedback control law for variable speed control moment gyros. *Journal of the Astronautical Sciences*, 46(3):307–28, 1998.

[41] D. Richie, P. Tsiotras, and J. Fausz. Simultaneous attitude control and energy storage using vscmgs:theory and simulation. In *Proc. American Control Conf.*, 2001. Arlington,VA.

[42] T.R. Kane and D.A. Levinson. *Dynamics:Theory and Applications.* McGraw-Hill, New York, 1985.

[43] R. A. Horn and C. R. Johnson. *Matrix Analysis.* Cambridge University Press, Cambridge, United Kingdom, 1985.

[44] A. Biran and M. Breiner. *MATLAB 5 For Engineers.* Addison, Wesley, Harlow, England, 1999.

[45] C. Hall, P. Tsiotras, and H. Shen. Tracking rigid body motion using thrusters and reaction wheels. In *AIAA/AAS Astrodynamics Specialists Conference*, Boston, MA, Aug. 10-12, 1998. AIAA Paper 98-4471.

FINAL NOTE

"Man's flight through life is sustained by the power of his knowledge." (Austin 'Dusty' Miller, the quote on the Eagle and Fledgling Statue at the US Air Force Academy).